Hydrological modeling of a Mongolian River basin under current and changed climate conditions using permafrost conceptualizations

Master thesis Civil Engineering and Management

January 18th, 2013

Author: Kor Heerema

Supervisors: Prof. Ir. E. van Beek (University of Twente), Dr. Ir. M.J. Booij (University of Twente), Dr. J.J. Warmink (University of Twente) and Ir. R. Huting (Royal HaskoningDHV)

UNIVERSITY OF TWENTE.

Royal HaskoningDHV
Enhancing Society Together

Document	Master Thesis
Date	18-1-2013
Status	Final
Author	Kor Heerema
	kor.heerema@gmail.com
Assigned by	University of Twente
	Royal Haskoning DHV
Graduation committee	Dr. Ir. M.J. Booij (WEM)
	Dr. J.J. Warmink (WEM)
	Prof. ir. E. van Beek (WEM)
	Ir. R. Huting (Royal HaskoningDHV)

UNIVERSITY OF TWENTE.

Royal HaskoningDHV
Enhancing Society Together

SUMMARY

Water resources are globally under severe pressure, mainly due to population growth, economic development and climate change. The process of permafrost degradation resulting from global warming increases the vulnerability of all climate dependent sectors affecting the economy in high-latitude Asia. The adverse consequences of climate change are likely to disrupt mountain and highland ecosystems in Central Asia. The consequences for downstream agriculture, which relies on water for irrigation, will (very) likely be unfavorable.

The same applies to Mongolia, which has a strong need of developing its own infrastructure and water resources in a more efficient way. Mongolia is a country predominated by mountain ranges with a continental climate, which promote occurrence and development of permafrost regions. Since permafrost is a thermal condition, it is potentially sensitive to climate change and human activities. Impacts of climate change coupled with human pressure for water are upsetting the balances in Mongolian river basins and the situation is forecasted to get worse.

In this study, a rainfall-runoff model is developed based on the general structure of the HBV model. The model has proven to be applicable in mountainous areas under extreme and cold climate conditions, as is common in Mongolia. The model is able to cover the most important runoff generating processes using a simple and robust structure, and a small number of parameters. The Buyant River basin in Western Mongolia is used as a case study to simulate discharges for the current climate and predict monthly changes under different climate change scenarios.

Permafrost conditions are adapted in the conceptual HBV model in this study, resulting in four different permafrost conceptualizations. Two conceptualizations describe the general structure of the HBV model and take permafrost conditions into account by calibrating under non-permafrost conditions. The other two conceptualizations incorporate freezing and melting functions which simulate the storage and melting of ice in the soil. A further distinction is made between the elevation zones (single and multiple) in the mountainous Buyant River basin. Due to lack of meteorological input data, 5 years of calibration and 5 years of validation are used. Results of the calibration are moderate to good for the conceptualizations simulating permafrost conditions all year round, whereas the conceptualization with one elevation zone performs better in the validation period than the conceptualization with multiple elevation zones.

The output of four different Global Circulation Models (GCMs) and three different emission scenarios are used to assess the uncertainty in climate change for the Buyant River basin. The delta approach method is used to translate output from GCMs to climate time series for future conditions. The outputs of these 12 climate change scenarios are combined with the most appropriate HBV conceptualization to assess the climate change impacts on the future discharges of the Buyant River.

The application of the single elevation zone with permafrost conditions conceptualization indicates that, under the present estimated climate scenarios of global warming for the period 2080-2100, the runoff in the summer will decrease, while the discharge in spring is likely to increase in the Buyant River basin. However, uncertainties in future climate change impacts are rather high as the incongruity between GCMs and emission scenarios and between different GCMs cause distinct runoff projections, the former being the cause for yielding low and the latter for high variability. Whilst the variability in the models and the coarse resolution yield projections that are at best conjecture, future refinement of these models may yield in more accurate and realistic scenarios.

PREFACE

The preparation of my master thesis started more than one year ago. The main topic of my master thesis is the hydrological modeling of a river basin predominated by permafrost. The area of this case study is located in the western part of Mongolia, and is called the Buyant River basin. I was twice given the opportunity to visit Mongolia and the area of interest to this thesis whilst conducting my research. The warm welcome and pleasant stay during both of my visits made me realize how fortunate I was to be involved in this project. In particular the three weeks of our field trip to the Buyant River were an unforgettable experience.

The Buyant River flows through the impressive landscape of western Mongolia. It rises in the Altai Mountains to a height of 3500 meters above sea level and is predominated by permafrost conditions. The river forms a unique ecosystem which is under threat from water shortages caused by evaporation, irrigation and infiltration into the soil.

The outcome of this master thesis is a conceptual hydrological model which simulates current and future discharges for the Buyant River, taking into account permafrost conditions. A permafrost conceptualization is applied within an existing conceptual hydrological model (HBV) and performed moderate to good for the Buyant River basin. This permafrost conceptualization can therefore be used as a tool for the simulation and forecasting of hydrological processes in other river basins prevailed by permafrost conditions.

The output of the permafrost conceptualization helps local government authorities to implement a range of measures to safeguard its sustainability in the Buyant River basin. This will help to ensure that enough water is left in the river to restore the ecosystem in the basin.

Conducting my research I gained a lot of experience with hydrological modeling and I became more and more familiar with the mathematical tool Matlab. In the early stadium of my thesis I tried a lot of different and, mostly, time consuming aspects to improve the HBV model. Although this has proven very effective at times, it made the research process very inefficient most of the time: my laptop was processing data and simulating various conceptualizations day and night, but a slight mistake in the model's parameters made simulation often worthless. A lot of data have been examined during this thesis. Special thanks go to my colleagues at the Institute for Meteorology, Hydrology and Environment in Mongolia for kindly supplying me with all the climatological data I asked for.

It took a while before I clearly had in mind what the end result should look like. The last three meetings provided me with many new ideas and data that substantially aided to improve progress on my thesis. During a sparring session with Ric new ideas popped up in our heads and insights were born. With the critical view of Martijn and Jord pieces quickly fell in to space. New input data from Mongolia provided even better model performances, resulting in a constantly improving drive to finish my master thesis project.

I wish you much pleasure in reading this thesis and hope you will find it enjoyable!

ACKNOWLEDGEMENTS

Many people helped me during the period of my graduation. Besides the support and interest of my friends and family, who are hopefully aware of my gratitude towards them, I would like to thank the following people and organizations for their invaluable contributions:

In The Netherlands…

- At the University of Twente, Enschede: Martijn Booij, Jord Warmink and Eelco van Beek.
- At Royal Haskoning DHV, Amersfoort: Ric Huting, Eisse Wijma, Harm Nomden and Tijmen Smolders.
- At Deltares, Delft: Jaap Kwadijk.

…and in Mongolia

- At the WWF office, Ulaanbaatar: Oyunmunkh, Purevdorj and Sanjaa.
- At the IMHE Mongolia, Ulaanbaatar: Odgarav, dr Davaa and mr Gomboluudev.
- At the IWRM project Mongolia, Ulaanbaatar: Wim van der Linden.

And of course my great (former) housemates Freek and Bob.

CONTENTS

LIST OF FIGURES

LIST OF TABLES

1. INTRODUCTION

1.1 General

Water resources are globally under severe pressure, mainly due to population growth, economic development and climate change. Problems in cold and arid areas in Central Asia are particularly serious [*IPCC-TGICA*, 2007]. In these areas precipitation is low and often highly variable in space and time. The resulting surface run-off represents a scarce water resource and it depends mainly on the melting of snow and ice as their main source of water [*Kang et al.*, 1999].

Impacts of climate change coupled with human pressure for water are upsetting the balances in these river basins and the situation is forecasted to get worse [*IPCC-TGICA*, 2007]. By 2080 increased temperatures under climate change are expected to make hot summer months becoming even hotter and dryer for Central Asia. This warming process will accelerate the melting of glaciers in mountainous areas [*Kang et al.*, 1999]. As glaciers melt, river runoff will initially increase in winter or spring but eventually will decrease as a result of loss of ice resources. Significant shortages in wintertime water availability for livestock are projected by the end of this century [*MARCC*, 2009].

Agricultural productivity in Central Asia is likely to suffer severe losses because of high temperature, severe drought, flood conditions and soil degradation [*MARCC*, 2009]. The process of permafrost degradation resulting from global warming increase the vulnerability of all climate dependent sectors affecting the economy in high-latitude Asia [*Kang et al.*, 1999]. The adverse consequences of climate change are likely to disrupt mountain and highland ecosystems in Central Asia. Consequences for downstream agriculture, which relies on water for irrigation, will (very) likely be unfavorable [*MARCC*, 2009].

The same applies to Mongolia, which has a strong need of developing its own infrastructure and water resources in a more efficient way [*MARCC*, 2009]. Water resources in the arid areas of Mongolia are distributed by mountainous inland river basins. At the low land plains and basins in front of the mountains runoff is scattering and water is abstracted for consumption and irrigation [*Kang et al.*, 1999].

1.2 Project background

The Buyant River basin, located in Western Mongolia, is one of those mountainous watersheds characterized by local permafrost, steep hills, glaciers, marshlands, and wide alluvial plains. Due to a changing climate, glaciers that feed the rivers are getting melted and dryness has increased [*MARCC*, 2009]. For efficient use of scarce water, effective management of available water is necessary. Managing recharge or storing flood water, for instance, can be used to mitigate the threats and to maximize available resources. The Mongolian Water Authority is therefore setting up water management plans to restore the water balance in the Buyant River basin to safeguard its sustainability [*MARCC*, 2009].

More knowledge about the change in discharge nowadays and in the future is a prerequisite for the development of these plans. For operational water management, spatial and temporal distributions of water resources become important to understand. Hydrological models are generally used to describe the hydrological processes in river basins, which are important to predict future discharges [*Liden and Harlin*, 2000].

Originally the HBV (Hydrologiska Byråns Vattenbalansavdelning) model was developed at the Swedish Meteorological and Hydrological Institute (SMHI) for runoff simulation and hydrological forecasting, but the scope of applications has increased steadily [*Lindström et al.*, 1997]. The conceptual hydrological model HBV has been applied in more than 60 countries all over the world and implemented in river basin with strongly different climatic conditions [*Liden and Harlin*, 2000]. The original HBV model was already expanded at the Swiss Federal Institute of Technology (ETH) in Zurich for the application in glaciered catchments [*Braun et al.*, 1993]. *Akhtar et al.* [2008] and *Konz et al.* [2007] conducted an HBV model study for the analysis of river basins in the high mountainous Himalaya region, respectively in Pakistan and Nepal. The model has been used in several catchments in Canada [*Moore*, 1993; *Stahl et al.*, 2008] and in inland river basins of Central Asia [*Hagg et al.*, 2007; *Kang et al.*, 1999]. A study by *Council et al.* [1999] applied an HBV model version for simulation and forecasting of hydrological catchment processes in permafrost areas. Based on these former studies the HBV model has proven to be applicable in a range of geographic regions similar to the Buyant River basin. Due to its former successes the rainfall-runoff model HBV will be applied to simulate the Buyant River discharges.

1.3 Objective and approach

The food security of inhabitants and water availability for their livestock in the Buyant River basin are important issues in the area. Both depend heavily on the discharge of, and possible abstractions from, the Buyant River. These discharges are most likely to be influenced by climate change. Getting reliable estimates of these discharges with the help of the simulations derived by the conceptual HBV model, the management of the water resource system can be improved and thus more efficient and effective in the future. The aim of this study is:

> *To predict the discharges of the Buyant River under current and changed climate conditions using the HBV model*

The quality of the hydrological simulation depends on the ability of the HBV model to describe and predict the hydrological processes in the Buyant River basin. The model needs to be adapted for permafrost conditions, than calibrated and hereafter validated. Different conceptualizations should be implemented in the HBV model and compared to select the most appropriate one. The uncertainty in the hydrological model [*Seibert*, 1997] should be considered before conclusions can be drawn from these conceptualizations. To determine the effect of a changing climate for the discharge of the Buyant River, different climate change scenarios should be used for the prediction of future discharges in the Buyant River basin.

To pursue the research aim the following research questions are defined:

1. What is the reliability of the available input data for the HBV model?
2. Which conceptualization of the HBV model gives the most accurate results in the Buyant River basin, given the specific permafrost conditions of this basin?
3. What are potential changes in river discharge downstream at the Buyant River under different climate scenarios?

Based upon the simulations of the discharges in the Buyant River for present and future conditions, a better understanding of the hydrological processes in the basin can be obtained. Combining the climate change scenarios and the HBV model results enables an assessment of climate change impacts and related uncertainties. These uncertainties sources are mainly derived from the performance of the HBV model and the differences in climate changes scenarios. The uncertainty in the HBV model performance is assumed to be represented by the difference between observed and simulated discharges. The uncertainties of the climate change are taken into account by using different emission scenarios and different Global Circulation Models (GCMs). Mean monthly projected discharges for different climate scenarios will be simulated for the Buyant River. Based on these discharges, predictions can be made about the water availability of the Buyant River basin for future scenarios.

1.4 Thesis outline

In chapter 2, the catchment characteristics in the Buyant River basin are described. The general structure of the HBV model and the permafrost routine are outlined in chapter 3. The availability, quality and preparation of the data input for the HBV model will be discussed in chapter 4. This chapter will answer the first research question. The methodology including the HBV conceptualizations and the climate change scenarios are outlined in chapter 5. The results of the most appropriate HBV conceptualization are presented in chapter 6, and thus the second research question will be answered. Applying the climate change scenarios in this HBV conceptualization, results in potential changes in river discharges and research question 3 will be answered. In chapter 7, conclusions of this study and recommendations for further research are outlined.

2. THE BUYANT RIVER BASIN

2.1 Location and topography

The Buyant River basin is located in Western Mongolia and squeezed between Russia, Kazakhstan, China and the Mongol heartland (Figure 1). The Buyant River drains to the Khovd River near its delta and is an essential part of the larger Mongolian river basin Khovd-Khar Us Nuur.

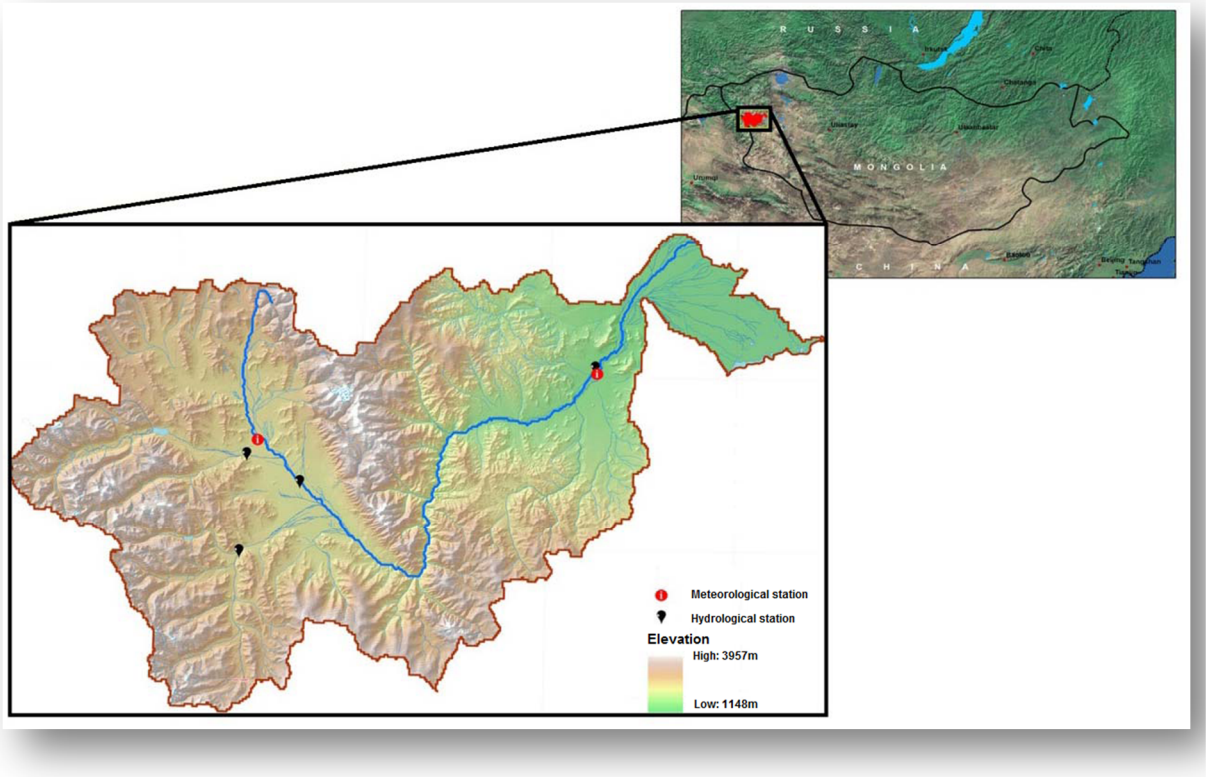

Figure 1 Location of the Buyant River basin in Mongolia (IMHE Mongolia, 2012)

The Buyant River basin drains an area of approximately 8370km². The Buyant River basin is mostly dominated by mountainous with steep slopes. The elevation of the Buyant River catchment ranges from 1148m till 3957m. The end of the Khokh Serkh mountain range is stretched from North to South-Eastwards in the middle region of the basin, see Figure 1.

2.2 Climate

In and around the Buyant River basin meteorological stations are located; these stations measure precipitation and temperature. The spatial distribution of the meteorological stations is shown in Figure 2. The meteorological stations Deluun and Khovd are located within the basin and the meteorological stations Duut and Khovd soum are located outside the boundaries of the catchment. Local temperature and precipitation data are only available for the Deluun and Khovd meteorological stations, beginning in 1993 and 1961 respectively. These meteorological stations are run by the Institute of Meteorology, Hydrology and Environment (IMHE) Mongolia. Both meteorological stations are located in a valley, thus no meteorological measurements are taken at high altitudes in the Buyant River basin. Data for the meteorological stations Khovd Soum and Duut Soum are not considered in this thesis.

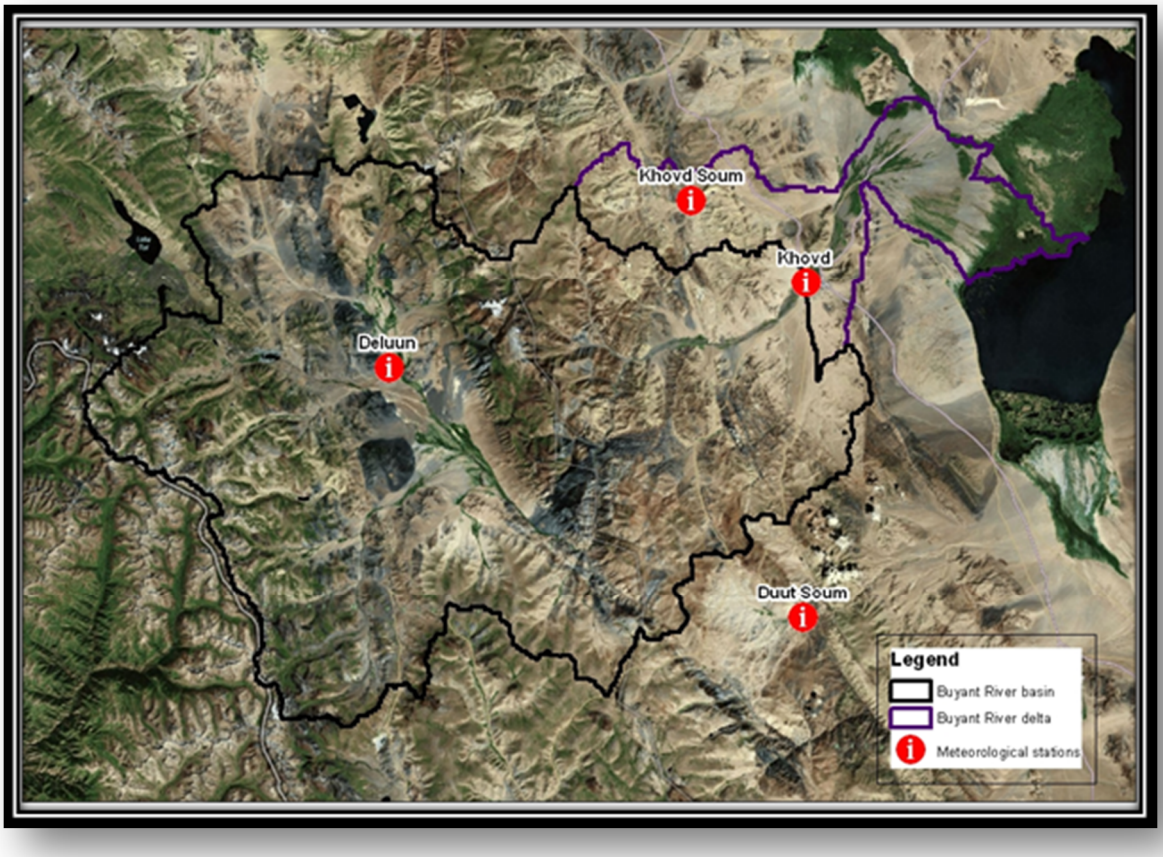

Figure 2 The spatial distribution of the meteorological stations in the Buyant River basin (IMHE Mongolia, 2012)

The annual mean temperatures vary from -2 to -6°C in the mountainous range, and from -3 to -1°C in the lower area of the Buyant River basin, see Figure 3. The highs and lows for Khovd and Deluun reach 20 °C and 15 °C in the summer, and drop to about -23 °C and -21 °C in the winter. The absolute maximum temperature is recorded at 37.6°C at meteorological station Khovd, and the absolute minimum temperature is recorded at -46.6°C at the same location.

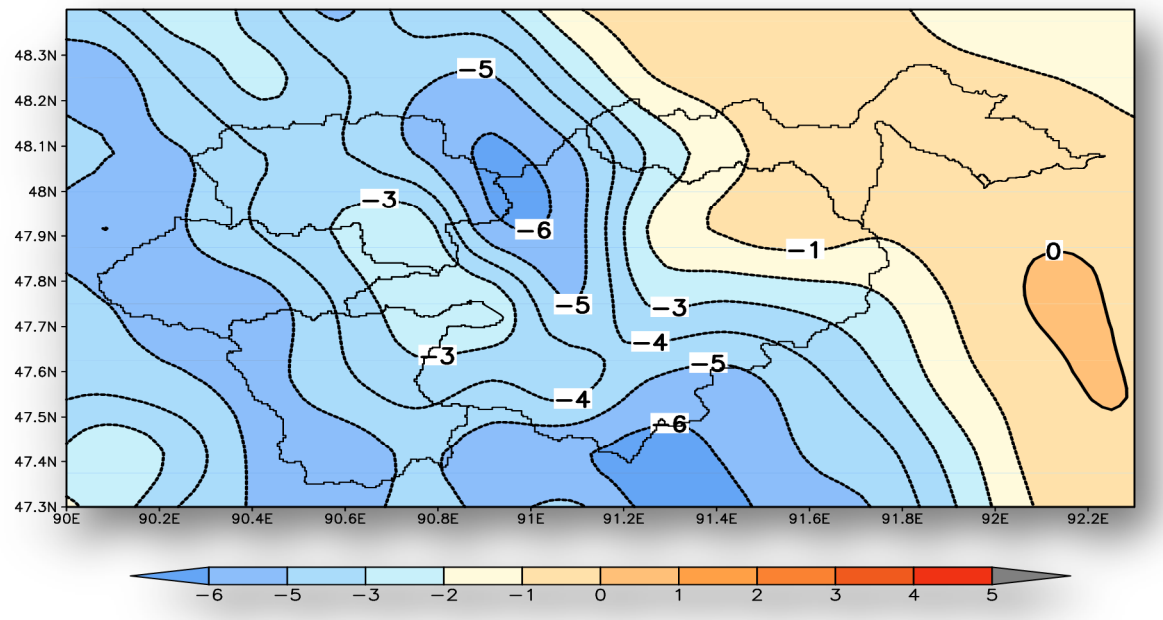

Figure 3 Mean annual temperature in the Buyant River basin (IMHE Mongolia, 2012)

Precipitation is higher in the mountain region than it is at lower altitudes in the Buyant River basin, see Figure 4. It varies from 200 to 240mm at the high altitudes and less than 100mm in the low land region. The majority of the total precipitation occurs during the months May till September. The daily maximum precipitation is observed at meteorological Khovd station, which recorded 37.8mm.

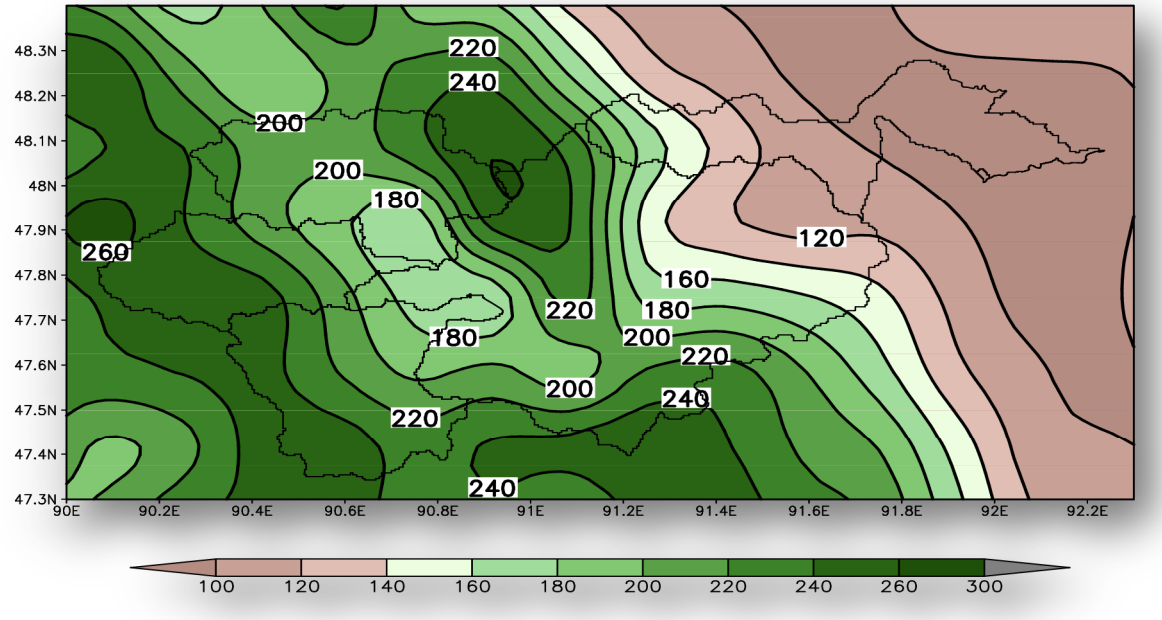

Figure 4 Mean annual precipitation in the Buyant River basin (IMHE Mongolia, 2012)

2.3 Hydrology

The Buyant River starts at 3500m above sea level from the Takhilt Mountain, and has a total length of 172km. The river passes Deluun and drains via a gorge in the mountain range to its delta near the city Khovd, see Figure 5. In the upper part of the basin two main tributaries drain into the Buyant River; the Chigertei River and the Gansmod River. Both tributaries contain river gauging stations, also near Deluun and Khovd river gauging stations are located, all run by the IMHE Mongolia.

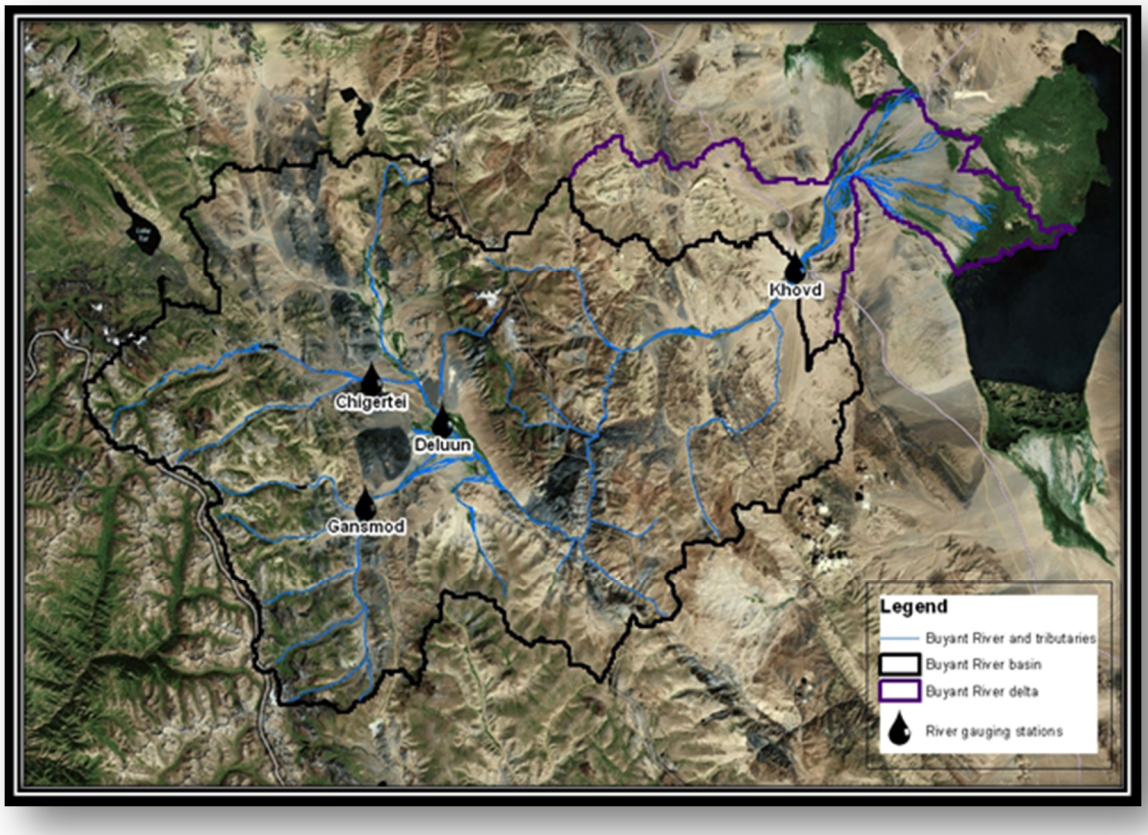

Figure 5 The spatial distribution of the river gauging stations in the Buyant River basin (IMHE Mongolia, 2012)

2.4 Permafrost

Mongolia is a country predominated by high and middle height mountains with a continental climate, which promote occurrence and development of permafrost [*Sharkhuu et al.*, 2007]. Permafrost is ground, soil or rock and included ice and organic material, that remains at or below 0 °C for at least two consecutive years [*Sharkhuu et al.*, 2007]. Permafrost terrain consists of an active layer at the surface that freezes and thaws each year, underlain by perennially frozen ground, see Figure 6. The top of permafrost is at the base of this active layer [*Osterkamp et al.*, 2009]. Due to climate fluctuation or change, some permafrost regions may develop an unfrozen layer between the active layer and the permafrost layer, this is called talik [*Sharkhuu et al.*, 2007]. Talik occurs because the ground that thawed in summer does not completely refreeze in winter.

The seasonally frozen ground in the Buyant River basin has a major impact on the water regime of the Buyant River. Due to the melting of ice and snow, discharges increase in summer time, while the freezing of water results in low to zero flow in winter time. Since permafrost is a thermal condition, it is potentially sensitive to climate change and human activities [*Sharkhuu et al.*, 2007]. A changing climate can alter the water regime of the Buyant River basin and therefore change the future water supply for the inhabitants of the basin. Near the meteorological stations Khovd and Deluun soil temperature measurements are taken from the active layer. The mean monthly soil temperature is nearly the same at both meteorological stations. In general, the top of the soil layer starts freezing at the end of October and begins melting in the middle of April.
For pragmatic reasons, reference in this thesis to permafrost conditions also include processes occurring within the active layer.

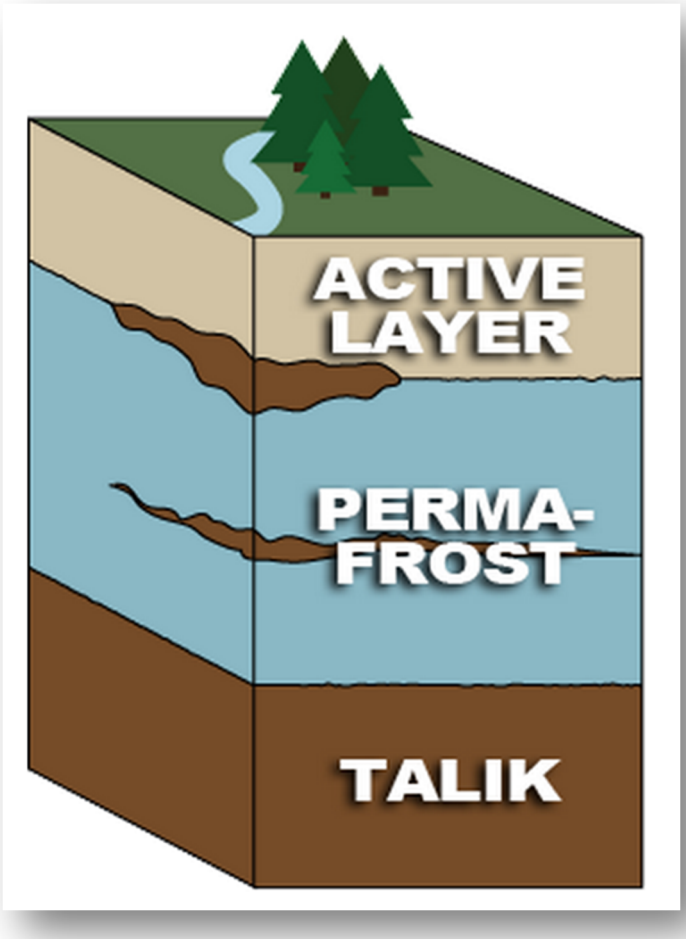

Figure 6 Idealized permafrost cross section (© Weather Underground).

3. HBV MODEL

3.1 General description

The HBV model is a conceptual model that simulates daily discharge using daily rainfall and temperature, and daily or monthly estimates of potential evapotranspiration as input [*Lindström et al.*, 1997]. The HBV model is a semi-distributed conceptual hydrological model. An important aspect of conceptual models is that although model parameters may have a physical meaning, they cannot be measured directly [*Liden and Harlin*, 2000]. Therefore, their values need to be obtained by means of model calibration. The model consists of subroutines for meteorological interpolation, evapotranspiration estimation, snow accumulation and melt, a soil moisture accounting procedure, routines for runoff generation, a transformation and routing routine [*Lindström et al.*, 1997].
The model structure of HBV is presented schematically in Figure 7. The figure only shows the most important characteristics of the model, a more detailed description of the HBV model is given by *Lindström et al.* [1997] and in Appendix A: HBV model. A list of symbols and their description is given at page 43.

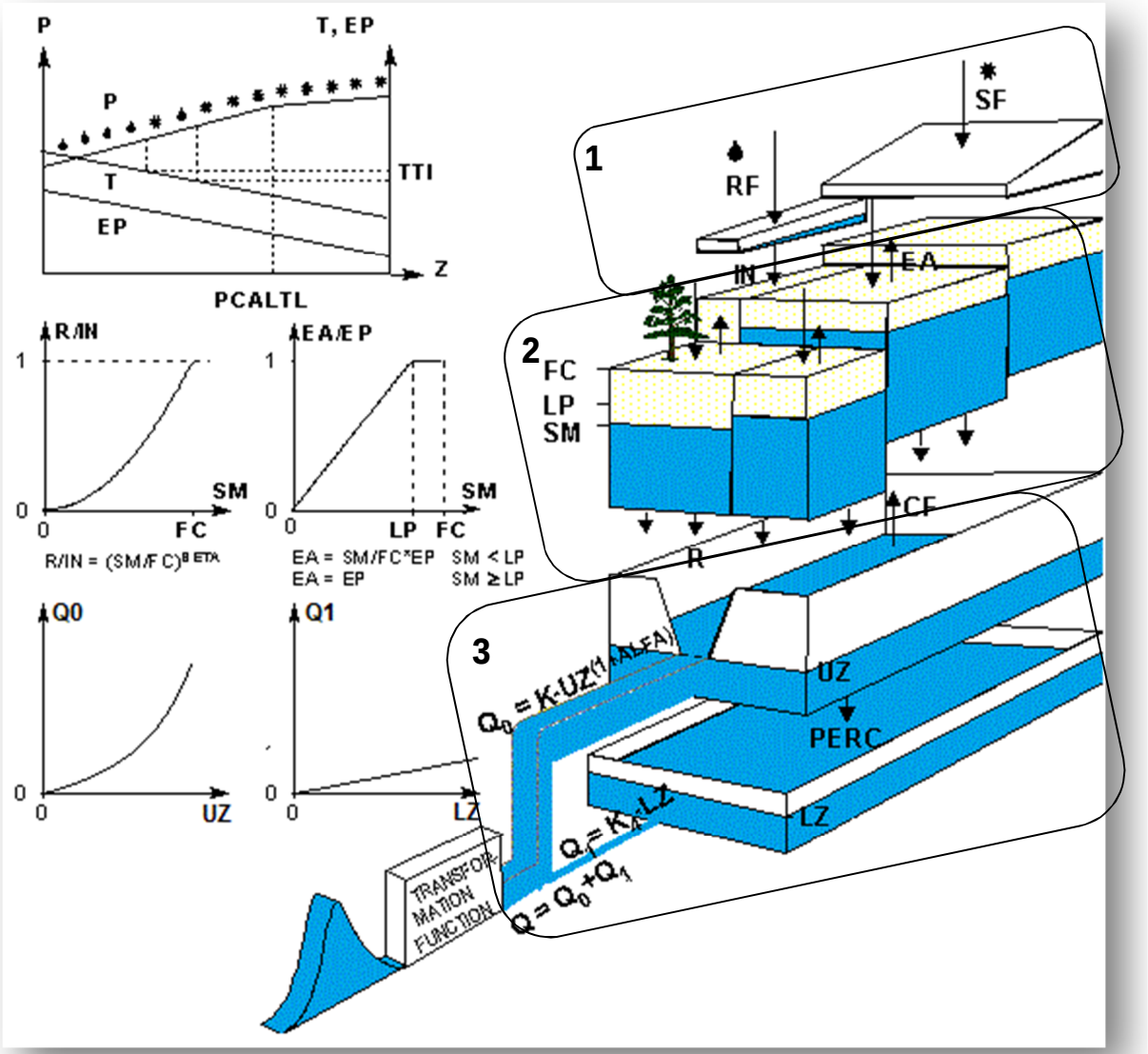

Figure 7 Schematic structure of the HBV-96 model [Lindström et al., 1997]

The in and output of water in the snowmelt routine is indicated by box 1 in Figure 7, the in and output of water in the soil and evapotranspiration routine is indicated by box 2 and the in and output of water in the response routines is indicated by box 3.

3.2 Mass balances

The overall water balance for the HBV model is as follows:

$$P(t) - EA(t) - Q(t) = \frac{d}{dt}[SSP(t) + SWC(t) + SSM(t) + SUZ(t) + SLZ(t)] \quad [3\text{- }1]$$

Where *P [mm/d]* is the daily precipitation, *EA [mm/d]* is the daily actual evapotranspiration and *Q [mm/d]* is the daily discharge, *SSP [mm]* is the daily storage of snow, *SWC [mm]* is the daily storage of water in the snow pack, *SSM [mm]* the storage of soil moisture, *SUZ [mm]* the storage of water in the upper zone and *SLZ [mm]* the storage of water in the lower zone. For every day, *t*, the water balance is solved, i.e. the difference between the daily input and output of water should be equal to the change in storage of water.

If the limit of water capacity in the snow pack is exceeded, excess of rain and melt water in the snow routine will infiltrate in the soil. However, If the snowpack is completely vanished, rain and melt water will infiltrate directly in the soil. The mass balances for snow and melt are given by:

$$SSP(t + \Delta t) = SSP(t) + SF(t) + REFR(t) - MELT(t) \quad [3\text{- }2]$$

$$SWC(t + \Delta t) = SWC(t) + RF(t) - REFR(t) + MELT(t) - IN(t) \quad [3\text{- }3]$$

Where *SF [mm/d]* is the daily snowfall, *REFR [mm/d]* is the daily freezing of water in the snow pack, *MELT [mm/d]* is the daily melting of snow or ice and *IN [mm/d]* is the excess of water from the snow routine infiltrating in the soil and evapotranspiration routine.

Actual evapotranspiration and recharge to the response routine reduce the amount of water in the soil, which is supplied with infiltration from the snow routine and capillary flow from the response box. The mass balance for the soil and evapotranspiration moisture storage box is given by:

$$SSM(t + \Delta t) = SSM(t) + IN(t) - R(t) + CF(t) - EA(t) \quad [3\text{- }4]$$

Where *R [mm/d]* is the direct and indirect recharge of water from the soil and evapotranspiration routine to the upper response box, *CF [mm/d]* is the daily freezing of water in the snow pack, *MELT [mm/d]* is the daily melting of snow or ice and *IN [mm/d]* is the excess of water from the snow routine infiltrating in the soil and evapotranspiration routine.

Direct and indirect recharge from the soil and evapotranspiration routine are the suppliers of water for the upper response box. Outflow of the upper response box is the capillary flow to the soil and evapotranspiration routine, percolation to the lower response box and direct runoff. The percolation to the lower response box has a maximum rate determined by the parameter *PERC*.

The mass balance for the upper response box is given by equation [3- 5], the mass balance for the lower response is given by [3- 6].

$$SUZ(t + \Delta t) = SUZ(t) + R(t) - [Q_0(t) + CF(t) + PERC(t)] \quad [3\text{- }5]$$

$$SLZ(t + \Delta t) = SLZ(t) + PERC(t) - Q_1(t) \quad [3\text{- }6]$$

Where Q_0 *[mm/d]* is the direct runoff from the upper response box, *PERC [mm/d]* is the percolation of water from the upper response box to the lower response box and Q_1 *[mm/d]* is the slow runoff from the lower response box.

3.3 Permafrost conditions

As an alternative to the general structure of the HBV model [*Lindström et al.*, 1997] this study emphasizes the influence of permafrost conditions in the Buyant River basin. Gradually freezing of the soil moisture during the winter period and gradually melting of the soil moisture in spring and summer are adapted in the general structure of the HBV model.
A former study by *Council et al.* [1999] adapted the soil and evapotranspiration routine in the HBV-model in order to account for the thawing and freezing of the active layer. In the *Council et al.* [1999] study the field capacity of the soil varies with the date in permafrost conditions. These adjustments in the soil and evapotranspiration routine gave very satisfying results for river basins in permafrost areas [*Council et al.*, 1999].
This study, however, simulate permafrost conditions by adding freezing and melt functions and storage of ice to each of the three routines indicated by box 2 and 3 in Figure 7. The added permafrost conditions are based on the snowmelt routine in the general structure of the HBV model [*Lindström et al.*, 1997]. Melt in the soil takes place according to a temperature lapse rate, this process starts when soil temperature is above the temperature limit for melting, *TTM [°C],* according to a simple degree-day expression, *CFMAX [mm/°C/d].* The same accounts for freezing of water in the soil, when the temperature decreases below the temperature limit for melting, this water in the soil freezes gradually according to a coefficient, *CFR [-].* The temperature for a daily time step, *t*, determines whether solid water is melting or liquid water is freezing. The bottom line is that when the observed soil temperature is below a certain threshold temperature, groundwater gradually freezes. If the soil temperature is above this threshold temperature, the soil will gradually thaw and groundwater is released into the basin and will contribute to the discharge of the Buyant River. The corresponding equations for the freezing are as follows:

$$ISM(t + \Delta t) = ISM(t) + [CFR \cdot CFMAX \cdot SSM(t)] \quad [3\text{- }7]$$

$$IUZ(t + \Delta t) = IUZ(t) + [CFR \cdot CFMAX \cdot SUZ(t)] \quad [3\text{- }8]$$

$$ILZ(t + \Delta t) = ILZ(t) + [CFR \cdot CFMAX \cdot SLZ(t)] \quad [3\text{- }9]$$

Where *ISM [mm]* represent the ice content in the storage of soil moisture, *IUZ [mm]* the ice content in the upper zone and *ILZ [mm]* the ice content of the lower zone in the response box. These equations are applied when the soil temperature is below the temperature limit for melting, *TTM*. The freezing of water in the three boxes is determined by the same soil temperature and applied in the same conceptual way for all boxes.

As soon as the soil temperature is above the *TTM*, ice in the soil gradually starts melting and the following equations are applied:

$$ISM(t + \Delta t) = max(ISM(t) - [CFMAX \cdot ISM(t)], 0) \quad [3\text{- }10]$$

$$IUZ(t + \Delta t) = max(IUZ(t) - [CFMAX \cdot IUZ(t)], 0) \quad [3\text{- }11]$$

$$ILZ(t + \Delta t) = max(ILZ(t) - [CFMAX \cdot ILZ(t)], 0) \quad [3\text{- }12]$$

The interaction between freezing of water and melting of ice in the soil and evapotranspiration routine is shown in Figure 8. The blue colored boxes indicate the storage of water, whereas the grey boxes represent the ice volume. In the winter months the water in the soil gradually freezes and become ice, and in the summer ice in the soil melts and the storage of water increases. The right-hand added box prevents that water is flowing out of the model, and thus cannot contribute to the discharges in the summer period.

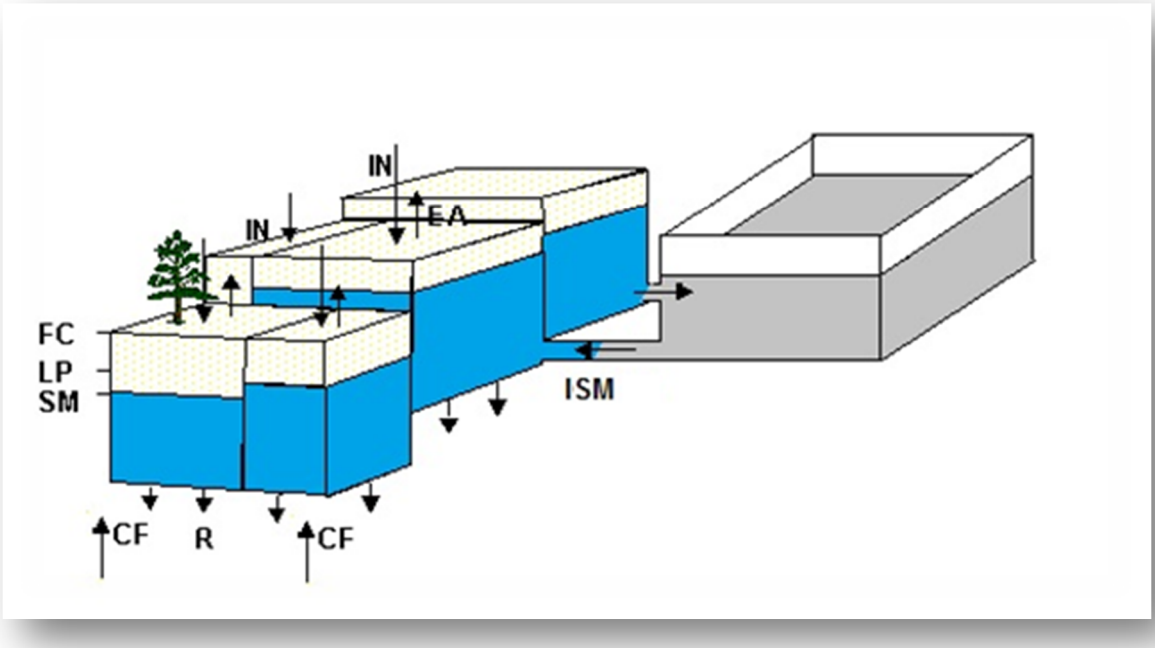

Figure 8 The inflow of freezing water (blue) and outflow of melted ice (grey) in the soil and evapotranspiration routine.

The new situation can be seen as additional storage of water during the winter period. In reality the water stays in the soil and evapotranspiration box. But to avoid complex calculations, soil water is distributed to the right-handed box were it becomes ice. When the temperature is above the temperature limit for melting, the ice content melts and the left boxes are refilled with water. Simulated discharges will increase when the soil temperature is above the temperature limit for melting, because more water is available to generate outflow of the HBV model.

The interaction between freezing and melting in the response routine is depicted in Figure 9. The filling of the right-handed boxes of ice not only prevents generating outflow of the HBV model, but also reduces or stops the simulated capillary flow (*CF*), percolation (*PERC*) and recharge (*R*) between the three boxes. The storage of ground water in the grey boxes results in low to zero outflow of the HBV model when the soil temperatures are below the temperature limit for melting.

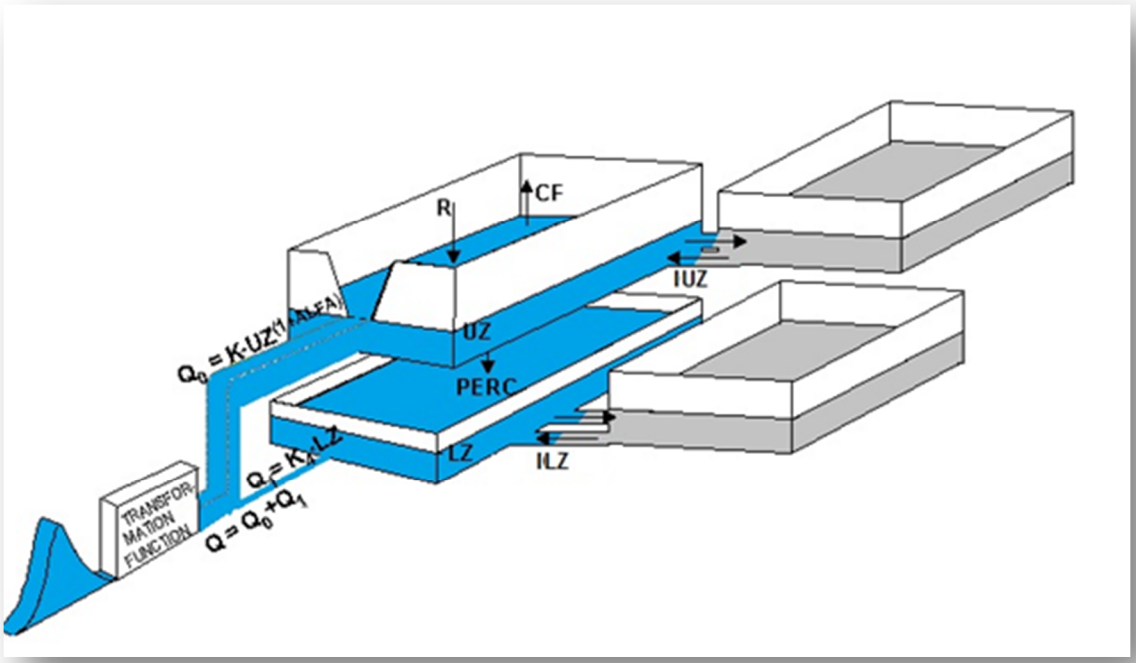

Figure 9 The inflow of freezing water (blue) and outflow of melted ice (grey) for the upper and lower response box.

The storage of water for the three boxes also change the water balances:

$$SSM(t+1) = SSM(t) + IN(t) + CF(t) - [R(t) + EA(t)] - [ISM(t+1) - ISM(t)] \quad [3\text{-}13]$$

$$SUZ(t+1) = SUZ(t) + R(t) - [PERC(t) + CF(t) + Q_0(t)] - [IUZ(t+1) - IUZ(t)] \quad [3\text{-}14]$$

$$SLZ(t+1) = SLZ(t) + PERC(t) - Q_1(t) - [ILZ(t+1) - ILZ(t)] \quad [3\text{-}15]$$

The permafrost conditions, added to the general HBV model structure of *Lindström et al.* [1997], might result in modeled discharges which have a good agreement with the observed discharges in the Buyant River basin, i.e. predicting high flows in the summer months and low to no-flow in the winter period.

4. MODEL INPUT

4.1 Available data

4.1.1 Meteorological data

As described in paragraph 2.2 two meteorological stations are located in the Buyant River basin; these stations measure precipitation, air temperature, soil temperature, wind speed and humidity. The meteorological station Deluun is located in the upper part of the Buyant River basin, where the meteorological station Khovd is located downstream near the delta of the Buyant River, see Figure 2. The periods of measured data are outlined in Table 1.

Table 1 Recorded data at the two meteorological stations in the Buyant River basin (IMHE Mongolia)

Meteorological station	*Precipitation*	*Temperature*		*Wind speed*	*Humidity*
		Air	Soil		
Khovd	1961-2010	1961-2010	1980-2010	1999-2011	1993-2011
Deluun	1993-2010	1993-2010	1987-2010	1999-2011	1999-2011

Automatic weather stations (AWS), shown in Figure 10 and Figure 11, measure the meteorological data in the Buyant River basin. The reliability of AWS has improved over the last two decades, so that measurements formally made manually at reference meteorological stations can be obtained at a higher frequency with data logged sensors [*Shaw et al.*, 2011]. The temperature, wind speed and humidity instruments are wired to data loggers, where the measurements for precipitation are manually recorded twice a day.

Precipitation data for the meteorological stations Khovd and Deluun are complete for the given data period. The meteorological station Khovd misses one year of average temperature data; the year 1998. However, maxima and minima temperature values are available for this year. In the year 1990 no average temperature is recorded for the month February and in 1995 recorded temperature values are missing for October, also for these months maxima and minima are available. Meteorological station Deluun also misses daily average temperature data in the month July of the year 1995, no minima and maxima are available for this month. The data for the soil temperature, wind speed and humidity are complete over the given periods shown in Table 1.

Figure 10 Meteorological station Khovd (IMHE Mongolia, 2011)

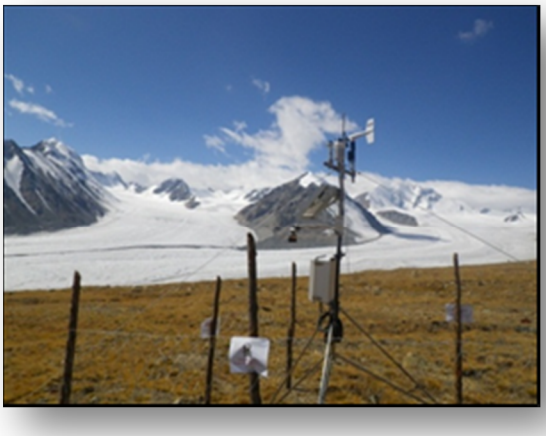

Figure 11 Meteorological station Deluun (IMHE Mongolia, 2010)

4.1.2 Hydrological data

In the Buyant River basin four river gauging points are located. At these gauging points water levels are measured. One is located in the Chigertei tributary, one in the Buyant River near Deluun, one in Gantsmod tributary and one in the Buyant River near the city Khovd, see Figure 5.
The river gauging point near Khovd contains 43 years of water level data, the gauging point near Deluun and Gantsmod contain both 36 years of water level data. The river gauging point at Chigertei contains 3 years of data before a period starts where no water levels were measured. Measurements restarted in 2003 for the Chigertei gauging point, see Table 2.

Table 2 Periods of waterlevel data for the four river gauging stations (IMHE Mongolia)

River gauging points	*Latitude [°]*	*Longitude [°]*	*Data period*
Khovd	91. 37	48.00	1967-2009
Deluun	90.50	47.47	1974-2009
Gantsmod	90.41	47.39	1974-2009
Chigertei	90.41	45.50	1988-1990, 2003-2009

Missing water level data at both the gauging points Khovd and Deluun are mostly during the winter months. The gauging point at Deluun misses water level data for the entire year 1982. The availability of water level data for the gauging point at Gantsmod is complete from 1986 till 2009. At the gauging point in the Chigertei tributary water level data for the first 3 years are not complete, only during summer all daily water levels are listed. The same accounts for the years 2003 till 2009, except for the year 2004.

The discharge is determined by the measured water level and the use of a calibrated stage-discharge rating curve. The water levels are measured by local observers twice a day, based on these water levels the stage is determined, see Figure 12. The stage-discharge relation is derived by an expert at IMHE Mongolia through regular once a month stage-discharge measurements. In order to calculate the discharges, flow velocities are determined for three different stages; high, low and intermediate flows. At each river gauging point the cross-sectional area is also determined. All the measured discharges, *Q*, are plotted against the corresponding mean stages, *h*. Once the rating curve is determined, discharges for measured water levels can be determined directly from the rating curve without additional flow velocity measurements.

Figure 12 Local observer measuring the water level in the Chigertei tributary (IMHE Mongolia, 2010)

4.2 Quality of data

4.2.1 Meteorological data

The quality of the meteorological data described in paragraph 4.1.1 has been checked, by plotting data as a function of time. An insight has been quickly gained about outliers, or values that do not appear to be consistent with the rest of the data. Also discontinuities could easily be determined. Next to the visual inspection of the meteorological data, annual sums of precipitation and the annual means of the temperature data have been determined. The data analysis report of the Buyant River basin can be found in Appendix B: Data Analysis Report.

The quality of meteorological data for the first three years (1995-1998) of the station Deluun is highly questionable. Besides, wind speed and humidity data recordings started in the year 1999 for both meteorological stations. Based upon the quality and the availability of the meteorological data the period 1999 until 2010 has been selected for the input data for the HBV model.

Next to the observed precipitation and temperature data, potential evapotranspiration is the third input variable for the HBV model. A large number of empirical methods have been developed over the last 50 years to estimate the potential evapotranspiration [*Zotarelli et al.*, 2010]. Of these methods the well-known Penman-Monteith equation has been selected, because it can estimate the evapotranspiration accurately and the climatic input variables [*Chen et al.*, 2005] for the equation are available for the Buyant River basin. The Penman-Monteith method combines both energy and mass balances to model the potential evapotranspiration and it is based on fundamental physical principles, which guarantee the universal validity of the method [*Chen et al.*, 2005].
The potential evapotranspiration was calculated using Penman-Monteith as proposed by the FAO in *Allen and Pruitt* [1988]. The potential evapotranspiration is calculated using the observed minimum and maximum temperature and the observed wind speed for the meteorological stations Deluun and Khovd. The incoming solar radiations were provided by the Prediction of Worldwide Energy Resource Project and were obtained from the NASA Langley Research Center Atmospheric Sciences Data Center. By filling in the latitude, longitude and altitude from the two meteorological stations, the amount of electromagnetic energy (solar radiation) incident on the surface of the earth was obtained. More can be found in Appendix C: PET calculations and projections.

4.2.2 Hydrological data

Also the quality of the hydrological data described in paragraph 4.1.2 has been analyzed in the report attached in Appendix B. Outcomes of this report show that the discharge data for the Gantsmod, Chigertei and Deluun sub-basins are highly questionable. Only the discharge data for Khovd are considered reliable. The river gauging point near Khovd is located downstream of the Buyant River, all streams have their outflow through this point.
Due to the quality and availability of the meteorological data the same periods should be selected for the output of the HBV model, namely 1999-2010. However, the available discharge data ends at the year 2009 for the river gauging point near Khovd. This means that discharges can be predicted for the year 2010, but validating of the model conceptualization for this year is not possible.

During the summer months the stage-discharge relation is used to determine the discharges for the river gauging point near Khovd. In general, the stage-discharge relation is applied during the 1st of April till the 1st of November, see Figure 13. In winter streams in the Buyant River basin freeze up due to the low air temperatures, resulting in zero discharges in these months.
Conditions in natural rivers are rarely stable over a period and thus the stage-discharge relationships were checked regularly by experts from the IMHE Mongolia. This also means that rating curves, shown in Figure 13, are not similar for each year, but changing in time.
For discharges higher than 5m³/s the rating curves show reasonable stage-discharge relations for the 11 years of data at the river gauging point Khovd. However, for discharges lower than 5m³/s the years 2001, 2002 and 2006 show unrealistic relations: at higher waterlevels lower discharges are determined. This should be taken into account during the calibration results of the HBV model conceptualizations.

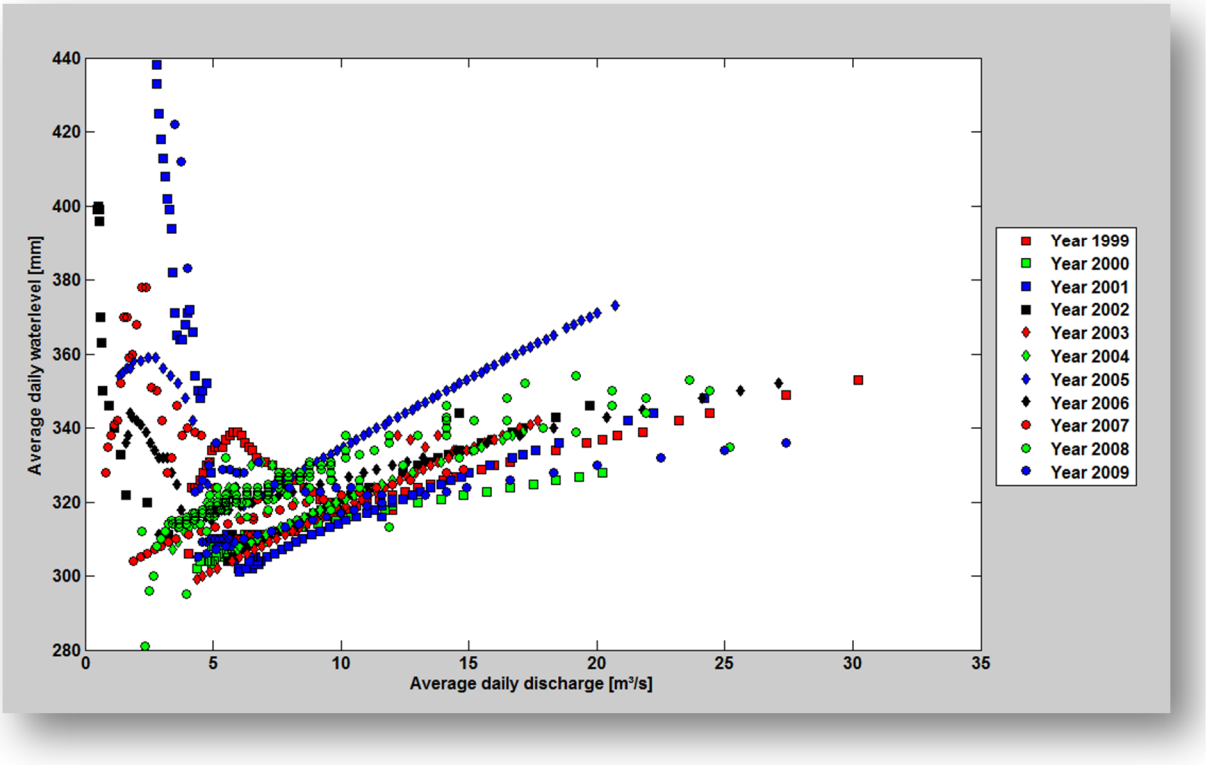

Figure 13 Rating curves showing the stage-discharge relation during the summer period (1st of April till the 1st of November) for the river gauging station Khovd

4.3 Data preparation

4.3.1 Elevation zones

The observed data at the meteorological stations Khovd and Deluun rely on point gauge measurements. For each input variable (precipitation, temperature, potential evapotranspiration) average time series should be calculated from the data of various stations [*Lindström et al.*, 1997]. Because the stations are on a different altitude, the input values need to be corrected to a mean altitude before calculating the areal average over the basin. Due to the lack of meteorological stations in the Buyant River basin two different strategies are applied to determine the areal data input for the HBV model; a single elevation zone and multiple elevation zones.

4.3.1.1 Single elevation zone

The single elevation zone is the simplest strategy in which the mean altitude of the basin is evenly distributed over the entire basin. In this strategy the areal precipitation, temperature and potential evapotranspiration are averaged and corrected for altitude for the Buyant River basin. The recorded data at the meteorological stations Khovd and Deluun are corrected to the mean elevation of the Buyant River basin. Default values for the altitude gradients are derived from *Lindström et al.* [1997]. The correction factors for the air temperature and soil temperature are considered equal in this study, both derived from equation [4- 2]. The corrected data series for precipitation, *P [mm/d]*, temperature, *T [°C/d]*, and potential evapotranspiration, *EP [mm/d]*, are given by:

$$P(t) = p(t) \cdot \{1 + PCALT(z) \cdot [Z(m) - Z_{ref}(m)]\} \quad [4\text{- }1]$$

$$T(t) = t(t) - TCALT(z) \cdot [Z(m) - Z_{ref}(m)] \quad [4\text{- }2]$$

$$EP(t) = ep(t) \cdot \{1 - ECALT(z) \cdot [Z(m) - Z_{ref}(m)]\} \quad [4\text{- }3]$$

Where *p [mm/d]* is the observed daily precipitation at the meteorological station, *PCALT [-]* is the altitude gradient for precipitation, *t [°C/d]* is the observed daily temperature at the meteorological station, *TCALT [-]* the temperature gradient, *ep [mm/d]* is the calculated daily potential evapotranspiration at the meteorological station and *ECALT [-]* is the potential evapotranspiration gradient. With these values the areal input data can be corrected to the mean elevation of the Buyant River basin. The altitude of the meteorological stations Khovd and Deluun is represented by Z_{ref} *[m].* The mean altitude for the Buyant River basin is indicated by *Z [m],* also shown in Table 3.

The mean altitude of the Buyant River basin is above the altitude for both the Khovd and Deluun meteorological station, thus correction results in higher values for the precipitation, lower values for temperature and lower values for potential evapotranspiration for both stations. The difference between the mean elevation height of the Buyant River basin and the elevation of the meteorological station is higher for Khovd situation than for Deluun meteorological station, thus factors for the correction for altitude for the input derived from the meteorological station Khovd are higher than those for the Deluun meteorological station.

The corrected input variables for both meteorological stations are hereafter weighted by the fractions, w_i, of the catchment area represented by the gauges, so-called Thiessen coefficients [*Shaw et al.*, 2011]. This results in average daily values for the input data of the single elevation zone conceptualizations in the Buyant River basin.

Table 3 Altitude for the meteorological stations Deluun and Khovd, the mean altitude of the Buyant River basin and the weight factors determined by Thiessen polygons

Meteorological station	Z_{ref} *[m]*	Z *[m]*	w_i *[-]*
Deluun	2160	2543	0.76
Khovd	1405	2543	0.24

4.3.1.2 Multiple elevation zones

In the mountainous Buyant River basins, the input values for the single elevation zone conceptualizations represent conditions at the mean elevation of the basin. In reality, however, conditions at mountaintop and valley locations will be much different. Such processes as local snowpack accumulation and melting cannot be studied accurately with the single elevation zone conceptualizations. This study also examines the input of multiple elevation zones in the Buyant River basin, in order to take the spatial variability of rainfall and snowfall in to account.

The standard version of the model [*Lindström et al.*, 1997] was applied using multiple elevation zones of equal vertical extent. The areas of nine elevation zones are calculated from a digital elevation model (DEM), which was intersected in ArcGIS. An input file containing the percentage of the area for each elevation zone in the Buyant River basin was created. For the model computations, the mean elevations for each of the nine elevation zones were used. The mean altitude of each elevation zone and the area as percentage of the entire Buyant River basin are shown in Figure 14.

The steps described for the single elevation zone are applied for each of the nine elevation zones, resulting in nine corrected data series for a single input variable. This also means that nine different water balances are drawn; one water balance for each elevation zone. These average daily values are applied for the input data of the multiple elevation zone conceptualizations in the Buyant River basin.

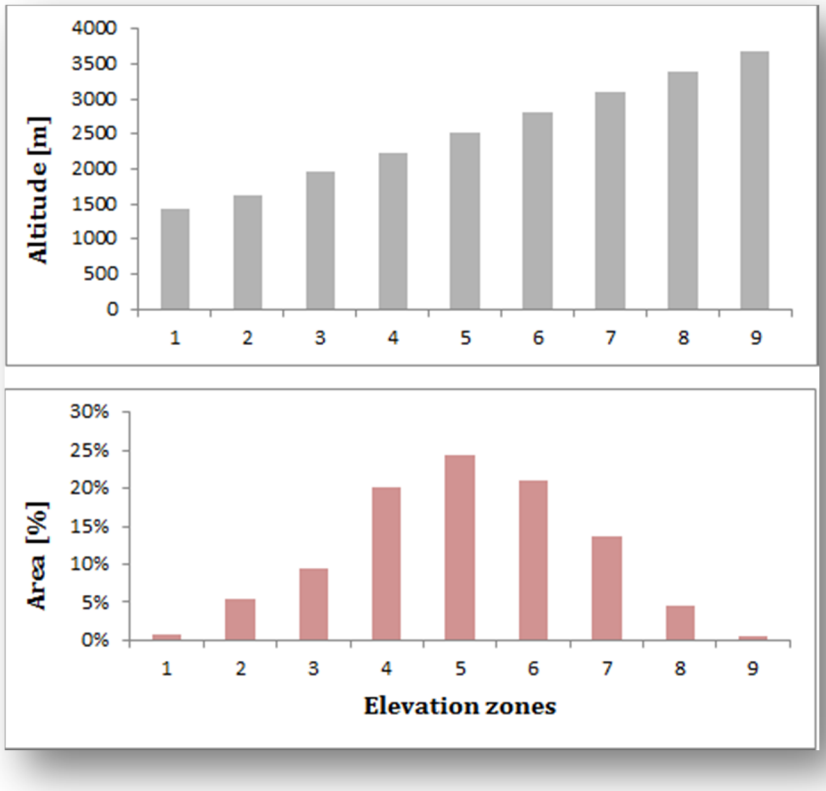

Figure 14 The mean altitude for each elevation zone and the percentage of area from the Buyant River basin for each elevation zones

4.4 Climate change

In principle, using the direct output of climate models is desirable because these results represent a physically consistent picture of future climate, including changes in climate variability and the occurrence of such various weather phenomena as extreme events [*Chiew et al.*, 2010]. In practice, this is rarely done because of simulation biases and the coarse spatial resolution of typical global simulations [*Andreasson et al.*, 2003].

The Buyant River basin drains an area of approximately 8300km², which equals a scale of 90km by 90km. GCMs provide information at a resolution (250-300km) that is too coarse to be used directly into the input values of the HBV model for the Buyant River basin. Several methods exist for developing regional GCM-based scenarios at the sub-grid scale of a river basin, a procedure also known as downscaling [*Chiew et al.*, 2010].

However, even when these corrections are applied, the projections, i.e. the future changes in the climate parameters, differ considerably from model to model. It is therefore, for impact assessment, recommended always to use an ensemble of models [*Andreasson et al.*, 2003]. The main source of uncertainty for regional climate change scenarios is also associated with different emission scenario projections from different GCMs [*Chiew et al.*, 2010]. Projections on climate change should be carried out using different GCMs assuming different emission scenarios.

The HadCM3, Hadley Centre Coupled Model from the UK, climate model represents the Mongolia climate best according to a study by *MARCC* [2009]. This study examined the performances of 12 GCMs related to the representation of temperature and precipitation for the current climate in Mongolia. Among the other models that showed good scores were the ECHAM5-CM model from the Max Planck institute in Germany; the CM2.0 model from the Geophysical Fluid Dynamics Laboratory (GFDL) from the USA and the CGCM2.3.2 from the Magnetic Resonance Imaging Institute (MRI) in Japan.
Next to these four GCMs, three greenhouse gas (GHG) scenarios, A2, A1B and B1, have been selected based on global socio-economic future trends [MARCC, 2009]. The output of 11 climate change scenarios were downscaled by experts of the IMHE Mongolia into the Buyant River basin to a 0.5 degree grid, using a bias correction downscaling method [Wood et al., 2004]. The ECHAM5-CM B1 climate change scenario could not be obtained from IMHE Mongolia, hence the output of 11 climate change scenarios are used. A total of 8 grid points are located in the vicinity of the Buyant River basin, each of these grid points contain monthly projections of temperature and precipitation for the period 2080-2100. The monthly increase/decrease for the precipitation and temperature is determined by the summation of the monthly projections times the fraction of the catchment area represented by each grid points.
The climate model output is used to determine future change in climate with respect to the model's present-day climate, by an absolute difference for temperature and a percentage change for precipitation. The absolute increase/decrease of monthly mean temperature over the period 2080-2100 is listed in Table 4 for the 11 climate change scenarios. All 11 climate change scenarios predict an increase of the monthly mean temperatures in the Buyant River basin for the period 2080-2100.

Table 4 Projections of the absolute difference in the monthly mean temperature for the Buyant River basin derived from 11 climate change scenarios for the period 2080-2100.

Climate change scenario	***Jan***	***Feb***	***Mar***	***Apr***	***May***	***Jun***	***Jul***	***Aug***	***Sep***	***Oct***	***Nov***	***Dec***
GFDL-USA A2	5.33	4.84	7.54	4.60	5.13	4.20	4.43	5.96	5.93	4.42	4.79	4.25
GFDL-USA A1B	2.47	5.85	5.37	6.00	4.44	4.52	5.63	5.71	5.27	4.59	4.90	2.92
GFDL-USA B1	1.75	4.54	4.26	2.69	3.71	3.49	2.87	3.99	3.38	2.82	2.17	2.10
HadCM3-UK A2	3.51	3.86	5.78	3.91	3.09	4.52	6.13	4.75	5.27	3.72	6.26	3.81
HadCM3-UK A1B	1.72	1.02	1.22	1.38	1.29	1.04	0.97	0.93	0.75	0.93	1.65	1.67
HadCM3-UK B1	3.45	3.24	4.30	4.10	2.79	3.20	4.23	3.83	2.84	2.50	4.06	2.43
MRICGCM-Japan A2	4.40	2.88	3.43	1.73	2.50	2.00	2.41	4.11	3.58	3.05	4.34	4.76
MRICGCM-Japan A1B	3.25	3.44	2.50	1.04	1.77	1.90	2.70	3.94	3.60	2.53	4.54	3.90
MRICGCM-Japan B1	3.59	2.62	2.92	1.96	2.16	1.98	1.70	3.44	4.03	3.21	3.63	3.91
ECHAM5-Germany A2	5.86	6.50	8.02	4.46	4.87	5.13	5.58	6.06	5.18	4.92	5.62	5.74
ECHAM5-Germany A1B	6.59	6.41	6.81	2.83	3.95	4.63	5.70	5.24	4.39	5.27	5.14	5.95
ECHAM5-Germany B1	NA	NA	NA	NA	NA	NA	NA	NA	NA	NA	NA	NA

Projections of the change in monthly mean precipitation derived from the 11 climate change scenarios for the period 2080-2100 are listed in Table 5. The percentage change in monthly mean precipitation is shown by its factor, values higher than 1 result in an increase and values below 1 in a decrease. For the months January till May all climate scenarios project an increase in the monthly mean precipitation, except for the ECHAM5-Germany A2 scenario which predicts a small decrease in the monthly mean precipitation for the month March. In the months June until September, a large variability in predicted precipitation change exists. In the month October both the GFDL-USA as the MRICGCM-Japan models predicts an increase in the monthly mean precipitation, whereas the HadCM3-UK A1B and B1 scenarios and the ECHAM5-Germany A1B scenario predict a decrease of the monthly mean precipitation in the month October. In the months November and December all climate change scenarios predict an increase in the monthly mean precipitation.

Table 5 Projections of the change in monthly mean precipitation for the Buyant River basin derived from 11 climate change scenarios for the period 2080-2100.

Scenario	***Jan***	***Feb***	***Mar***	***Apr***	***May***	***Jun***	***Jul***	***Aug***	***Sep***	***Oct***	***Nov***	***Dec***
GFDL-USA A2	1.30	1.63	1.61	1.26	1.28	0.93	0.68	0.31	0.52	1.37	1.38	1.25
GFDL-USA A1B	1.16	1.65	1.52	1.30	1.15	0.85	0.42	0.50	0.67	1.04	1.22	1.06
GFDL-USA B1	1.13	1.81	2.03	1.61	1.43	1.08	1.13	0.79	1.01	1.64	1.39	1.15
HadCM3-UK A2	1.94	1.52	1.33	1.29	1.13	1.02	1.00	0.86	0.81	1.08	1.65	1.62
HadCM3-UK A1B	1.72	1.02	1.22	1.38	1.29	1.04	0.97	0.93	0.75	0.93	1.65	1.67
HadCM3-UK B1	1.38	1.16	1.42	1.15	1.22	0.99	0.97	1.05	0.84	0.92	1.22	1.40
MRICGCM-Japan A2	1.42	1.37	1.15	1.31	1.51	1.24	1.05	0.99	0.91	1.52	1.85	1.77
MRICGCM-Japan A1B	1.38	1.48	1.43	1.36	1.39	1.11	0.81	1.01	1.07	1.10	1.46	1.41
MRICGCM-Japan B1	1.09	1.53	1.20	1.33	1.34	1.21	1.38	1.16	0.71	1.28	1.45	1.66
ECHAM5-Germany A2	1.48	1.44	0.99	1.03	1.08	0.78	0.49	0.37	0.70	1.27	1.20	1.75
ECHAM5-Germany A1B	1.84	1.55	1.18	1.46	1.02	1.02	0.60	0.53	1.19	0.94	1.02	1.32
ECHAM5-Germany B1	NA	NA	NA	NA	NA	NA	NA	NA	NA	NA	NA	NA

Variability in the change for temperature is smaller than the variability for the change in precipitation. An increase in temperature seem to be significant for all months, where an increase in precipitation seem to be only significant during winter (DJF) and spring (MAM), taking into account the variability in these variables as a result of three different emission scenarios and different output values of the four GCMs.

5. METHODS

5.1 Modeling approach

Four different permafrost conceptualizations are examined within the HBV model. Two conceptualizations take permafrost into account by only calibrating under non-permafrost conditions. The other two conceptualizations incorporate permafrost conditions (PC) which simulate the freezing and melting of ice. Apart from the differences in permafrost conditions accounted for by the model, a distinction is made by a single elevation zone (SEZ) and multiple elevation zones (MEZ).

First the SEZ and MEZ conceptualizations are calibrated to determine parameter sets for both the single elevation zone as for multiple elevation zones. After selecting the most sensitive parameters from both parameter sets, the SEZ and MEZ conceptualizations are recalibrated. The same parameter sets are applied for the calibration of the SEZ-PC and MEZ-PC conceptualizations, with the additional permafrost parameters described in paragraph 3.3. Hereafter, a comparison between the model performances of the four conceptualizations is made, to determine which conceptualization is most appropriate to predict the current climate conditions. The conceptualization which yields best in the validation period is used to simulate the future climate change effects for the Buyant River basin.

5.2 Monte Carlo Analysis

A Monte Carlo Analysis (MCA) is applied for the calibration of the four conceptualizations. The MCA is a technique in which, through numerous model simulations, a best objective function value is sought by using random parameter values within a pre-defined model parameter space [*Booij and Krol*, 2010].
In some cases a typical range of likely parameter values can be given, but it is in general not possible to determine the parameters from physiographic, climatic and soil physical characteristics [*Madsen et al.*, 2002]. In studies by *Lindström et al.* [1997], *Seibert* [1999] and *Liden and Harlin* [2000] sensitivity of parameters is demonstrated and results of these studies are used for selection of model calibration parameters. Thirteen parameters are selected that require optimization while for the remaining model parameters default values are used following *SMHI* [1999]. The high amount of parameters may result in different parameter combinations giving equally good output performances, which is usually labeled as overparameterisation [*Booij*, 2005]. The model parameter ranges are determined by evaluating model parameter ranges applied in former HBV studies [*Akhtar et al.*, 2008; *Booij and Krol*, 2010; *Seibert*, 1999].

5.2.1 Data period

Klemes [1986] proposed a hierarchical scheme for systematic testing of hydrological models. Based on this hierarchical scheme a split-sample test will be applied in this study. For the split-sample test different data periods are used, calibration based on one time period and validation on another period.
The data period is split into a calibration period of (2000-2004) and a validation period of (2005-2009). The year 1999 is considered as a warm-up period, before the calibration is started. In this first year the different boxes in the HBV model can be filled with water generated from the infiltration of snow, ice melt and rainfall.
The calibration and validation years are hereafter equally distributed, both periods contain 5 years of data. This equal length was chosen with the aim to include as much variety in the hydrological regimes as possible.

5.2.2 Objective functions

The goal of the calibration procedure is to adjust the model's parameters to decrease the difference between observed and simulated stream flow values [*Viviroli et al.*, 2009]. In this study the objective of the model calibration is to simulate a good agreement of the shape of the hydrograph and a good water balance.
To examine these objectives the Nash-Sutcliffe coefficient (*NS*) and the relative volume error (*RVE*) are selected [*Madsen et al.*, 2002]. Next to these two criteria the objective function *Y* will be investigated, this criterion is a combination of both the NS and the RVE values [*Akhtar et al.*, 2009]. These three objective functions are described below:

$$NS = 1 - \frac{\sum_{i=1}^{N}[Q_m(i) - Q_o(i) \cdot W(J)]^2}{\sum_{i=1}^{N}[Q_o(i) - \bar{Q}_o]^2} \quad [5\text{-}1]$$

$$RVE = 100 \cdot \frac{\sum_{i=1}^{N}[(Q_m(i) - Q_o(i)) \cdot W(J)]}{\sum_{i=1}^{N} Q_o(i)} \quad [5\text{-}2]$$

$$y = \frac{NS}{1 + |RVE|} \quad [5\text{-}3]$$

Where *i* is the time step, *N* is the total number of time steps, *Q* is the discharge and subscripts '*o*' and '*m*' means observed and modeled. In the numerator of the NS-value and RVE-value, an extra weight, *W,* has been added. This weight factor enables to eliminate differences in the winter months between the modeled and the observed discharges. The winter periods are defined by Julian days, *J*, referring to the day number in a calendar year.
For the calibration of the SEZ and MEZ conceptualizations the weight factor is set to zero, the difference between the observed and modeled discharge is eliminated and will not contribute to the determination of the objective function. In other words, the SEZ and MEZ conceptualizations are calibrated over a period in where non-permafrost conditions occur.
For the calibration of the SEZ-PC and MEZ-PC conceptualizations a weight factor of one is applied. This results in the correct difference between the observed and modeled discharge. Thus, the SEZ-PC and MEZ-PC conceptualizations are calibrated over the entire calibration period.

The *NS* value ranges between -∞ and 1, with higher values indicating a better agreement between observed and modeled values and 1 being a perfect fit [*Nash and Sutcliffe*, 1970]. For a NS value of 0 the model does not perform any better than the mean value of the observed discharges [*Bergström*, 1992]. The Nash-Sutcliffe efficiency is very sensitive to peak flows, at the expense of performance during low flow conditions [*Nash and Sutcliffe*, 1970]. The RVE vary between -∞ and ∞, but performs best when a value of zero is generated.

The objective function *Y*, is a combination of both the NS and the RVE values [*Akhtar et al.*, 2009]. Goal of the calibration is to find a parameter set which describes the peaks during summer time the best. However, the water balance in the Buyant River basin should also be taken into account, thus low flow conditions are equally important. For this reason the performance of the HBV model will be determined using the objective function *Y*, as described by [*Akhtar et al.*, 2009].

5.3 Sensitivity analysis

First optimal parameter sets are examined for the SEZ and MEZ conceptualizations under non-permafrost conditions. A total of 13 model parameters are applied in the MCA for both conceptualizations. To be certain that the entire model parameter space is examined, a sufficient number of runs should be executed [*Booij and Krol*, 2010]. In a former HBV study by *Seibert* [1997] 14 model parameters are calibrated by generating 500,000 parameter sets. [*Shrestha et al.*, 2009] found that statistics for testing convergence were stable after 5,000-10,000 simulations for an HBV model study with nine calibration parameters. Therefore, 500,000 simulations used for the calibration of the SEZ and MEZ conceptualizations can be seen as reasonable.

The weight factor, *W*, eliminates the difference in the winter months between the modeled and the observed discharges, by multiplying the difference with zero. For all other days the difference between the modeled and the observed discharge is multiplied by one.
Both periods are determined using Julian days *(J).* The value for J starts at 1 for the first of January and ends on 365 or 366 on the 31st of December, depending on the leap year once every four years. The weight factor is one from day 91 until day 304 or 92 until 305 for a leap year, which corresponds to the first of April until the last day of October. The stage-discharge relation has been applied in this period by the experts of the IMHE Mongolia, and therefore selected as non-permafrost conditions.

The model parameters calibrated for the SEZ and MEZ conceptualizations are analyzed to identify the most sensitive parameters. The purpose of this sensitivity analysis is to determine which input parameters exert the most influence on the model results [*Hamby*, 1994]. This information allows to eliminate less important parameters and provides direction for recalibration in order to reduce parameter uncertainties and increase the model accuracy [*Hamby*, 1994].
The parameter sensitivity for the SEZ and MEZ models is determined qualitatively by scatterplots of the parameter values versus the objective function *Y* value. Parameter sensitivity depends, not only on the range and distribution of an individual input parameter, but also on those of other parameters to which the model is sensitive [*Hamby*, 1994].

Also a local sensitivity analysis [*Crick et al.*, 1987] has been performed to determine the most sensitive parameters for the SEZ and MEZ conceptualization. The constant values of the parameter are determined by the optimal parameter set obtained from the MCA. A sensitivity ranking is determined by increasing each parameter by a given percentage while leaving all others constant, and quantifying the change in the value of the objective function *Y* value. The most sensitive parameters are compared between the SEZ and MEZ models. In this way the effect of multiple elevation zones can already be determined.

5.4 Calibration of the four conceptualizations

The four most sensitive parameters are selected for the SEZ conceptualization and for the MEZ conceptualization. These sensitive parameters are recalibrated for the SEZ conceptualization and for the MEZ conceptualization, using a MCA of 100,000 simulations, in order to increase the model accuracy. As described in paragraph 3.3 the parameters *CFMAX* and *STCF* play a major role in the permafrost condition routine for the SEZ-PC and MEZ-PC conceptualizations. These two parameters are combined with the four parameters obtained from the sensitivity analysis for the SEZ conceptualization and for the MEZ conceptualization. This results in a total of 6 parameters for the calibration of the SEZ-PC conceptualization and MEZ-PC conceptualization, again using a MCA of 100,000 simulations.
The recalibration for the SEZ and MEZ conceptualizations are applied with a weight factor of zero for the period of permafrost conditions. The calibration for the SEZ-PC and MEZ-PC conceptualizations are performed with a weight factor of one for the entire calibration period.
During the validation a weight factor of one is applied for all four conceptualizations. In this way a comparison can be made between the model performances of the four conceptualizations. The conceptualization which has the highest objective function *Y* value in the validation period, 2005-2009, is selected for the simulation of the climate change scenarios.

5.5 Climate change scenarios

To determine the climate change effects, described in paragraph 4.4, the delta approach method applied in a study by *Akhtar et al.* [2008] is used. This method has been implemented in many hydrological impact studies [*Andreasson et al.*, 2004; *Arnell*, 1998; *Lettenmaier et al.*, 1999; *Middelkoop et al.*, 2001]. Its simplicity makes it possible to rapidly apply the method to a large set of climate change scenarios [*Andreasson et al.*, 2004]. The observed climate time series are adapted from the output of four GCMs with three different emission scenarios, see paragraph 4.4. The delta approach method [*Akhtar et al.*, 2008] makes strong assumptions about the nature of the changes, including a lack of change in variability and spatial patterns of climate [*Buytaert et al.*, 2009]. One highly questionable consequence of this assumption is that the future frequency and magnitude of extreme weather events are the same relative to the mean climate of the future as they are in present- day climate [*Buytaert et al.*, 2009]. Other bias-removal methods have been developed, but none are nearly so widespread, or they are versions of the delta method.

The delta approach method only considers the difference between climate model control simulations and their respective scenario simulations. The hydrological model scenario input is generated from baseline observations [*Akhtar et al.*, 2008] following:

$$T_{f,daily} = T_{o,daily} + \left(\overline{T_{f,monthly}} - \overline{T_{p,monthly}}\right) \quad [5\text{-}4]$$

$$P_{f,daily} = P_{o,daily} \cdot \frac{\overline{P_{f,monthly}}}{\overline{P_{p,monthly}}} \quad [5\text{-}5]$$

$$EP_{f,daily} = EP_{o,daily} \cdot \frac{\overline{EP_{f,monthly}}}{\overline{EP_{p,monthly}}} \quad [5\text{-}6]$$

Where $T_{f,daily}$ *[°C]* is the future daily air/soil temperature, $T_{o,daily}$ *[°C]* is the present daily observed air/soil temperature, $T_{f,monthly}$ *[°C]* is the future monthly mean air/soil temperature, $T_{p,monthly}$ *[°C]* is the present monthly mean air/soil temperature, $P_{f,daily}$ *[mm]* is the future daily precipitation, $P_{o,daily}$ *[mm]* is the present daily observed precipitation, $P_{f,monthly}$ *[mm]* is the future monthly mean precipitation, $P_{p,monthly}$ *[mm]* is the present monthly mean precipitation, $EP_{f,daily}$ *[mm]* is the future daily potential evapotranspiration, $EP_{o,daily}$ *[mm]* is the present daily observed potential evapotranspiration, $EP_{f,monthly}$ *[mm]* is the future monthly mean potential evapotranspiration and $EP_{p,monthly}$ *[mm]* is the present monthly mean potential evapotranspiration.

The output of the 11 climate change scenarios for the period 2080-2100 are projected on the current climate data over the period 1980-2000. The monthly mean temperature and precipitation are shown in Table 4 and Table 5. The projections for the potential evapotranspiration for the period 2080-2100 are shown in Appendix C: PET calculations and projections.

6. RESULTS AND DISCUSSION

6.1 Result sensitivity analysis

Scatterplots are prepared for the SEZ and the MEZ conceptualization to illustrate the calibration results using the objective function *Y* value, see Figure 15 and Figure 16. The calibration results are obtained from the MCA after 500,000 simulations. Figure 15 and Figure 16 only show the results for the 13 model parameters against the objective function *Y* values above zero. From the 13 model parameters, the *ALFA*, *K* and K_4 parameters show optimal values towards their minimum parameter values for both conceptualizations. All other parameters are more evenly distributed over their parameter ranges.

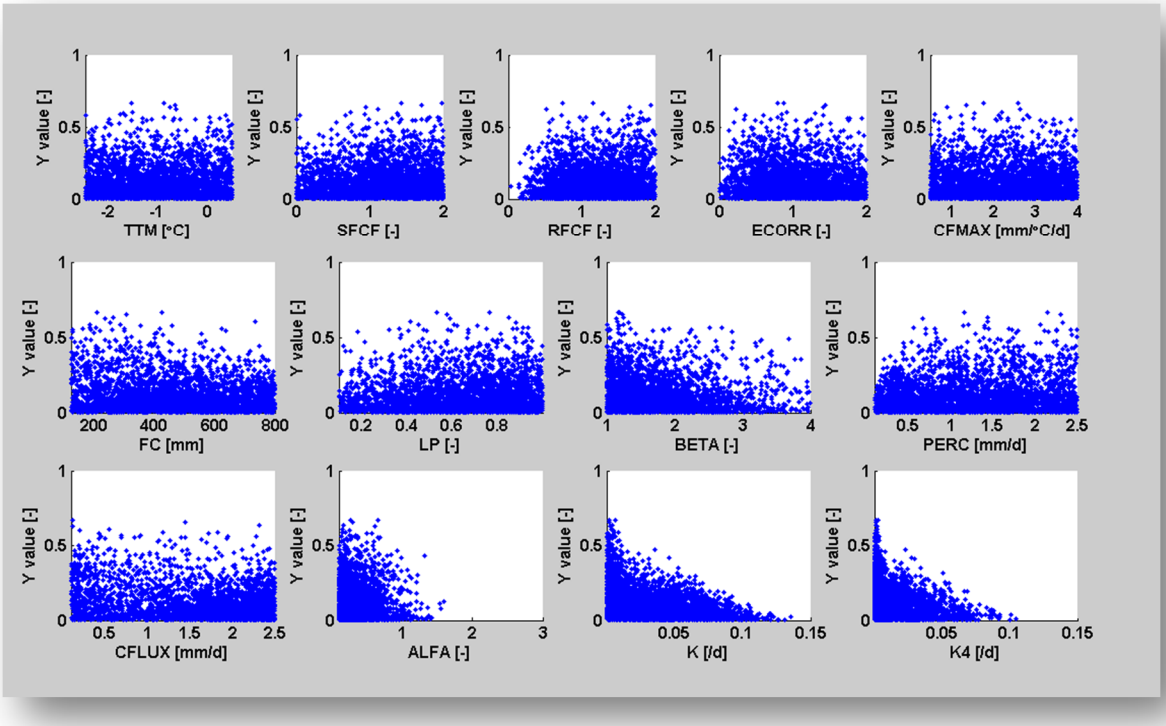

Figure 15 Scatterplots of the 13 model parameters versus the objective function Y value in the SEZ conceptualization after a MCA of 500,000 simulations.

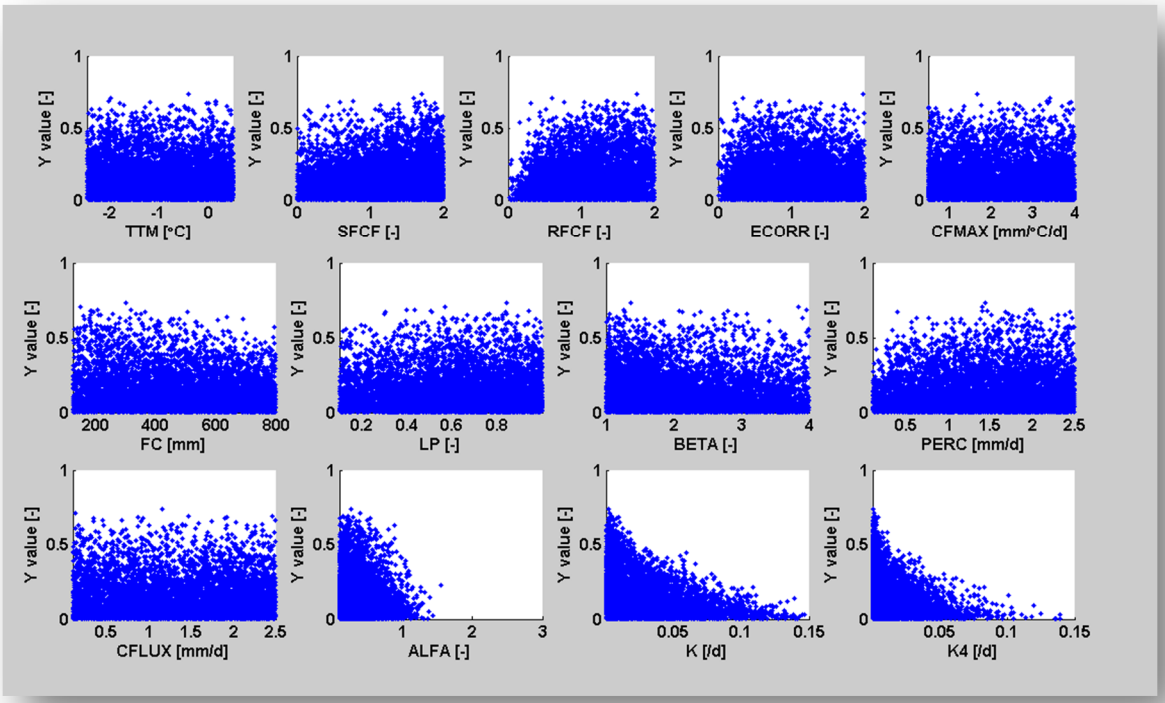

Figure 16 Scatterplots of the 13 model parameters versus the objective function Y value in the MEZ conceptualization after a MCA of 500,000 simulations.

The most sensitive parameters for the SEZ conceptualization are the *LP*, *PERC* and *ALFA* parameters. The most sensitive parameters for the MEZ conceptualization are the *LP*, *BETA* and *ALFA* parameters. Due to the direct relation between the *ALFA* and *K* parameters also *K* should be (re)calibrated for the four conceptualizations.

For the SEZ conceptualization the *LP, PERC, ALFA* and *K* parameters are recalibrated, the values for the other parameters are set to their optimal value obtained after the 500,000 simulations. For the MEZ conceptualization the *LP, BETA, ALFA* and *K* parameters are recalibrated, the values for the other parameters are set to their optimal value obtained after the 500,000 simulations.
For the SEZ-PC conceptualization the *CFMAX*, *LP, PERC, ALFA, K* and *TSCF* parameters are calibrated, the values for the other parameters are set to their optimal value obtained after the 500,000 simulations for the SEZ conceptualization. For the MEZ-PC conceptualization the *CFMAX*, *LP, BETA, ALFA, K* and *TSCF* parameters are calibrated, the values for the other parameters are set to their optimal value obtained after the 500,000 simulations for the MEZ conceptualization. The optimal parameter sets can be found in Appendix D: Calibrated parameter values.

6.2 Model performances

Scatterplots of the recalibrated model parameters for the SEZ and MEZ conceptualizations are shown in Figure 17 and Figure 18. The calibration results are obtained from the MCA after 100,000 simulations. Optimal parameter sets for the SEZ conceptualization are significant better than those for the MEZ conceptualization. The value for the objective function *Y* is 0.682 for the SEZ conceptualization, where the objective function *Y* value is 0.426 for the MEZ conceptualization. Clear optimal values for the *LP* and *K* parameter are obtained for the SEZ conceptualization. The optimal value of the *K* parameter for the MEZ conceptualization is close to its minimum, like the optimal values for the *ALFA* parameter in both conceptualizations. The calibration results for the remaining parameters are evenly distributed over their parameter spaces.

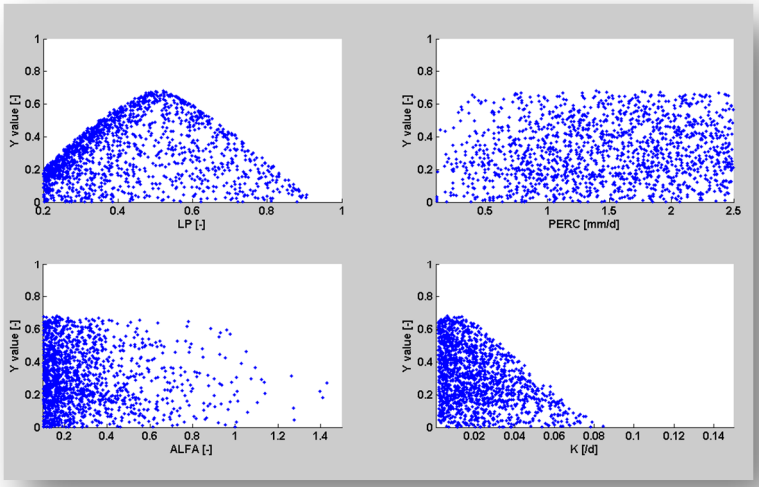

Figure 17 Recalibration results of the model parameters in the SEZ conceptualization after a MCA of 100,000 simulations.

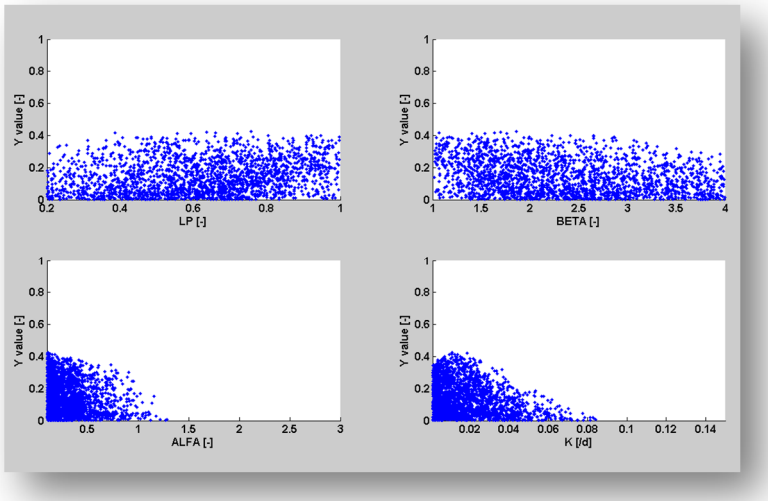

Figure 18 Recalibration results of the model paramters in the MEZ conceptualization after a MCA of 100,000 simulations.

Scatterplots of the calibrated model parameters for the SEZ-PC and MEZ-PC conceptualizations are shown in Figure 19 and Figure 20. The optimal parameter set for the SEZ-PC conceptualization results in an objective function *Y* value of 0.510, while the MEZ-PC conceptualization results in an objective function *Y* value of 0.423. The values of the added parameters *CFMAX* and *TSCF* are evenly distributed over their parameter space for both conceptualizations after the MCA of 100,000 simulations.

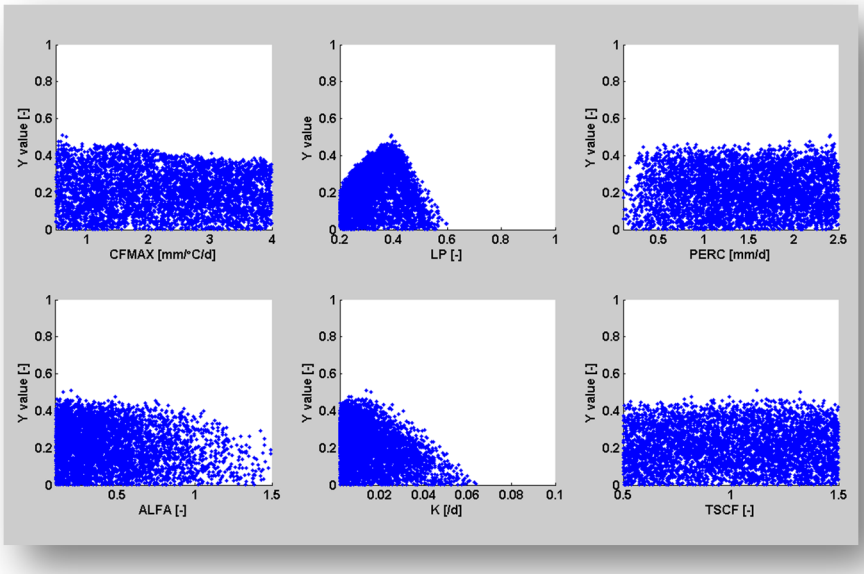

Figure 19 Results of the calibrated model parameters for the SEZ-PC conceptualization after a MCA of 100,000 simulations.

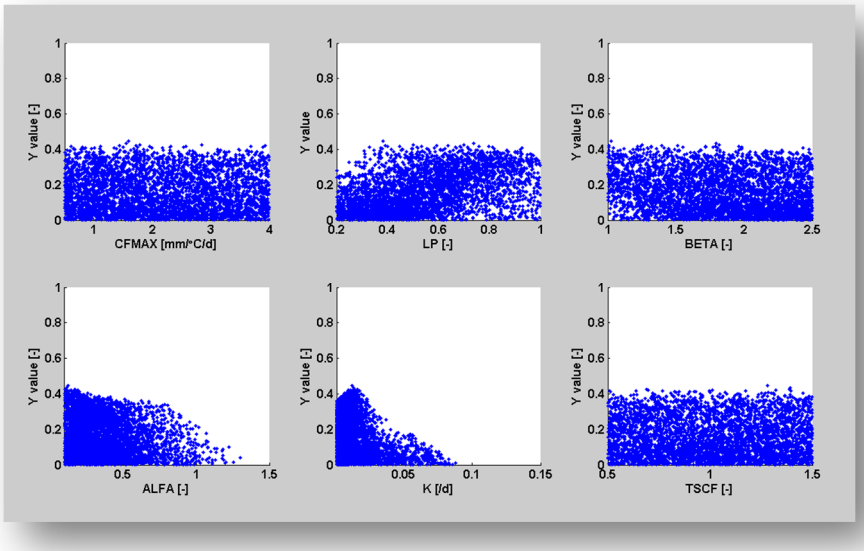

Figure 20 Results of the calibrated model parameters for the MEZ-PC conceptualization after a MCA of 100,000 simulations.

The optimal parameter sets obtained during the calibration are used to validate the four conceptualizations. The model performances for the four conceptualizations are listed in Table 6. The best model performance for the validation period is obtained with the SEZ-PC conceptualization (*Y=0.737*). Both the SEZ-PC and MEZ-PC conceptualizations perform better than the conceptualizations calibrated under non-permafrost conditions. The validated MEZ conceptualization is, however, performing better than the validated SEZ conceptualization, despite the poorer calibration results.

Table 6 Model performances of the four conceptualizations in the validation period (2005-2009).

Conceptualization	*NS (-)*	*|RVE| (%)*	*Y (-)*
SEZ	-0.098	55.8	**-0.063**
MEZ	0.301	17.4	**0.256**
SEZ-PC	0.759	3.00	**0.737**
MEZ-PC	0.438	3.64	**0.321**

The hydrographs for the SEZ and MEZ conceptualizations are shown in Figure 21. The poor model performances of both conceptualizations are mainly caused by the simulation of groundwater flow in winter. Despite the calibration of the SEZ and MEZ conceptualization over the non-permafrost conditions period, groundwater flow is generated during the months when permafrost conditions occur. The lower reservoir in the HBV model continues emptying during winter months and thus generating groundwater flow, represented by the linear red lines Figure 21, resulting in significantly overestimating the discharges in winter. Poor model performances are yielded, while in the validation of the models the weight factor in equations [5- *1*] and [5- *2*] are set to 1, meaning that both conceptualizations are validated over the entire period (2005-2009).

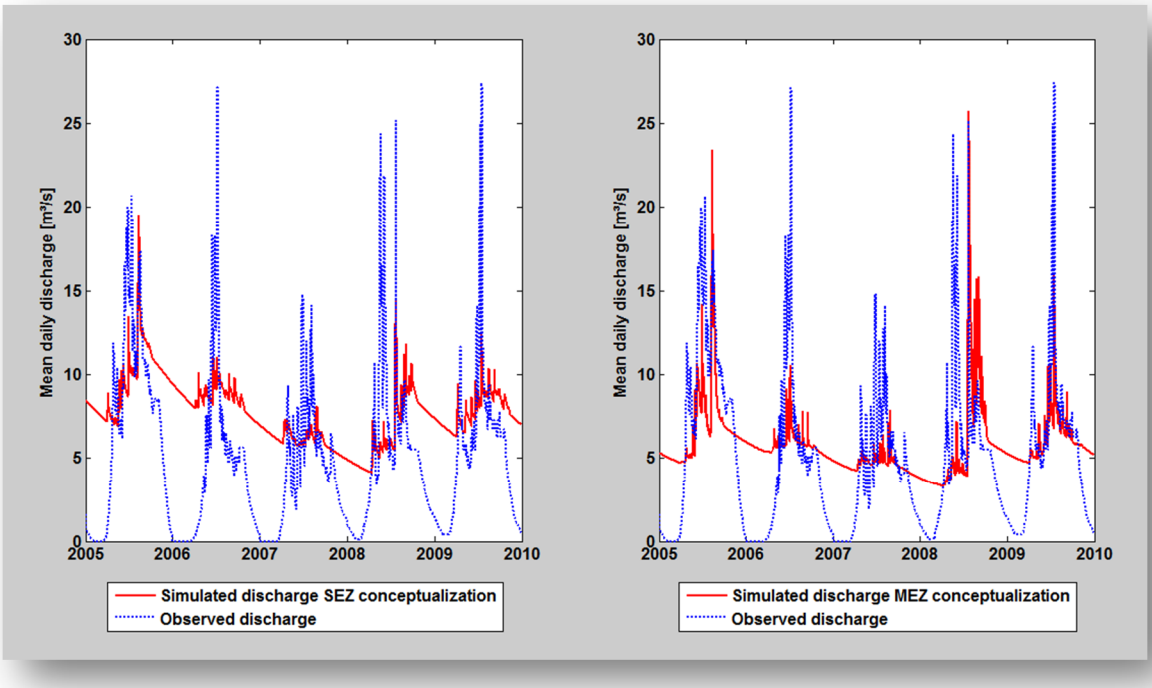

Figure 21 The hydrographs for the SEZ and the MEZ conceptualizations plotted with the observed mean daily discharges at the river gauging point Khovd for the validation period (2005-2009).

The influence of the permafrost conditions are clearly shown in the hydrographs obtained from the SEZ-PC and MEZ-PC conceptualizations; see Figure 22. The storage of frozen soil- and groundwater in the added boxes results in low to zero flow for both model structures during periods where permafrost conditions occur. The quick release of melted groundwater contributes to the discharges in the beginning of April, yielding in moderate model performances in spring. However, the MEZ-PC model is overestimating the low flows and underestimating the peaks in summer time. This may explain the small value for the RVE objective function, because overestimated low flows and underestimated peaks cancel each other out and thus balance the overall agreement between observed and modeled discharges. A small value for the *RVE* objective function also results in a high value for the objective function *Y*.

Yet, the results for the SEZ-PC model are more satisfying in both the objective function *Y* value as in the hydrograph. The conceptualization with a single elevation zone and simulating permafrost conditions by adding freezing and melt functions resulted in a reasonable degree of coherence between the observed and modeled discharges for the validation of the model. This conceptualization is the most appropriate one to simulate the current climate of the Buyant River basin.

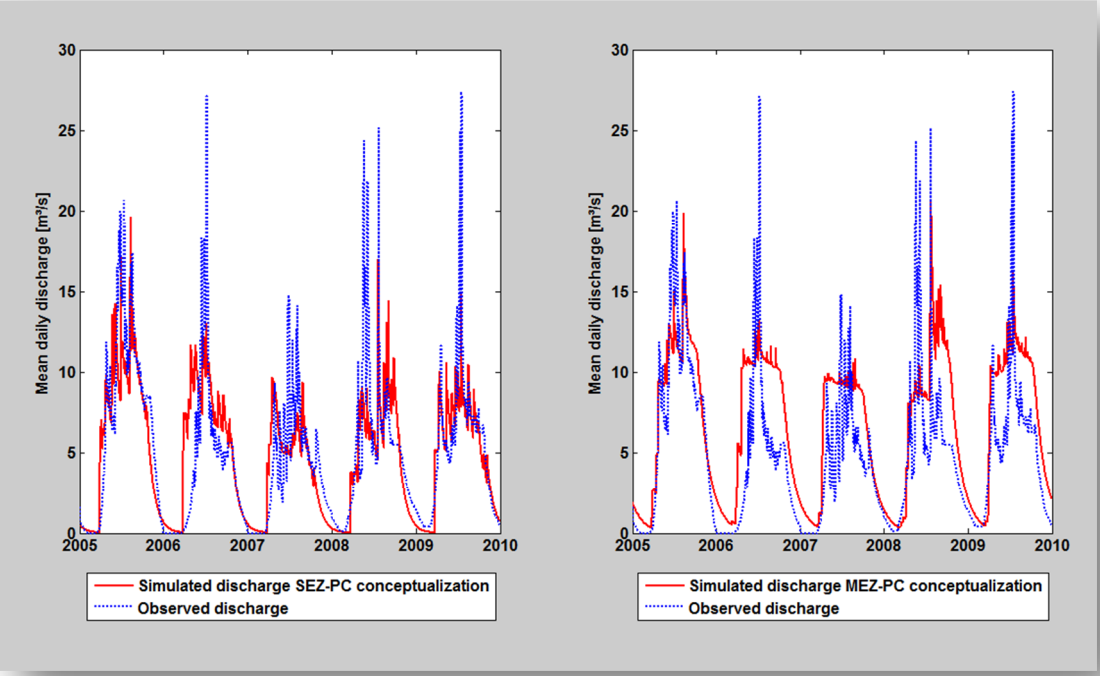

Figure 22 The hydrographs for the SEZ-PC and the MEZ-PC conceptualizations plotted with the observed mean daily discharges at the river gauging point Khovd for the validation period (2005-2009).

6.3 Optimal HBV conceptualization

Model performances have been examined for the SEZ-PC conceptualization for each year in the calibration and validation period, 2000-2009. The yielded yearly model performances for the SEZ-PC conceptualization determined by the three objective functions are listed in Table 7.

Table 7 Yearly model performances for the SEZ-PC conceptualization

	Year	*NS (-)*	*RVE (%)*	*Y (-)*
Calibration	2000	0.578	-19.2	0.485
	2001	0.165	-38.3	0.119
	2002	0.764	-15.6	0.661
	2003	0.766	-11.8	0.685
	2004	0.735	17.8	0.624
Validation	2005	0.867	-11.3	0.779
	2006	0.560	28.5	0.436
	2007	0.623	-6.7	0.584
	2008	0.667	-11.7	0.597
	2009	0.845	-6.1	0.797
	Overall	**0.707**	**-9.44**	**0.646**

The simulation for the year 2001 is poor (*Y=0.119*), the simulated hydrograph is underestimating almost all observed high flows in this year. The poor model performance for the year 2001 can also be assigned to the quality of the discharge data, see paragraph 4.2.2. Stage-discharge relationships showed multiple rating curves for the year 2001, so that it was not clear whether the quality of the discharge is ensured. Quality of the observed discharge data for the year 2006 was also questionable, the poor model performance (*Y=0.436*) for this year should not be weighted so hard.

Yet, in general the SEZ-PC conceptualization shows relatively high yearly values, despite the lack of meteorological input data. Worldwide testing of conceptual models [*Rango*, 1992] has shown that *NS* values higher than 0.8 are above average for runoff modeling in glaciated catchments. Even higher values were obtained in the years 2005 and 2009 with the SEZ-PC conceptualization, *NS* values of *0.867* and *0.845* respectively. The overall model performance of the SEZ-PC conceptualization (*Y=0.646*) is more than satisfying given the lack of input data. The SEZ-PC conceptualization is therefore applied to predict discharges under changed climate conditions for the Buyant River basin.

6.4 Impact climate change on discharge

The delta change method is used to translate the monthly projections for the precipitation, temperature and potential evapotranspiration for the climate change impact assessment. The projected monthly mean discharge for the 11 climate change scenarios are simulated by the SEZ-PC conceptualization and are shown in Figure 23. The four GCMs are separated by different colors, while the three emission scenarios have different marker types. It is evident from Figure 23 that projections of a single GCM are less variable than emission scenarios. The MRICGCM predicts an increase of discharges for the three emission scenarios for all months, except the months August and September for the A1B scenario. During spring the HadCM3 and the B1 emission scenario for the GFDL predict also an increase in discharge. However, projections for the ECHAM5, HadCM3 and GFDL show a decrease of the monthly mean discharges in summer.

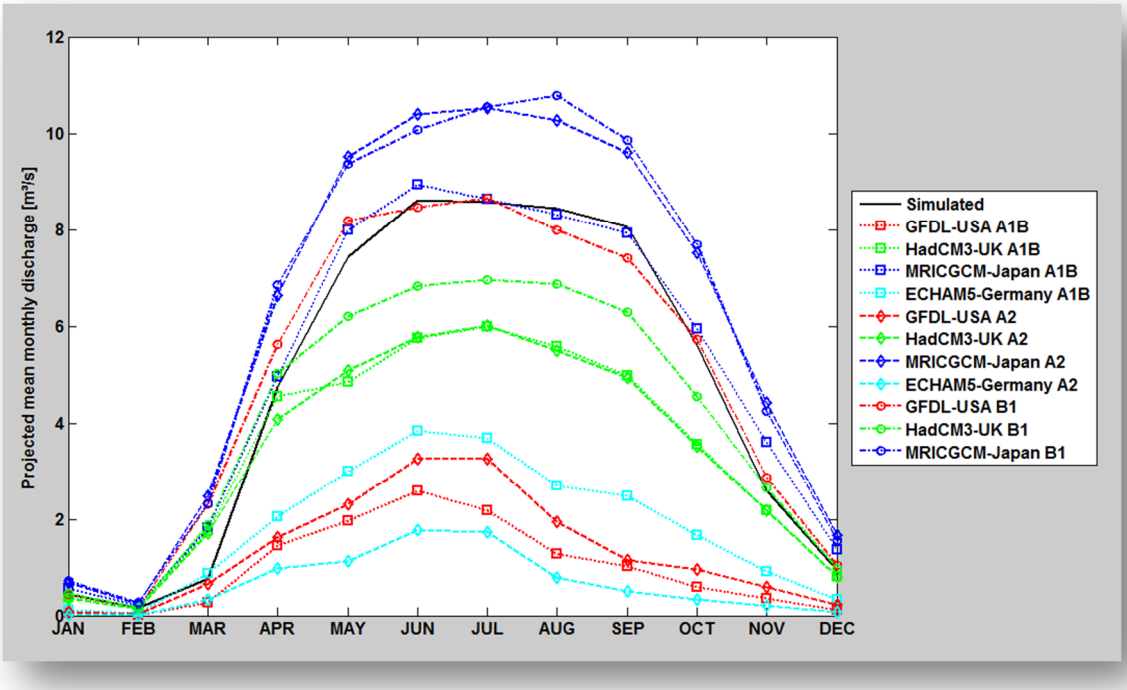

Figure 23 Projected mean monthly discharge for 11 climate change scenarios for the period 2080-2100.

The application of the SEZ-PC conceptualization in the Buyant River basin, indicates that, under the present estimated climate scenarios of global warming for the period 2080-2100, most probably the runoff in the summer will decrease, while the discharge in spring is likely to increase. However, uncertainties in these climate change impacts are rather high, whereas different GCMs are found to be more important than the uncertainty due to different emission scenarios.

7. CONCLUSIONS AND RECOMMENDATIONS

7.1 Conclusions

The HBV model is a conceptual model that simulates discharge using precipitation, temperature and estimates of potential evapotranspiration as input variables. Daily temperature and precipitation data was obtained from two meteorological stations in the Buyant River basin. The potential evapotranspiration has been estimated using the well-known Penman-Monteith equation, because it can estimate the potential evapotranspiration accurately and the climatic input variables for this equation were available for the Buyant River basin. A selection of data has been made according to the periods in which the meteorological data was complete, in order to increase the reliability of the meteorological input data. Despite the scarce number and poor distribution of meteorological stations in the mountainous river basin, the conceptualizations for a single elevation zone were able to simulate the hydrological processes of the Buyant River basin moderately to well.

The conceptualization with a single elevation zone and simulating permafrost conditions by adding freezing and melt functions resulted in a reasonable degree of coherence between the observed and modeled discharges for the calibration and validation of the model. Although the model yielded poor performances for two years, the overall model performance is remarkably high, especially given the lack of meteorological data. Conceptualizations with multiple elevation zones, however, did not yield better model performances compared to the single elevation zone conceptualizations.

The most appropriate conceptualization in the Buyant River basin indicates that, under the present climate scenarios of global warming for the period 2080-2100, the runoff in the summer will most likely decrease, while the discharge in spring is likely to increase. However, uncertainties in future climate change impacts are rather high as the incongruity between GCMs and emission scenarios and between different GCMs cause distinct runoff projections, the former being the cause for yielding low and the latter for high variability. In particular, uncertainties in precipitation account for the large degree of fluctuation in the projections for the future discharges in the Buyant River basin. Whilst the variability in the models and the coarse resolution yield projections that are at best conjecture, future refinement of these models may yield in more accurate and realistic scenarios. It is therefore necessary to carry out a further study of climate change scenarios in order to simulate impacts in the Buyant River basin more accurately.

7.2 Recommendations

The existing meteorological and hydrological stations are few in number in the Buyant River basin and the experimental studies on the hydrological processes are therefore rare in this mountainous river basin. Applying more field observations for the meteorological input data and more observations of precipitation and temperature at different altitudes may help to describe the hydrological processes in mountainous river basins more accurately. This may reduce the uncertainty in the model parameters and result in more optimal parameter values, thus yielding higher model performances for the conceptualizations. In addition, observed temperature and precipitation at higher altitudes may result in better model performances of the multiple elevation zones conceptualizations in the Buyant River basin.

It is difficult to study the impact of climate changes on the runoff of the Buyant River basin, while the uncertainties in the climate change impact are large. The development and implementation of downscaling techniques has an important role to play for further research of climate change in the Buyant River basin. A more refined resolution of this area will provide a better representation of the local climate patterns and processes in the mountainous Buyant River basin. Processes such as local snowpack accumulation and melting cannot be studied accurately on the basis of the resolution implemented in this study. The resolution adopted in this study also limits the accuracy of representation of small-scale processes. A good example of this is precipitation; the use of stochastic rainfall simulators, for instance, may eliminate the use of highly uncertain precipitation forecasts from the current GCM outputs in this study. If the variability of precipitation in the climate change scenarios can be reduced, better projections in future discharges can be drawn.

The most appropriate HBV conceptualization in this study yielded poor model performances for two years in the calibration and validation period. However, the quality of discharge data for these years is highly questionable. A subsequent study should examine the reliability of the stage-discharge relationships for both years. More data about snow and ice cover in the basin may help to model the melting of ice and snow more accurately in the snow and permafrost routine. As a result, the conceptualization should be able to simulate higher discharges, thereby providing for higher degrees of coherence between the observed and modeled discharges. This will improve the model performance of the conceptualizations.

The conceptualizations simulating permafrost conditions by adding a freezing and melting routine has shown significant improvement compared to the general HBV model structure. These conceptualizations should also be applied in similar river basins in western Mongolia or northwest China to determine if the model is applicable as a tool for the simulation and forecasting of hydrological river processes in permafrost areas.

LIST OF SYMBOLS

ALFA	Measure for non-linearity of flow in upper zone box
AWS	Automatic weather stations
BETA	Parameter in soil routine
CFLUX	Maximum value of capillary flux
CFMAX	Degree day factor
CFR	Refreezing factor
CGCM2.3.2	Model from the Magnetic Resonance Imaging Institute in Japan.
DEM	Digital Elevation Model
EA	Actual evapotranspiration
ECALT	Evapotranspiration correction factor for altitude
ECHAM5	Model from the Max Planck institute in Germany
ECORR	Evaporation correction factor
FC	Maximum soil moisture content
GCM	Global Circulation Models
GFDL	Geophysical Fluid Dynamics Laboratory, the USA
HadCM3	Hadley Centre Coupled Model
HBV	Hydrologiska Byråns Vattenbalansavdelning
ILZ	The ice content of the lower zone in the response box
IMHE	Institute of Meteorology, Hydrology and Environment
ISM	The ice content in the storage of soil moisture
IUZ	The ice content in the upper zone and
J	Julian day
K	Recession coefficient for runoff from upper zone box
K4	Recession coefficient for runoff from lower zone box
LP	Limit for potential evapotranspiration
MCA	Monte Carlo Analysis
MEZ	Multiple elevation zones conceptualization
MEZ-PC	Multiple elevation zones conceptualization with permafrost conditions
NS	Nash-Sutcliffe coefficient
P	Precipitation
PCALT	Precipitation correction factor for altitude
PERC	Percolation rate occurring when water is available
Q	Discharge
RF	Rainfall
RFCF	Rainfall correction factor
RVE	Relative Volume Error
SEZ	Single elevation zone conceptualization
SEZ-PC	Single elevation zone conceptualization with permafrost conditions

SF	Snowfall
SFCF	Snowfall correction factor
SLZ	Storage of water in the lower zone
SMHI	Swedish Meteorological and Hydrological Institute
SSM	Storage of soil moisture
SSP	Storage of snow
SUZ	Storage of water in the upper zone
SWC	Storage of water in the snow pack
TCALT	Temperature correction factor for altitude
TSCF	Temperature soil correction factor
TT	Temperature limit for snow/rain
TTI	Temperature interval with a mixture of snow and rain
TTM	Temperature limit for melting
WHC	Water holding capacity

REFERENCES

Akhtar, M., N. Ahmad, and M. J. Booij (2008), The impact of climate change on the water resources of Hindukush-Karakorum-Himalaya region under different glacier coverage scenarios, *J Hydrol*, *355*(1-4), 148-163.

Akhtar, M., N. Ahmad, and M. J. Booij (2009), Use of regional climate model simulations as input for hydrological models for the Hindukush-Karakorum-Himalaya region, *Hydrol Earth Syst Sc*, *13*(7), 1075-1089.

Allen, R. G., and W. O. Pruitt (1988), Rational Use of the Fao Blaney-Criddle Formula - Closure, *J Irrig Drain E-Asce*, *114*(2), 375-380.

Andreasson, J., S. Bergstrom, B. Carlsson, and L. P. Graham (2003), The effect of downscaling techniques on assessing water resources impacts from climate change scenarios, *Water Resources Systems - Water Availability and Global Change*(280), 160-164.

Andreasson, J., S. Bergstrom, B. Carlsson, L. P. Graham, and G. Lindstrom (2004), Hydrological change - Climate change impact simulations for Sweden, *Ambio*, *33*(4-5), 228-234.

Arnell, N. W. (1998), Climate change and water resources in Britain, *Climatic Change*, *39*(1), 83-110.

Bergström, S. (1992), The HBV model - its structure and applications, edited by SMHI.

Booij, M. J. (2005), Impact of climate change on river flooding assessed with different spatial model resolutions, *J Hydrol*, *303*(1-4), 176-198.

Booij, M. J., and M. S. Krol (2010), Balance between calibration objectives in a conceptual hydrological model, *Hydrolog Sci J*, *55*(6), 1017-1032.

Braun, L. N., W. Grabs, and B. Rana (1993), Application of a Conceptual Precipitation-Runoff Model in the Langtang-Khola Basin, Nepal Himalaya, *Iahs-Aish P*(218), 221-237.

Buytaert, W., R. Celleri, and L. Timbe (2009), Predicting climate change impacts on water resources in the tropical Andes: Effects of GCM uncertainty, *Geophys Res Lett*, *36*.

Chen, D., G. Gao, C.-Y. Xu, J. Guo, and G. Ren (2005), Comparison of the Thornthwaite method and pan data with the standard Penman-Monteith estimates of reference evapotranspiration in China, *Clim Res*, *28*, 123-132.

Chiew, F. H. S., D. G. C. Kirono, D. M. Kent, A. J. Frost, S. P. Charles, B. Timbal, K. C. Nguyen, and G. Fu (2010), Comparison of runoff modelled using rainfall from different downscaling methods for historical and future climates, *J Hydrol*, *387*(1-2), 10-23.

Council, N. E. R., I. o. Hydrology, F. M. INSTITUTE., F. E. Institute, SINTEF-NHL., and U. O. COPENHAGEN (1999), *LAPP: Land Arctic Physical Processes contract No. ENV4-CT95-0093.Final report for the period 1st April 1996 to 31st March 1999*, NERC.

Crick, M. J., J. Brown, Z. Hussain, and A. Walmsley (1987), Identification of Important Parameters in Urban Dose Assessment, *Radiat Prot Dosim*, *21*(1-3), 181-188.

Hagg, W., L. N. Braun, M. Kuhn, and T. I. Nesgaard (2007), Modelling of hydrological response to climate change in glacierized Central Asian catchments, *J Hydrol*, *332*(1-2), 40-53.

Hamby, D. M. (1994), A Review of Techniques for Parameter Sensitivity Analysis of Environmental-Models, *Environ Monit Assess*, *32*(2), 135-154.

IPCC-TGICA (2007), General Guidelines on the Use of Scenario Data for Climate Impact and Adaptation Assessment*Rep.*, 66 pp, Prepared by T.R. Carter on behalf of the Intergovernmental Panel on Climate Change, Task Group on Data and Scenario Support for Impact and Climate Assessment.

Kang, G. D. Cheng, Y. C. Lan, and H. J. Jin (1999), A model for simulating the response of runoff from the mountainous watersheds of inland river basins in the arid area of northwest China to climatic changes, *Sci China Ser D*, *42*, 52-63.

Klemes, V. (1986), Operational Testing of Hydrological Simulation-Models, *Hydrolog Sci J*, *31*(1), 13-24.

Konz, M., S. Uhlenbrook, L. Braun, A. Shrestha, and S. Demuth (2007), Implementation of a process-based catchment model in a poorly gauged, highly glacierized Himalayan headwater, *Hydrol Earth Syst Sc*, *11*(4), 1323-1339.

Lettenmaier, D. P., A. W. Wood, R. N. Palmer, E. F. Wood, and E. Z. Stakhiv (1999), Water resources implications of global warming: A US regional perspective, *Climatic Change*, *43*(3), 537-579.

Liden, R., and J. Harlin (2000), Analysis of conceptual rainfall-runoff modelling performance in different climates, *J Hydrol*, *238*(3-4), 231-247.

Lindström, G., B. Johansson, M. Persson, M. Gardelin, and S. Bergstrom (1997), Development and test of the distributed HBV-96 hydrological model, *J Hydrol*, *201*(1-4), 272-288.

Madsen, H., G. Wilson, and H. C. Ammentorp (2002), Comparison of different automated strategies for calibration of rainfall-runoff models, *J Hydrol*, *261*(1–4), 48-59.

MARCC (2009), Mongolia Assessment Report on Climate Change 2009*Rep.*, Ministry of Environment, Nature and Tourism, Mongolia.

Middelkoop, H., K. Daamen, D. Gellens, W. Grabs, J. C. J. Kwadijk, H. Lang, B. W. A. H. Parmet, B. Schadler, J. Schulla, and K. Wilke (2001), Impact of climate change on hydrological regimes and water resources management in the rhine basin, *Climatic Change*, *49*(1-2), 105-128.

Moore, R. D. (1993), Application of a Conceptual Streamflow Model in a Glacierized Drainage-Basin, *J Hydrol*, *150*(1), 151-168.

Nash, J. E., and J. V. Sutcliffe (1970), River flow forecasting through conceptual models part I — A discussion of principles, *J Hydrol*, *10*(3), 282-290.

Osterkamp, T. E., M. T. Jorgenson, E. A. G. Schuur, Y. L. Shur, M. Z. Kanevskiy, J. G. Vogel, and V. E. Tumskoy (2009), Physical and Ecological Changes Associated with Warming Permafrost and Thermokarst in Interior Alaska, *Permafrost Periglac*, *20*(3), 235-256.

Rango, A. (1992), Worldwide Testing of the Snowmelt Runoff Model with Applications for Predicting the Effects of Climate Change, *Nord Hydrol*, *23*(3), 155-172.

Seibert (1997), Estimation of parameter uncertainty in the HBV model, *Nord Hydrol*, *28*(4-5), 247-262.

Seibert (1999), Regionalisation of parameters for a conceptual rainfall-runoff model, *Agr Forest Meteorol*, *98-9*, 279-293.

Sharkhuu, A., N. Sharkhuu, B. Etzelmuller, E. S. F. Heggem, F. E. Nelson, N. I. Shiklomanov, C. E. Goulden, and J. Brown (2007), Permafrost monitoring in the Hovsgol mountain region, Mongolia, *J Geophys Res-Earth*, *112*(F2).

Shaw, E. M., K. J. Beven, N. A. Chappel, and R. Lamb (2011), *Hydrology in practice*, Fourth ed., Spon Press, London.

Shrestha, D. L., N. Kayastha, and D. P. Solomatine (2009), A novel approach to parameter uncertainty analysis of hydrological models using neural networks, *Hydrol Earth Syst Sc*, *13*(7), 1235-1248.

SMHI (1999), Integrated hydrologic modelling system (IHMS). *Manual version 4.3*.

Stahl, K., R. D. Moore, J. M. Shea, D. Hutchinson, and A. J. Cannon (2008), Coupled modelling of glacier and streamflow response to future climate scenarios, *Water Resour Res*, *44*(2).

Viviroli, D., M. Zappa, J. Gurtz, and R. Weingartner (2009), An introduction to the hydrological modelling system PREVAH and its pre- and post-processing-tools, *Environmental Modelling & Software*, *24*(10), 1209-1222.

Wood, A. W., L. R. Leung, V. Sridhar, and D. P. Lettenmaier (2004), Hydrologic implications of dynamical and statistical approaches to downscaling climate model outputs, *Climatic Change*, *62*(1-3), 189-216.

Zotarelli, L., M. D. Dukes, C. Romero, K. W. Migliacciao, and K. T. Morgan (2010), Step by step calculation of the Penman-Monteith Evapotranspiration (FA)-56 Method), 12.

Appendix A: HBV model

Appendix B: Data Analysis Report

Appendix C: PET calculations and projections

Appendix D: Calibrated parameter values

APPENDIX A: HBV MODEL

1.1 Routines

1.1.1 Input routine

All equations and routines are derived from *Lindstrom et al.* [1997]. Input variables for the HBV model are weighted means for precipitation, temperature and potential evapotranspiration. The relations for the input variables are given by:

$$p(t) = \sum w_i \cdot P_{i,obs}$$

$$t(t) = \sum w_i \cdot T_{i,obs}$$

$$ep(t) = \sum w_i \cdot EP_{i,obs}$$

The daily precipitation, p (mm), is determined by the sum of the observed precipitation, $P_{i,obs}$ (mm), at the meteorological stations in the river basin multiplied by the weight for each station, w_i (-). The same calculations are made for the temperature, t (°C), and potential evapotranspiration, ep (mm).

A threshold temperature is used to distinguish the precipitation into daily rainfall, *RF* (mm), and daily snowfall, *SF* (mm). With the use of the parameter *TTI (°C)*, the threshold is extended to an interval and within this interval precipitation is assumed to be a mix of rain and snow. For mountainous basins also a distinction is made in altitude. At higher elevations, *Z* (m), precipitation will increase. Temperature, *T (°C)*, and potential evapotranspiration, *EP* (mm), will decrease for higher elevations. These three variables are determined by their altitude gradients. At a certain altitude level *PCALTL* (m), the gradient of the altitude correction for precipitation will slightly change, resulting in less snowfall per altitude level rise.

Due to the rather crude weighting and lapse rates for computation of areal precipitation, air temperatures and potential evapotranspiration, correction factors are applied to determine the rainfall, snowfall and evapotranspiration:

$$RF(t) = RFCF \cdot p(t) \qquad if\ T \geq \frac{TT + TTI}{2}$$

$$SF(t) = SFCF \cdot p(t) \qquad if\ T \leq \frac{TT - TTI}{2}$$

$$EP(t) = ECORR \cdot ep(t)$$

Where RFCF (-) is the rainfall correction factor, SFCF (-) is the snowfall correction factor and ECORR (-) is the evapotranspiration correction factor.

1.1.2 Snowmelt routine

The standard snowmelt routine of the HBV model is a degree-day approach, based on air temperature, with a water holding capacity of snow which delays runoff. Melt is further distributed according to the temperature lapse rate. The melt process starts when air temperature is above the temperature limit for melting, *TTM (*°C*)*, according to a simple degree-day expression, *CFMAX (*mm/°C/d*)*. The same accounts for refreezing of water in the snowpack, when temperature decreases below the temperature limit for melting, this water refreezes gradually. Liquid water within the snow pack, *WC* (mm), refreezes according to a refreezing coefficient, *CFR (-)*. The temperature for a daily time step, *t*, determines whether solid water is melting or liquid water is refreezing.

$$MELT(t) = CFMAX \cdot (T(t) - TTM) \qquad if\ T > TTM\ (MELT \leq SP)$$

$$REFR(t) = CFMAX \cdot CFR \cdot (TTM - T(t)) \qquad if\ T < TTM\ (REFR \leq WC)$$

SP (mm) is the frozen part of the snowpack. The snowpack is assumed to retain melt water as long as the amount does not exceed a certain fraction of the snow, given by the parameter *WHC (-)*.

The liquid water, *WC* (mm), in the snow and the infiltration of water, *IN* (mm/d) from the snow cover into the soil are given by:

$$WC(t) = WC(t-1) + MELT(t) + RF(t) \qquad if\ WC < WHC \cdot SP$$

$$IN(t) = MELT(t) + RF(t) \qquad if\ WC \geq WHC \cdot SP$$

1.1.3 Soil and evapotranspiration routine

The amount of soil moisture, *SM* (mm), in the catchment is computed with a soil moisture reservoir, representing the unsaturated soil. The calculated infiltration from the snow melt routine determines the input of water in to the soil. As long as the maximum soil moisture storage determined by its field capacity, *FC* (mm), is not exceeded, water infiltrates into the soil moisture reservoir. If no more water can infiltrate in the soil it becomes directly available for runoff.

As long as the sum of infiltration and soil moisture storage does not exceed the maximum soil moisture storage there is no direct runoff. A part of the infiltrating water will contribute to the soil moisture content; the other part will run through the soil layer as recharge, *R* (mm/d). The infiltrated water will leave the soil moisture storage box as recharge given by:

$$R(t) = \left(\frac{SSM(t)}{FC}\right)^{BETA} \cdot IN(t)$$

The parameter *BETA (-)* controls the contribution to the response function or the increase in soil moisture storage from each millimeter of rainfall or snow melt. In order to avoid problems with non-linearity, the soil moisture routine is fed in millimeter steps by water from rainfall or snowmelt. The routine results in a small contribution to runoff when the soil is dry and a great contribution when conditions are wet. For a specific amount of soil moisture, the higher the parameter BETA, the lower the runoff coefficient [*Aghakouchak and Habib*, 2010]. As the soil moisture approaches the field capacity, the runoff coefficient increases.

Actual evapotranspiration, *EA* (mm), is calculated based on potential evapotranspiration and the available amount of water for evapotranspiration in the soil. The actual evapotranspiration increases with increasing soil moisture storage according to a linear relationship. The parameter *LP* (-) is the value of soil moisture storage above which evapotranspiration reaches its potential value. The relations are given by:

$$EA(t) = \frac{SM(t)}{LP \cdot FC} \cdot EP(t) \qquad SM(t) < LP \cdot FC$$

$$EA(t) = EP(t) \qquad SM(t) \geq LP \cdot FC$$

The value for LP is a soil moisture limit for evapotranspiration, meaning that when the soil moisture is less than LP, the actual evapotranspiration is less than the potential evapotranspiration. If the value for LP is small, the soil moisture storage will reach its potential value sooner. A small value for LP means that more water in the soil evaporates, and vice versa.

Besides the outflow from the soil moisture the amount of water in the soil can also be refilled by capillary flow. The capillary flow, *CF* (mm/d), is determined by the soil moisture storage, the maximum soil moisture storage and the parameter *CFLUX* (-). If the soil moisture storage box is ´fully saturated´ no capillary flow occurs, thus the capillary flow is limited by the available space in the soil moisture storage box. The capillary flow is also limited by the amount of water available in the upper response reservoir:

$$CF(t) = CFLUX \cdot \left(1 - \frac{SSM(t)}{FC}\right) \qquad (CF \leq SUZ)$$

Where S*UZ* (mm) is the storage of water in the upper response box.

1.1.4 Response routine

The runoff generation routine is the response function which transforms excess water from the soil moisture zone to runoff. The response routine consists of one upper, non-linear, and one lower, linear, box. These are the origin of the quick (peak flow) and slow (base-flow) runoff components of the hydrograph.

The fast runoff routine generates runoff from the surface water storage in the upper response box. This runoff is non-linear and depends on the water level, *SUZ* (mm/d), in the upper response box and the flow recession coefficients *K* (d^{-1}) and *ALFA (-)*:

$$Q_0 = K \cdot SUZ^{(1+ALFA)}$$

The parameter *ALFA* introduces non linearity in the relation between Q_0 and *SUZ*. Besides the outflow from the upper response box, two more water fluxes appear in the upper reservoir. These are capillary flow to the soil and evapotranspiration routine and percolation to the lower response box.

The maximum amount of percolation is given by the parameter *PERC* (mm/d). If a small amount of water is available in the upper response box, than this water is first divided to the fast runoff routine, than the remaining water is available for capillary flow and percolation to the lower response box.

The slow runoff routine generates runoff from the lower response box. Only two water fluxes are applied on the lower ground water reservoir: inflow from the upper response box and outflow due to the slow runoff. The slow runoff is determined by:

$$Q_1 = K_4 \cdot SLZ$$

Where K_4 (mm/d) is the recession parameter and *SLZ* (mm) the water level in the ground water reservoir. The total discharge is computed as the sum of Q_0 (mm/d or m^3/s) and Q_1 (mm/d or m^3/s).

References

Aghakouchak, A., and E. Habib (2010), Application of a Conceptual Hydrologic Model in Teaching Hydrologic Processes, *Int J Eng Educ*, *26*(4), 963-973.

Lindstrom, G., B. Johansson, M. Persson, M. Gardelin, and S. Bergstrom (1997), Development and test of the distributed HBV-96 hydrological model, *J Hydrol*, *201*(1-4), 272-288.

University of Twente

Data analyse Buyant River basin, Mongolia

Final Report

Kor Heerema

16 December 2012

Preface

To complete my Water Management and Engineering program I decided to attend a so-called Capita Selecta (CS) course. This CS course enables you to define individual assignments which are equal to a regular master course, i.e. equal to 7,5 ECTS. Using the CS course I had the opportunity to already do preparation work for my master thesis. Main topic of this master thesis is the hydrological modeling of a river basin, to simulate present and future river discharges.

The study area of my master thesis is located in the Western part of Mongolia and is called the Buyant River basin. This mountainous river basin is characterized by local permafrost, steep hills, glaciers, marshlands, and wide alluvial plains. The climate in the basin is harsh with low temperatures, ice covered rivers and minimal precipitation in winter and warm and dry summers.

One part of my CS course was a trip to Mongolia, to visit the Buyant River basin. Goal of this visit was to learn more about the study area and the local problems inhabitants are facing. During my stay I was able to obtain available data about the Buyant River basin by the Institute of Meteorology and Hydrology (IMH) Mongolia. With the help of these data series it is aimed to simulate the discharges of the Buyant River for its current situation and for climate scenarios. This report outlines the obtained data, describing the availability and analyzing the reliability of the data.

Contents

1 Introduction

The Mongolian Water Authority is setting up water management plans to restore the water balance in the Buyant River basin. More knowledge about the change in availability of water nowadays and in the future is a prerequisite for the development of these plans.

In mountainous basins, such as the Buyant River basin, meteorological parameters vary with elevation. As these are usually the main input to hydrological models, the accuracy of such data is very important in runoff modeling. In order to account for the spatial variation of such variables, a semi distributed rainfall-runoff model is required. To simulate the discharges of the Buyant River the hydrological HBV model will be used (See Research plan Kor Heerema). Main input values of the HBV model are precipitation, temperature and potential evapotranspiration, the model generates discharges as its output.

IMH Mongolia provided data series describing precipitation, temperature and observed discharges within the Buyant River basin. Also topographical and geological data about the Buyant catchment is available. With this data it is aimed to simulate dischargers of the Buyant River.

1.1 Aim and research questions

Aim of this report is to determine the quality of the available data and to determine which adjustments are needed before the modeling procedures can be started. To achieve this aim the following research questions are defined:

- ✓ What data is available?
- ✓ Which methods were used to obtain this data?
- ✓ What data should be used for modeling of the Buyant River basin?

1.2 Study area

The Buyant River in the western part of Mongolia is located in a mountainous and semi-arid area. The river basin is characterized by permafrost, steep hills, glaciers, marshlands, and wide alluvial plains. The climate in the basin is harsh with low temperatures, ice covered rivers and minimal precipitation in winter and warm and dry summers. The Buyant River catchment drains an area of approximately 8370km² and the river has a length of 172km.

1.3 Outline report

First the available data for the Buyant River basin is described in chapter 2. In this chapter obtained topography, geology, meteorological and discharge data are outlined. In Chapter 3 methods are described to determine the quality of the obtained data. Based on the quality of this data, preparations are described to repair unreliable data and interpolate data for missing days. Results of these operations are shown in chapter 4. Conclusions and recommendations are outlined in the last chapter.

2 Data

2.1 Topography and geology

Topographical and geological characteristics of the Buyant River basin can be displayed using a Geographical Information System (GIS). Using layers provided by IMH Mongolia main characteristics of the Buyant basin are depicted in the program ArcMap.

The Buyant river starts in the North-western part of the basin and drains via the gorge, located in the southern part, to its delta North-east of the basin. The basin is bounded by mountain tops from which precipitation and meltwater drains into the tributaries of the Buyant River. The Buyant River basin is mostly dominated by mountainous relief features with steep slopes. Intermountain valleys, gorges and flat plains are only located downstream of the river. On the upper north slopes alpine meadow consist of high mountains with rock debris. In the mountain slopes dry steppe and lower flat plains are more common [*Nandintsetseg et al.*, 2010]. The elevation height of the Buyant catchment is roughly between 1150-4000m above sea level. The main Buyant River passes Deluun in the upstream part and the Khovd downstream of the river, see Figure 1.

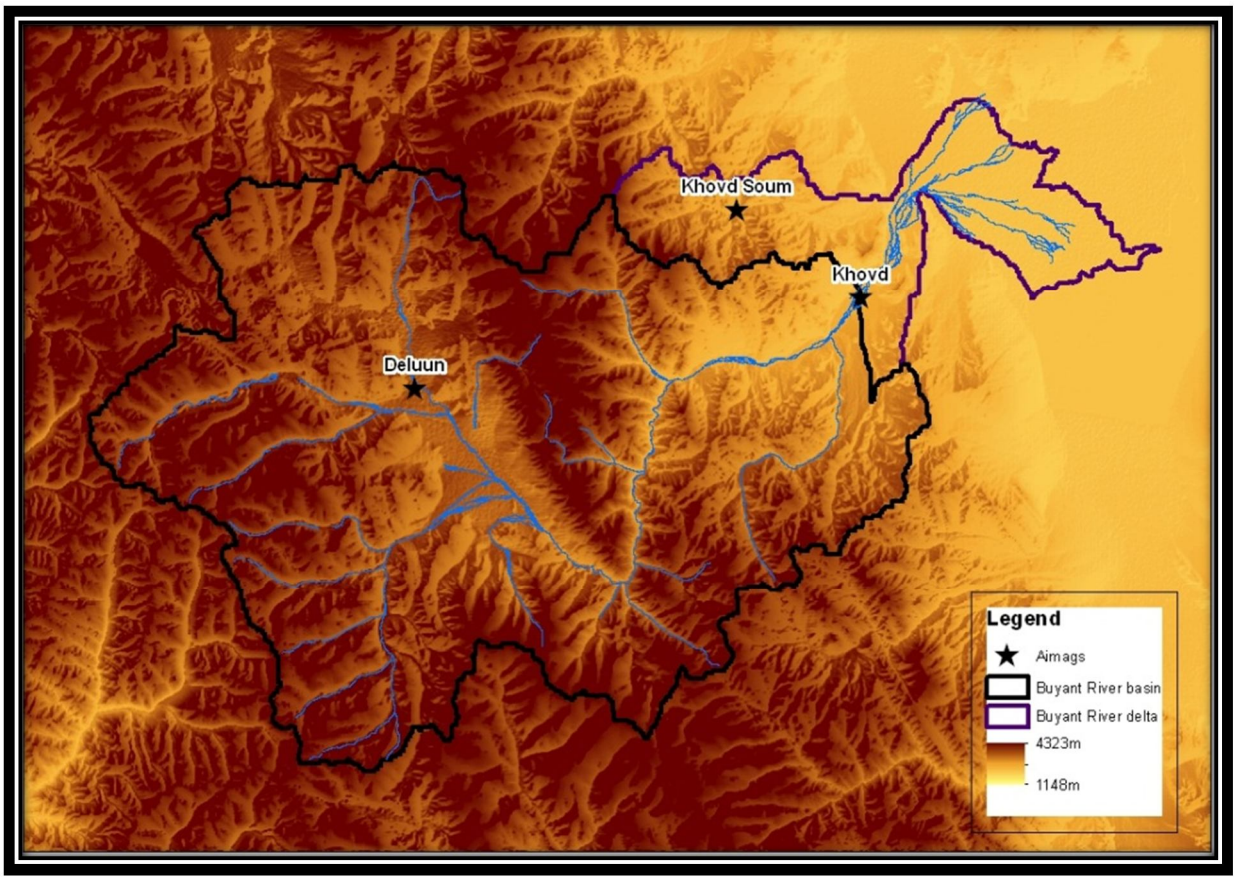

Figure 1 Buyant River basin displaying elevation heights, aimags and the borders of the basin and its delta (IMH Mongolia)

In the upper (western) part of the basin two main tributaries drain into the Buyant River; the Chigertei River and the Gansmod River. These two tributaries coincide into the Buyant River near Deluun aimag. The largest lake of the Buyant River basin is located in the Chigertei River. Small remaining of glaciers can be found at the highest peaks in the basin and around the western border of the Buyant basin, see Figure 2.

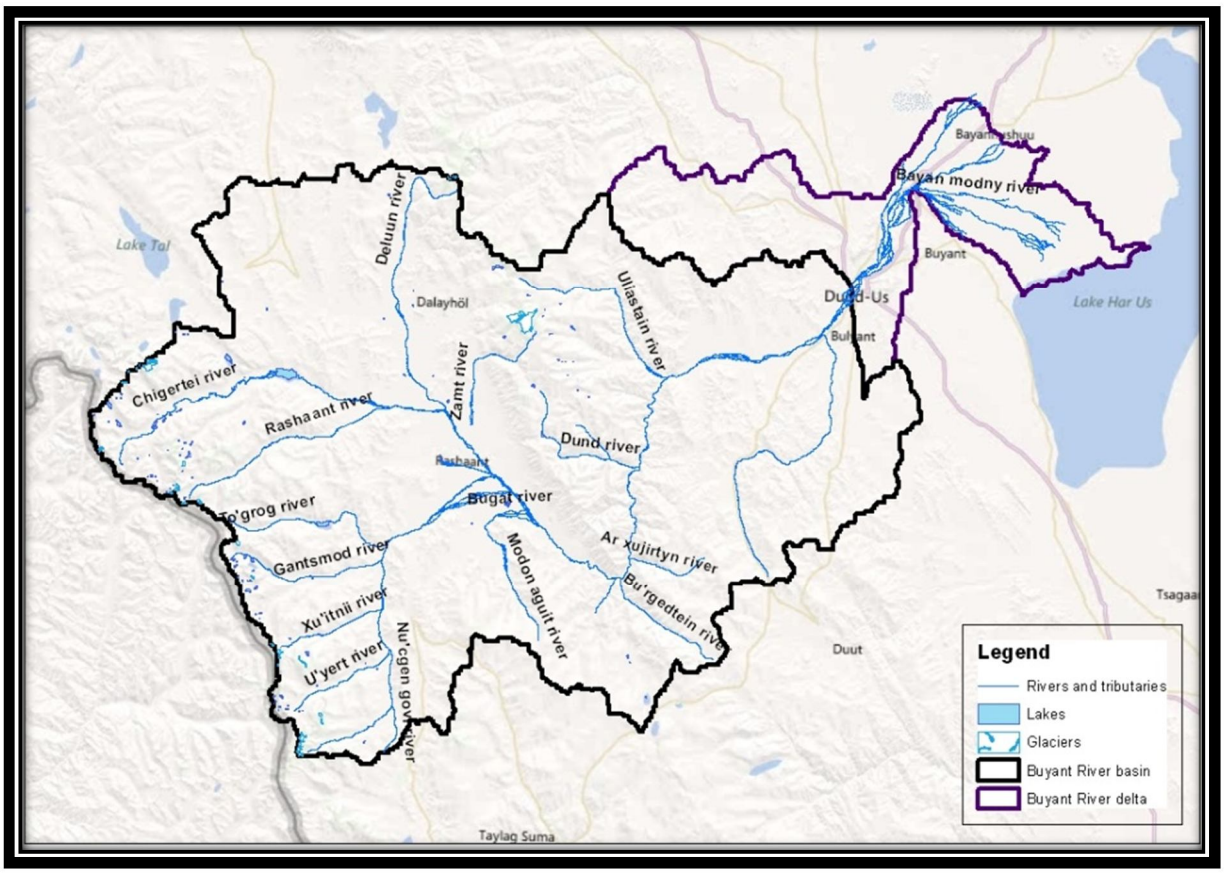

Figure 2 Buyant River basin displaying main rivers, tributaries, lakes and glaciers (IMH Mongolia)

Permafrost exists in the higher altitude part of the basin; this permanently frozen ground remains at or below 0°C for at least two years [*Nandintsetseg and Shinoda*, 2011]. The underground is merely hard rock or loose rocky soil, and partly alluvial plain.

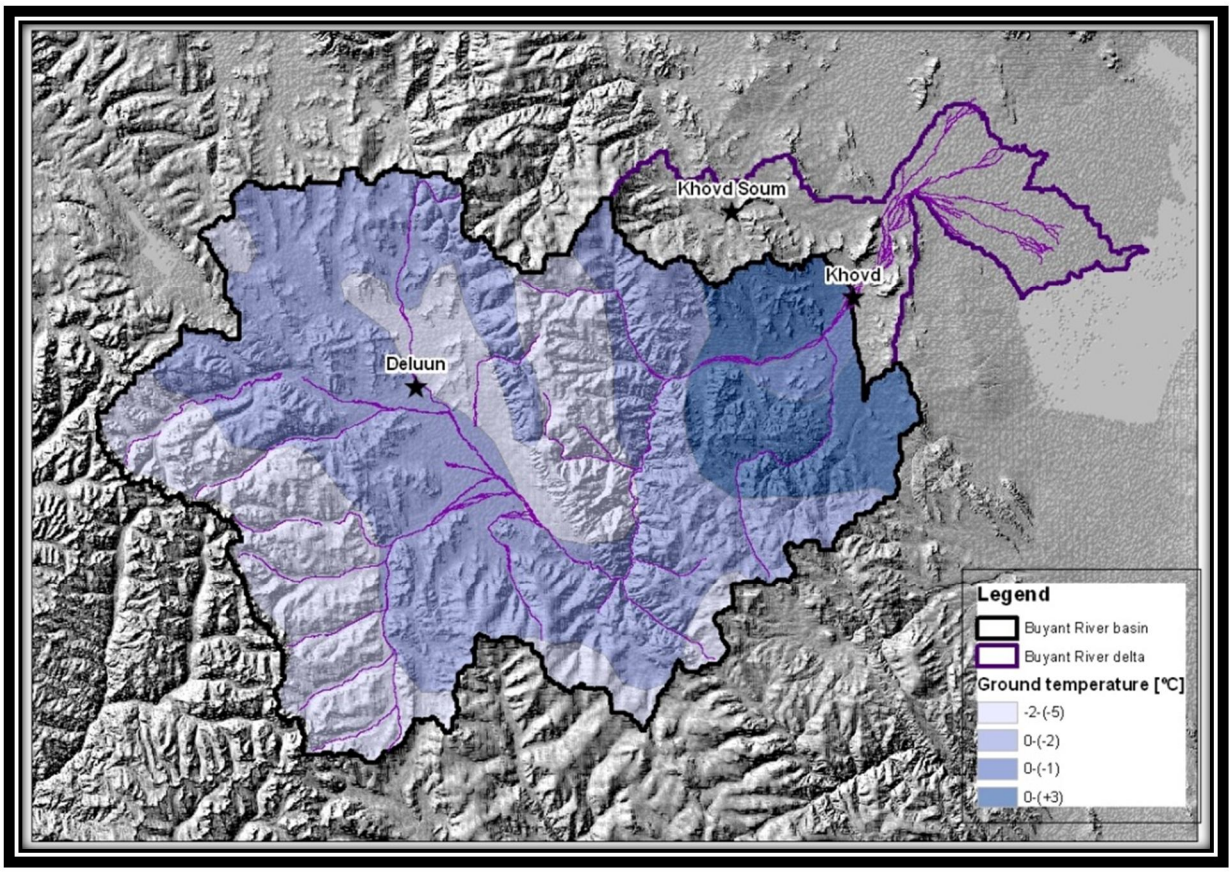

Figure 3 Buyant River basin displaying zones of frozen ground (IMH Mongolia)

2.2 Meteorological data

In and around the Buyant River basin meteorological stations are located; these stations measure precipitation and temperature. The spatial distribution of the meteorological stations is shown in Figure 4. The meteorological stations Deluun and Khovd are located within the basin and the meteorological stations Duut and Khovd soum are located outside the boundaries of the catchment.

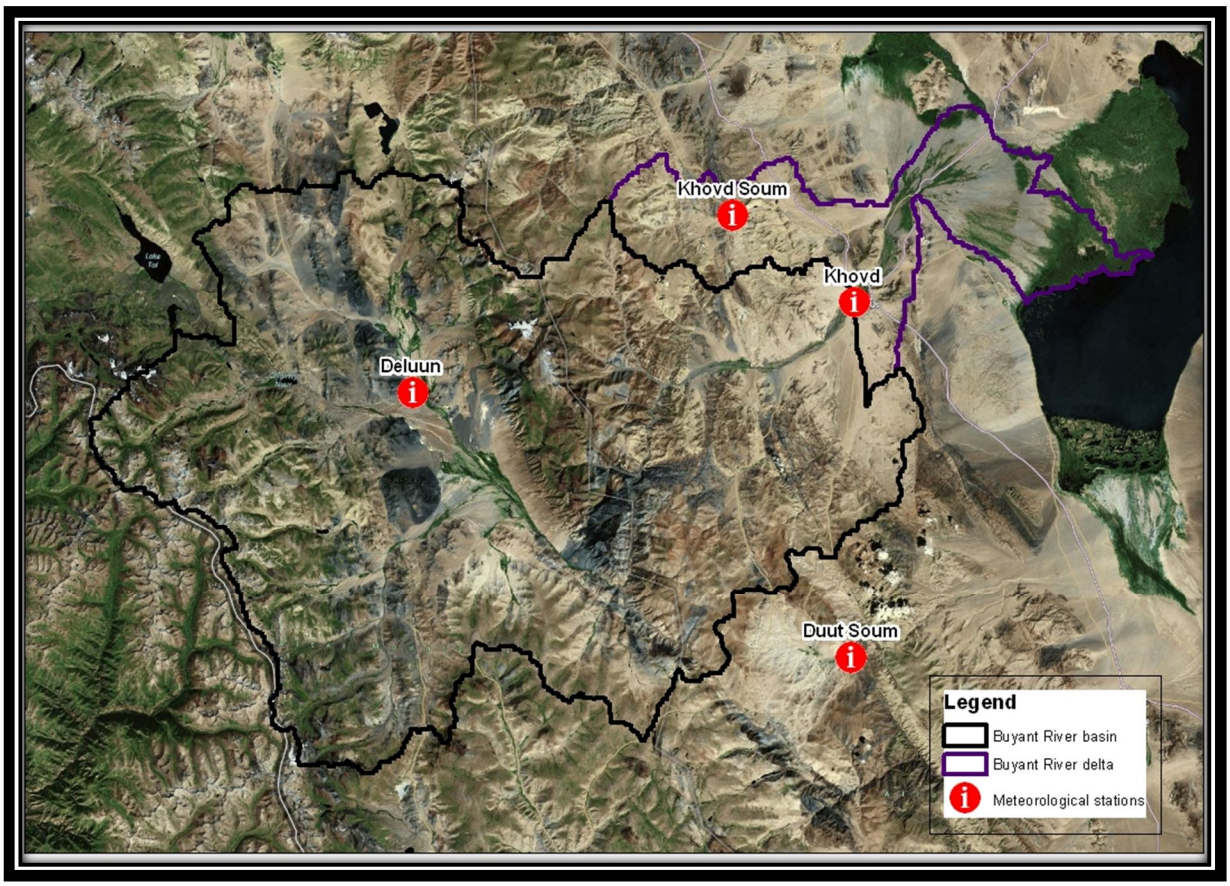

Figure 4 Buyant River basin displaying locations of the meteorological stations (IMH Mongolia)

2.2.1 Availability meteorological data

Locations of each meteorological station are outline in Table 1. The meteorological station Khovd provides 50 years of precipitation data, the meteorological station Deluun 18 years of data, as the meteorological stations Khovd soum and Duut only have records for 2 and 6 years respectively.

The same length of data recordings for precipitation is available for temperature data at the meteorological stations Khovd, Deluun and Duut Soum. The data period for Duut Soum has a length of 5 years.

Next to the measurements of precipitation and temperature the meteorological station Khovd also measured evaporation. All available meteorological data periods are shown in Table 1.

Table 1 Location coordinates and data period of the meteorological stations within and near the Buyant River basin (IMH Mongolia)

Meteorological stations	Latitude [º]	Longitude [º]	Altitude [m]	Data period precipitation	Data period temperature	Data period evaporation
Khovd	48.02	91.65	1405	1961-2010	1961-2010	2005-2009
Deluun	47.88	90.77	2160	1993-2010	1993-2010	-
Khovd Soum	48.12	91.37	1700	2009-2010	2006-2010	-
Duut Soum	47.52	91.65	2280	2005-2010	2005-2010	-

2.2.2 Missing meteorological data

The missing precipitation data is depicted in Table 2. Precipitation data for the meteorological stations Khovd and Deluun are complete for the given data period. Meteorological station Duut Soum misses daily precipitation data for the years 2005, 2007, 2008 and 2010. The period of measured data for the meteorological station Khovd Soum is complete.

Table 2 The availability of daily precipitation data for the 4 meteorological stations within and near the Buyant River basin, displayed for each year (IMH Mongolia)

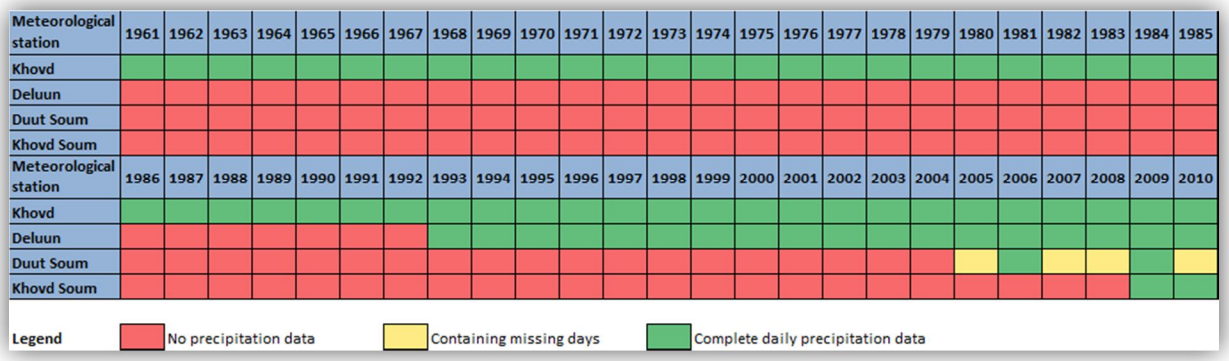

The missing temperature data is depicted in Table 3. The meteorological station Khovd misses one year of average temperature data; the year 1998. However, maxima and minima temperature values are available for this year. In the year 1990 no average temperature is measured for the month February and in 1995 recorded temperature values are missing for October, also for these months maxima and minima are available.

Meteorological station Deluun also misses daily average temperature data in the month July of the year 1995, no minima and maxima are available for this month. The data period of Duut Soum misses average daily temperature data in the years 2005, 2007, 2008 and 2010. No data is measured in the months September 2005 and 2007, April 2008 and February 2010. The data period for meteorological station Khovd Soum is complete.

Table 3 The availability of daily average temperature data for the 4 meteorological stations within and near the Buyant River basin, displayed for each year (IMH Mongolia)

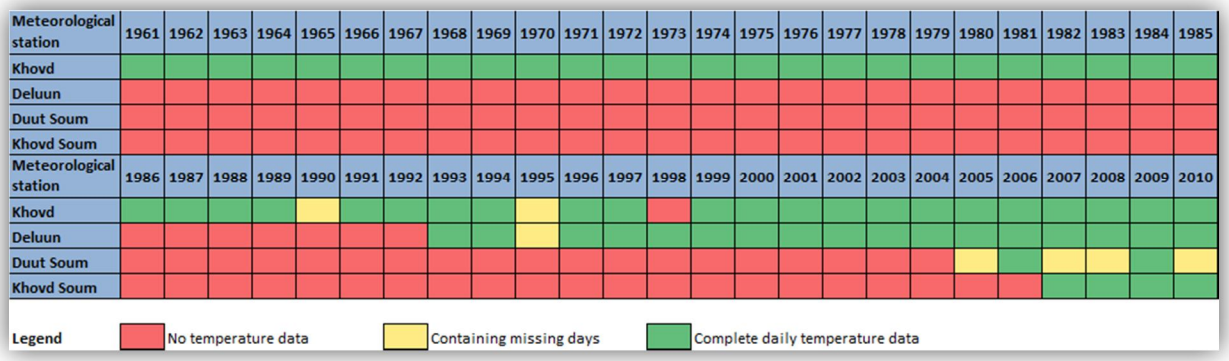

The recorded evaporation data is shown in Table 4. The availability of data is distinguished by the 12 months in one year. Missing data occurs during the months October till April, which means that only during 5 months per year evaporation is measured.

Table 4 The availability of daily evaporation data for the meteorological station Khovd, displayed for each month (IMH Mongolia)

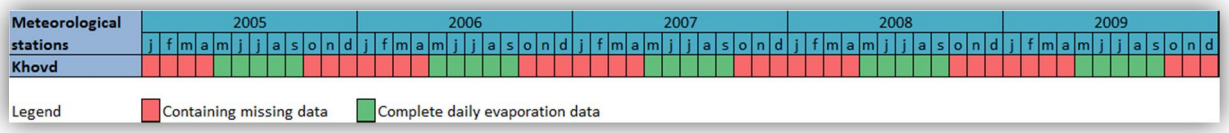

2.3 Discharge data

In the Buyant River basin four river gauging points are located. At these gauging points water levels are recorded. One is located in the Chigertei tributary, one in the Buyant River near Deluun, one in Gansmod tributary and one in the Buyant River near the city Khovd. These permanent river gauging points are indicated in Figure 5.

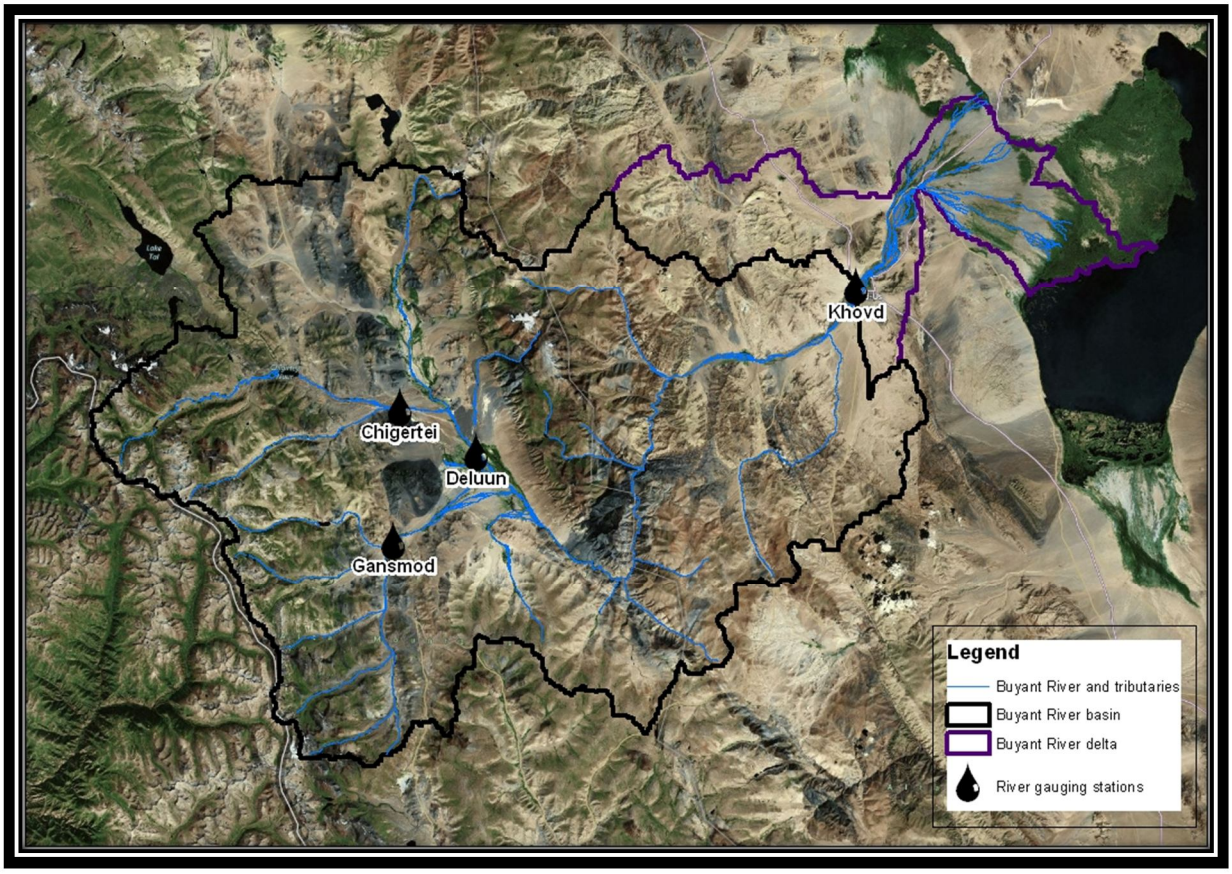

Figure 5 Buyant River basin displaying locations of the river gauging stations (IMH Mongolia)

2.3.1 Availability discharge data

The river gauging point near Khovd provides 43 years of discharge data, the gauging point near Deluun 36 years of data and gauging point Gantsmod also 36 years. The river gauging point at Chigertei contains 3 years of data before a period starts where no discharge is measured. At the end 7 years of discharge data is available for this gauging point, see Table 5.

Table 5 Data period of the river gauging stations within the Buyant River basin (IMH Mongolia)

Gauging points	Latitude [°]	Longitude [°]	Data period
Khovd	91. 37	48.00	1967-2009
Deluun	90.50	47.47	1974-2009
Gantsmod	90.41	47.39	1974-2009
Chigertei	90.41	45.50	1988-1990, 2003-2009

2.3.2 Missing discharge data

The missing discharge data is depicted in Table 6. The availability of data has been distinguished by the four seasons in one year; spring (s), summer (s), autumn (a) and winter (w). The gauging point near Khovd misses 4 complete years of discharge data; 1970, 1972, 1978 and 1979. Missing discharge data at both the gauging points Khovd and Deluun is mostly during the winter months. The gauging point at Deluun misses discharge data for the entire year 1982. The availability of discharge data for the gauging point at Gantsmod is complete from 1986 till 2009. At the gauging point in the Chigertei tributary discharge data for the first 3 years is not complete, only during summer complete daily discharge has been listed. The same accounts for the years 2003 till 2009, except for the year 2004.

Table 6 The availability of daily discharge data for the river gauging stations in the Buyant basin (IMH Mongolia)

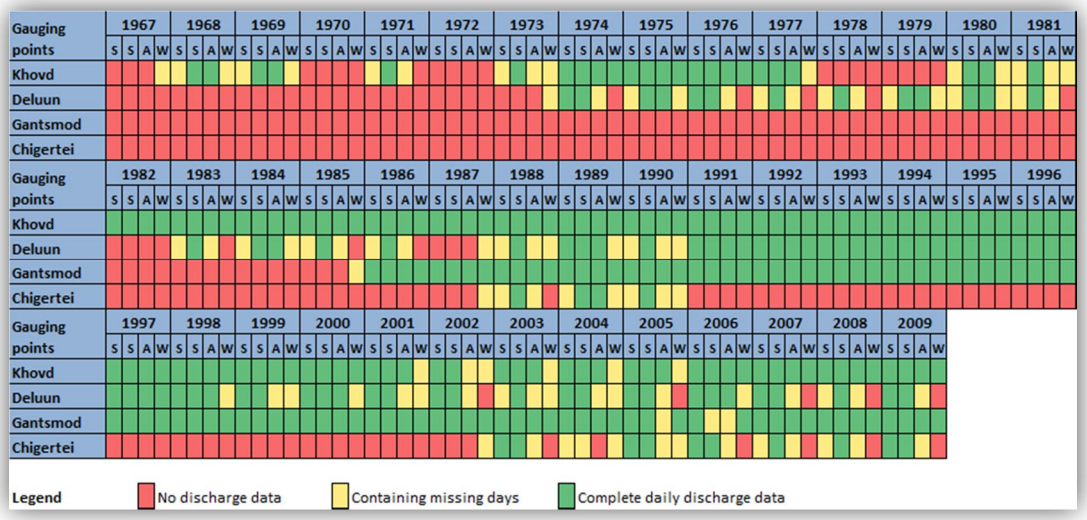

3 Methods

3.1 Buyant River basin

Ajami et al. [2004] considered three different calibration strategies in their studied catchment area. By dividing the basin into sub basins a lumped, semi-lumped and semi-distributed strategy were obtained. They worked from a lumped model towards a semi-distributed model, and determined for each sub-basin separated parameters based on soil characteristics and their contribution to the stream flow at the outlet [*Ajami et al.*, 2004]. IMH Mongolia already divided the Buyant basin into 4 sub-basins. The division of these basins is based on the location of the river gauging stations and the area which drains into each gauging point. Using these 4 sub-basins a lumped, semi-lumped and semi-distributed model has been obtained. The lumped model describes the entire Buyant River basin with its discharge outlet near Khovd, see Figure 6. Characteristics of each model are outlined in the table below:

Table 7 Description of the sub-basins and the calculated area for each calibration model.

Model	Sub-basins	Area
Lumped	Chigertei, Deluun, Gantsmod and Khovd combined	7142 km²
Semi-lumped	Chigertei and Deluun combined	2284 km²
	Khovd and Gantsmod combined	4859 km²
Semi-distributed	Chigertei,	902 km²
	Deluun,	1382 km²
	Gantsmod,	1035 km²
	Khovd	3824 km²

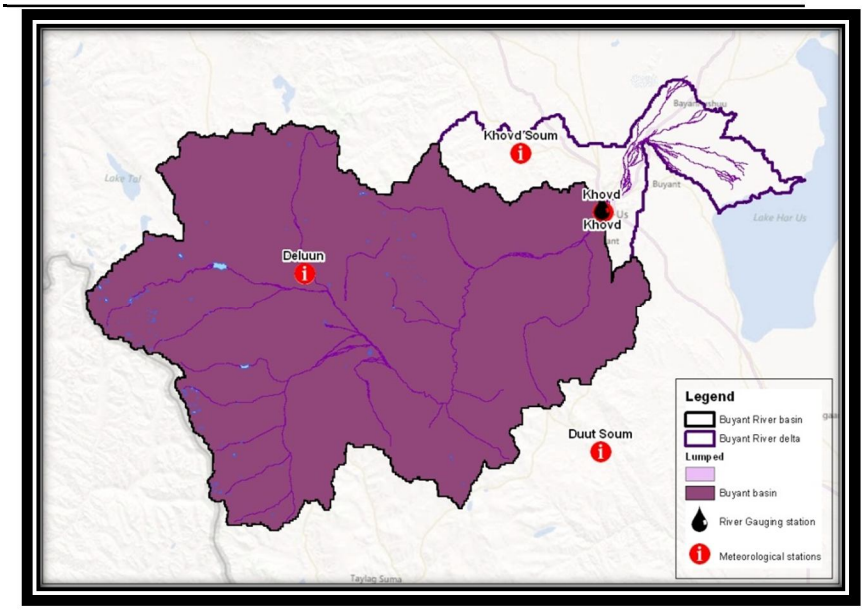

Figure 6 Lumped model of the Buyant River basin with its discharge outlet at Khovd (IMH Mongolia)

The semi-lumped model divides the basin into 2 areas, one discharge outlet near Deluun and one near Khovd, see Figure 7.

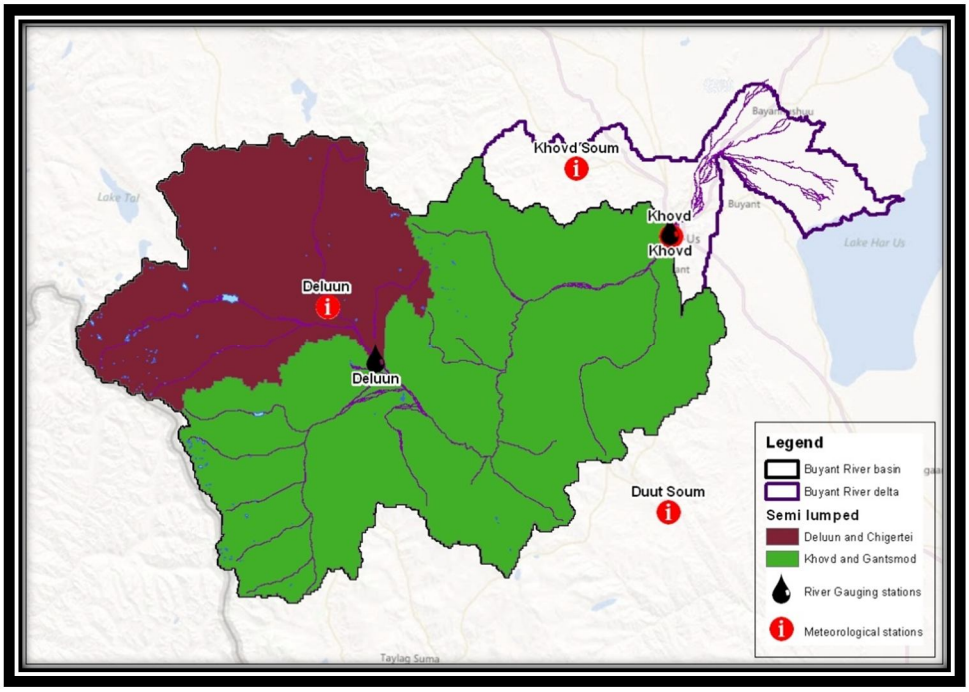

Figure 7 Semi-lumped model of the Buyant River basin with its discharge outlets at Khovd and Deluun (IMH Mongolia)

The semi-distributed model contains 4 sub-basins based on the 4 river gauging stations, see Figure 8.

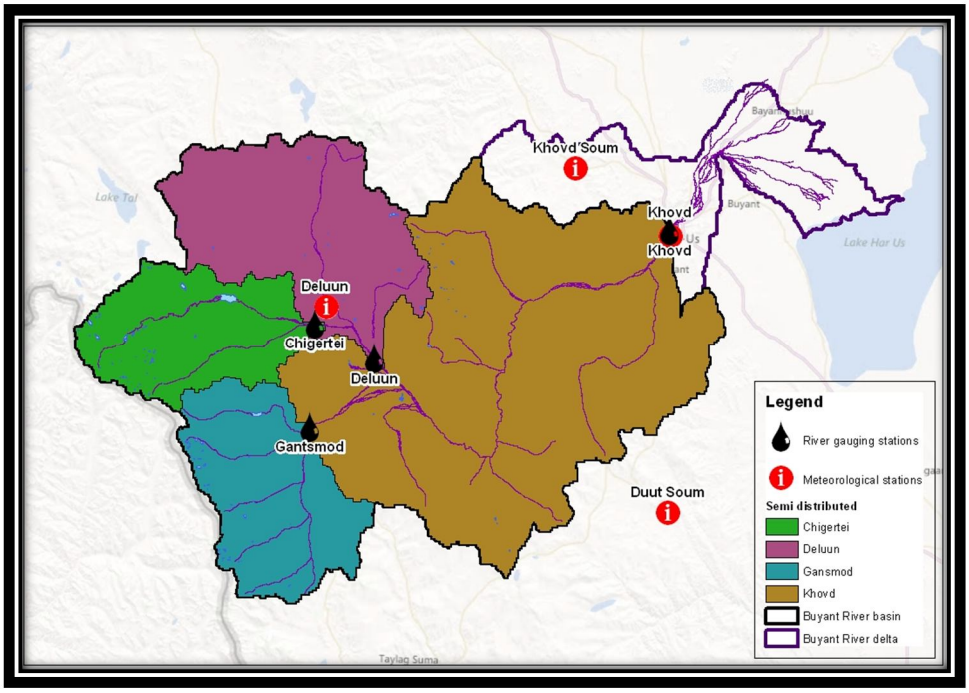

Figure 8 Semi-distributed model of the Buyant River basin with its discharge outlets at Chigertei, Deluun, Gantsmod and Khovd (IMH Mongolia)

3.2 Measurements

3.2.1 Meteorological data measurements

Measurements of daily precipitation and daily temperature are made by automatic weather stations [*Shaw et al.*, 2011]. Two of the four meteorological stations are shown in Figure 9 and Figure 10. All 4 meteorological stations measure precipitation twice a day. The sum of these measurements has been listed in tables by IMH Mongolia, in mm per day.

Data loggers at the Khovd and Deluun meteorological stations have recorded air temperature for every 3 hour (8 times per day). Data loggers at the meteorological stations at Khovd Soum and Duut Soum have recorded air temperature for every 8 hour (3 times a day). Of these records the daily maximum and minimum temperatures are listed by IMH Mongolia. Based on the recorded air temperatures for each day, average daily temperatures are calculated and also listed by IMH Mongolia.

Figure 9 Meteorological station Khovd (IMH Mongolia)

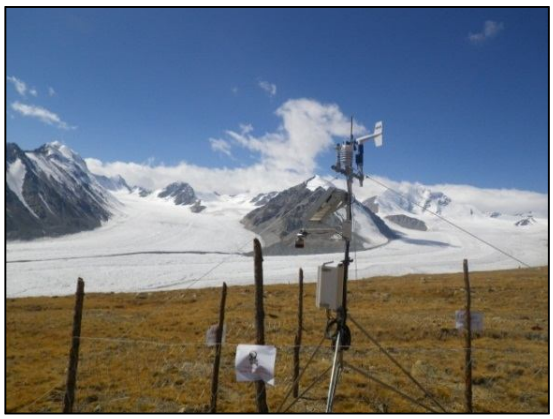

Figure 10 Meteorological station Deluun (IMH Mongolia)

The evaporation data at the meteorological station Khovd has been measured using an evaporation pan (IMH Mongolia). The water level in the pan is daily measured with a hook gauge and the difference between two readings gives a daily value of evaporation [*Shaw et al.*, 2011]. During the months October till April evaporation could not be measured due to low temperatures in these months.

3.2.2 Discharge measurements

At the four river gauging stations the water level has been measured. The water level at a gauging station, is the most important measurement in river hydrometry, it is generally known as the stage [*Shaw et al.*, 2011]. The recorded stage for the river gauging stations is the mean of a twice per day measurement at 8AM and 8PM. The measured stage is the length from datum to water surface in centimeter (IMH Mongolia).

With the stage measurements discharges are calculated using a rating-curve. The rating curve describes the relation between the discharge and the stage. The rating curve performs best when discharges are available for different water stages; high, low and intermediate flows [*Shaw et al.*, 2011]. In order to calculate the discharges, flow velocities are determined for these stages (IMH Mongolia). At each river gauging point the cross-sectional area is also determined. Discharges are calculated using the following equations:

$$Q = vA$$

$$A = wh$$

Where:

Q = Discharge (m^3/s)

A = Cross-sectional area (m^2)

h = Stage (average) (m)

v = Flow velocity (average) (m/s)

All the measured discharges (Q) are plotted against the corresponding mean stages (h). Once the rating curve is determined, discharges for measured stages can be calculated directly from the rating curve without additional flow velocity measurements.

Figure 11 Mr. H. Bagdad, gauging man doing measurements in Chigertei river at Deluun gauge in June, 2011 (IMH Mongolia)

However, conditions in a natural river are rarely stable for any length of time and thus the stage-discharge relationship must be checked regularly [*Shaw et al.*, 2011]. This also means that rating curves are not similar for each year, but changes in time. The rating curves for the four gauging stations are depicted in Figure 12.

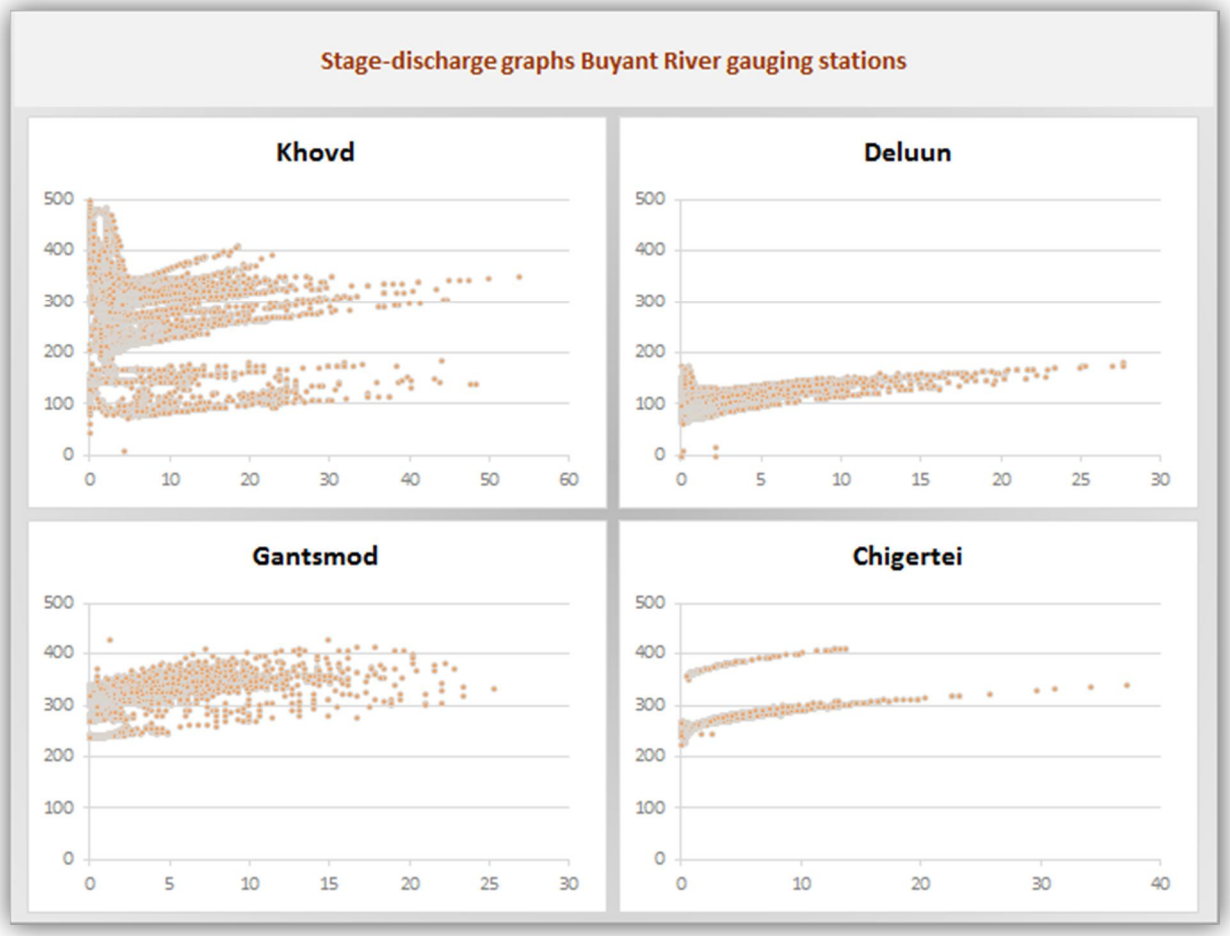

Figure 12 Rating curves which represent the relation between the stage [mm] (vertical axes) and the discharge [m³/s] (horizontal axes) for the four river gauging points (IMH Mongolia).

3.3 Quality

3.3.1 Meteorological data

The quality of meteorological data will be checked, by plotting data as a function of time. An insight can be quickly gained about outliers, or values that do not appear to be consistent with the rest of the data. Also discontinuities can be easily determined.

3.3.1.1 Precipitation data

Looking at the graphs for the recorded precipitation values, no odd observations can be determined, see Figure 13. Comparing the daily precipitation between the years 1993 and 1994 for the meteorological station Deluun, a large difference can be observed. It looks that the data for the year 2003 is not reliable, due to the very low values.

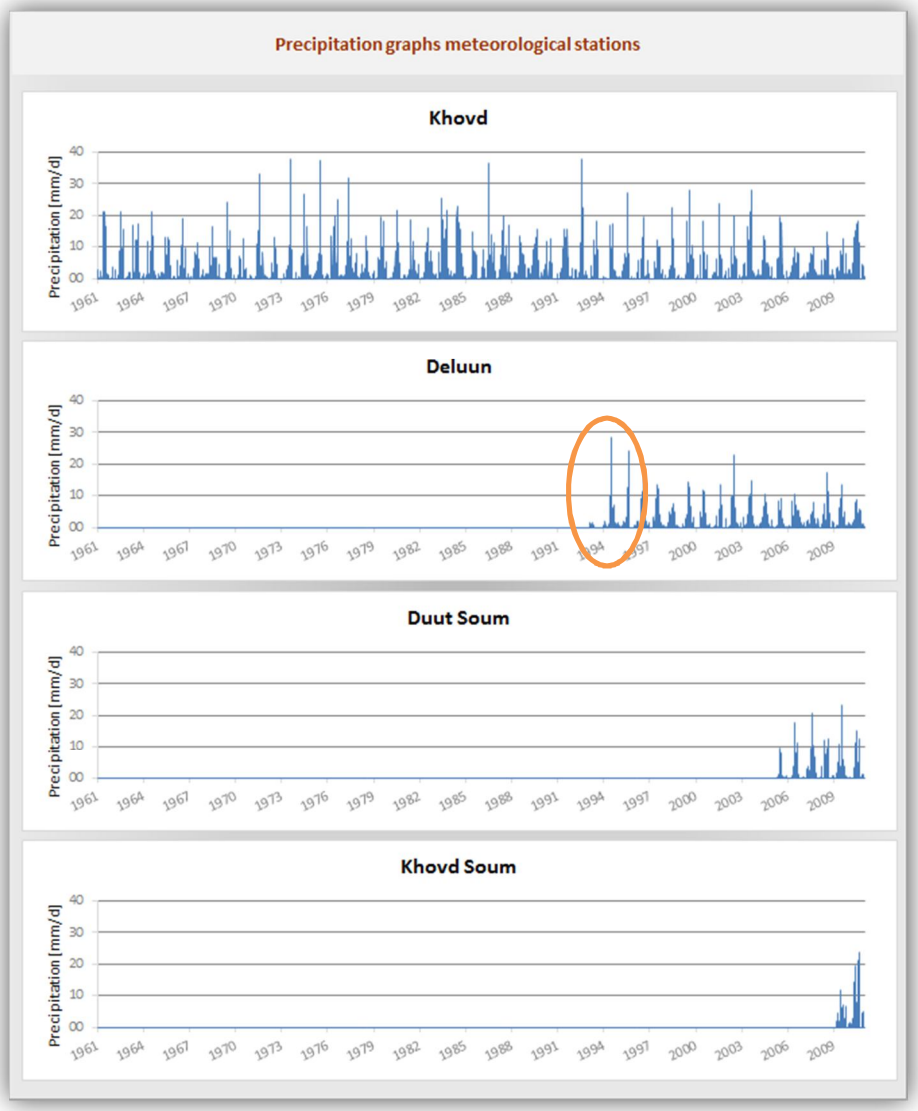

Figure 13 The daily precipitation measurements are plotted against time for all 4 meteorological stations (IMH Mongolia)

3.3.1.2 Temperature data

Looking at the graphs for the recorded temperature values, no outliers can be determined, see Figure 14. The horizontal line representing the year 1998 for the meteorological station Khovd is due to missing daily average temperature data.

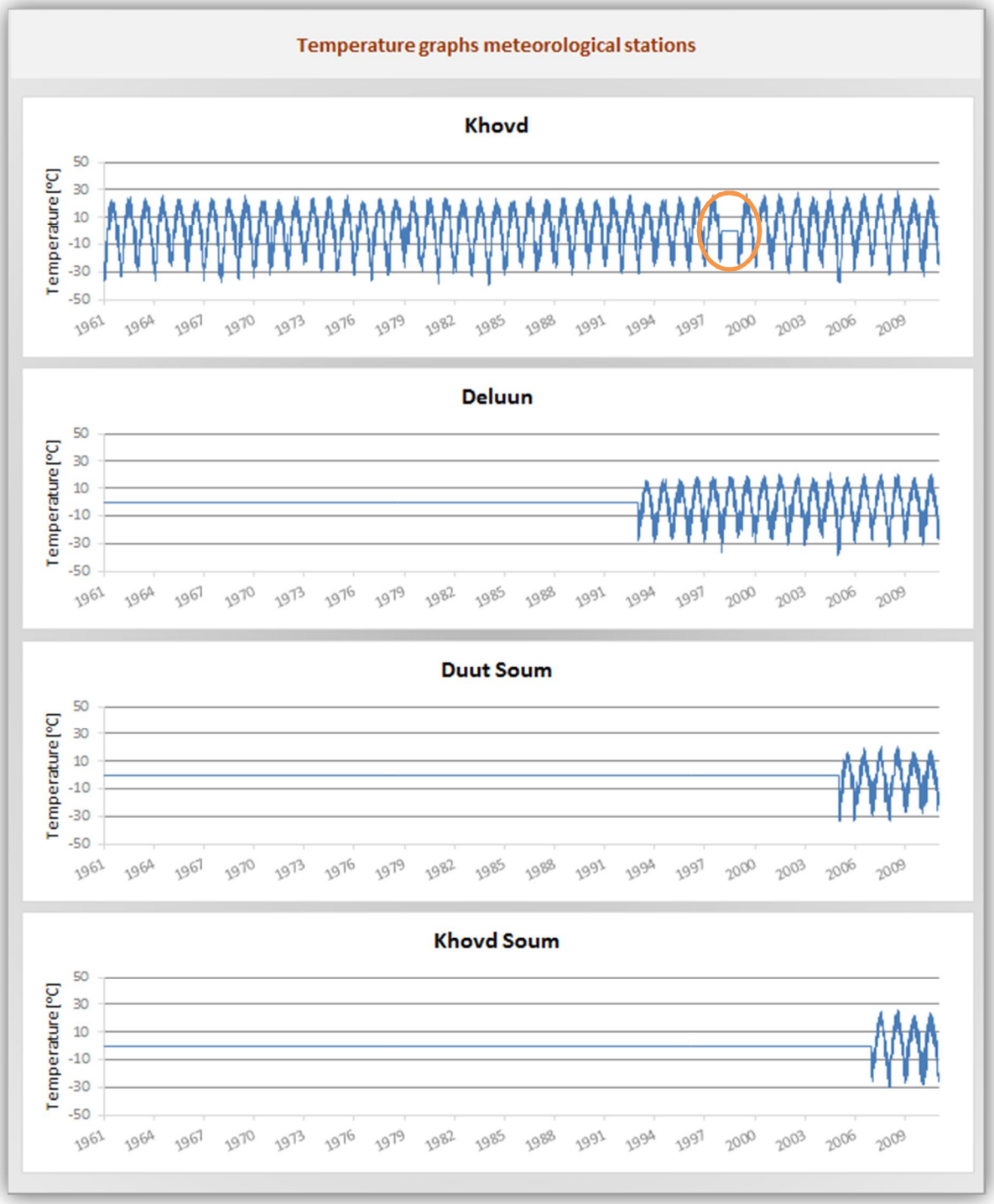

Figure 14 The daily average temperature measurements are plotted against time for all 4 meteorological stations (IMH Mongolia)

3.3.1.3 Potential evapotranspiration

Next to the precipitation and temperature data, potential evapotranspiration is also a necessary input value for the HBV model. Evaporation pans provide a measurement of the combined effect of temperature, humidity, wind speed and sunshine on the reference crop evapotranspiration. At the meteorological station Khovd, such an evaporation pan has been used to measure daily evaporation over the months May till September.

The Penman-Monteith method is recommended as the sole standard by the FAO [*Allen et al.*, 1998]. It combines both energy and mass balances to model the potential evapotranspiration. It is based on fundamental physical principles, which guarantee the universal validity of the method [*Chen et al.*, 2005]. However, it needs a number of meteorological variables which are not available for the Buyant River basin (IMH Mongolia).

Therefore the temperature based method called the Blaney and Criddle equation [*Blaney and Criddle*, 1950] is used to calculate the potential evapotranspiration. This formula, based on an empirical model, requires only mean daily temperatures T (C) over each month. This equation is also implemented in a study by Menzel (2008) for the Kharaa River basin in the Northern part of Mongolia. This formula, based on an empirical model, requires only mean daily temperatures T (°C) over each month:

$$PE = p \cdot (0{,}46 \cdot T + 8)\ [mm/d]$$

Where *p* is the mean daily percentage (for the month) of total annual daytime hours.

3.3.2 Discharge data

To check the quality of the discharge data yearly rating curves are displayed for each river gauging point. These rating curves are determined by filtering the days without measured stages and/or without measured discharges. Using the XY-plot function rating curves can be drawn, which represents the relation between the stages and corresponding discharges. For each year of its data period the available rating curves are determined for the four gauging stations.

3.3.2.1 Gauging station Khovd

The rating curves for the gauging point Khovd are depicted in Figure 15. Especially for the first decade the variability in rating curves is large. At each decade unreliable data has been highlighted by red boxes. Unreliable data are those values which do not match with the rating curves. In particular for the years 1967 till 1980 rating curves show a large diversity. At the last decade low discharges occur during very high water levels, which is not realistic. The stage-discharge relations for the years 1985 and 1998 are unreliable due to the scattered dots.

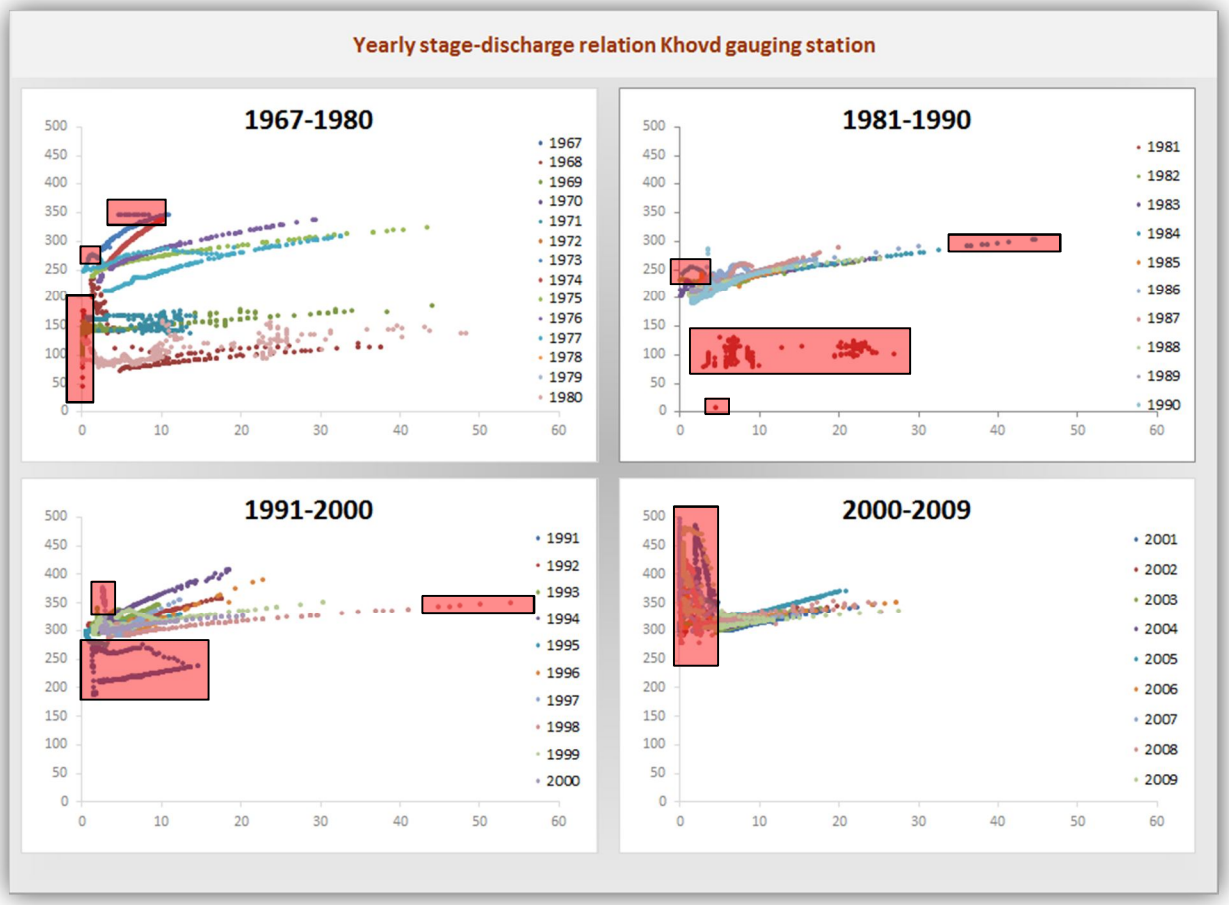

Figure 15 Yearly rating curves which represent the relation between the stage [mm] (vertical axes) and the discharge [m³/s] (horizontal axes) for the river gauging points at Khovd (IMH Mongolia). Unreliable data has been highlighted by red boxes.

3.3.2.2 Gauging station Deluun

The rating curves for the gauging point Deluun are depicted in Figure 16. For meteorological station Deluun unreliable discharge data should be deleted by filtering discharges below 1 m³/s, as depicted by the small red rectangles. Mainly due to the large diversity of the dots at these low discharges, data is not reliable. The overall variability in rating curves is smaller than those at the gauging station Khovd.

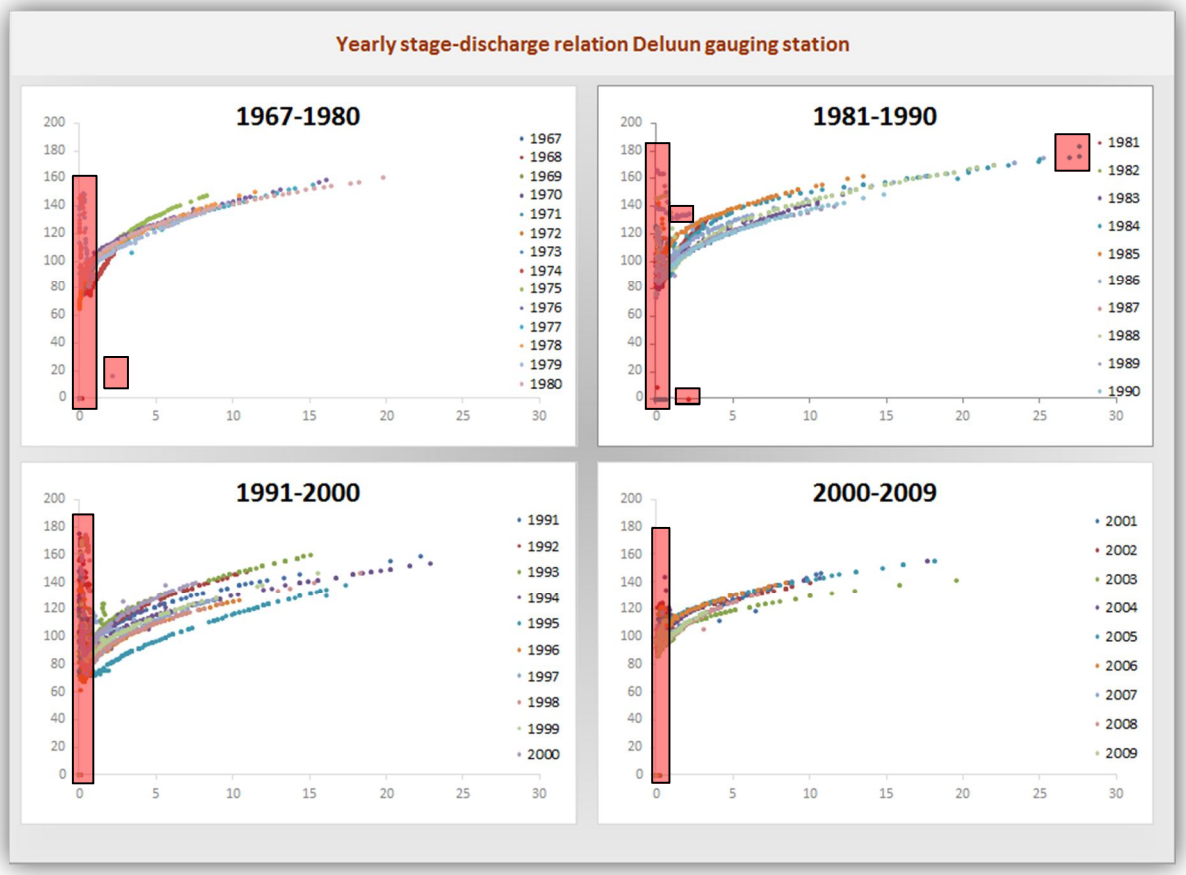

Figure 16 Yearly rating curves which represent the relation between the stage [mm] (vertical axes) and the discharge [m³/s] (horizontal axes) for the river gauging points at Deluun (IMH Mongolia). Unreliable data has been highlighted by red boxes.

3.3.2.3 Gantsmod

The rating curves for the gauging point Gantsmod are depicted in Figure 17. The relation between the stages and discharges for this gauging point are very well described. All relations have smooth curves and there are only a few points which seem not reliable. The four boxes at point (0,0) represents measurement days where no water level is measured and therefore no discharge is determined. Comparing the overall graphs the two dots for the year 1993 are representing very high discharges and do not look reliable. As for all other years maximum discharge is not exceeding 50 m³/s.

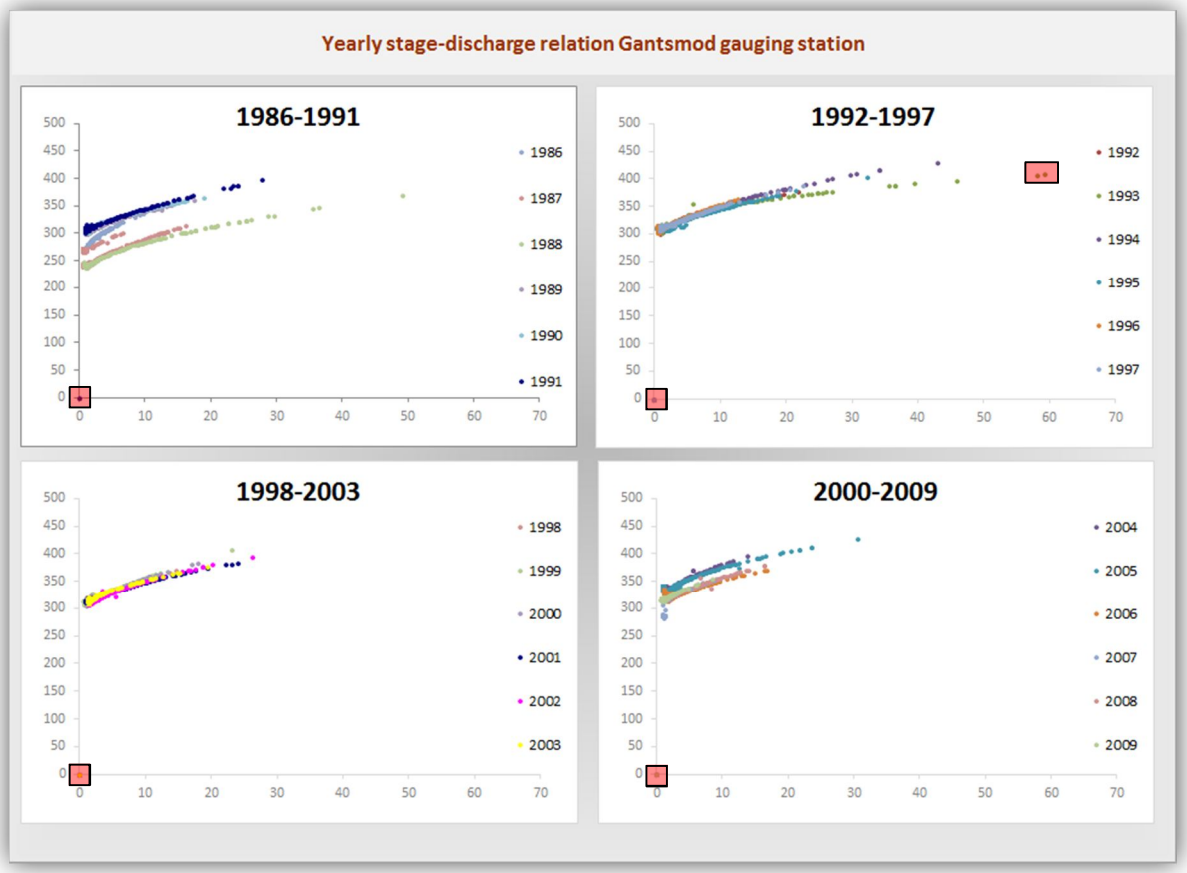

Figure 17 Yearly rating curves which represent the relation between the stage [mm] (vertical axes) and the discharge [m³/s] (horizontal axes) for the river gauging points at Gantsmod (IMH Mongolia). Unreliable data has been highlighted by red boxes.

3.3.2.4 Chigertei

The rating curves for the gauging point Gantsmod are depicted in Figure 18. The curves for the years 1988-1990 are describing the same relationship. Only low discharges seem unreliable for this first period due to the diversity of the dots. At the second period, years 2003-2009, the rating curve for the year 2003 is describing the same rating curve as all others, except at a higher stage. It seems that 100mm (250mm and 350mm) is differentiating the rating curves, which can be caused by incorrect reading during the measurements. The quality of the discharge data for 2003 seems reliable.

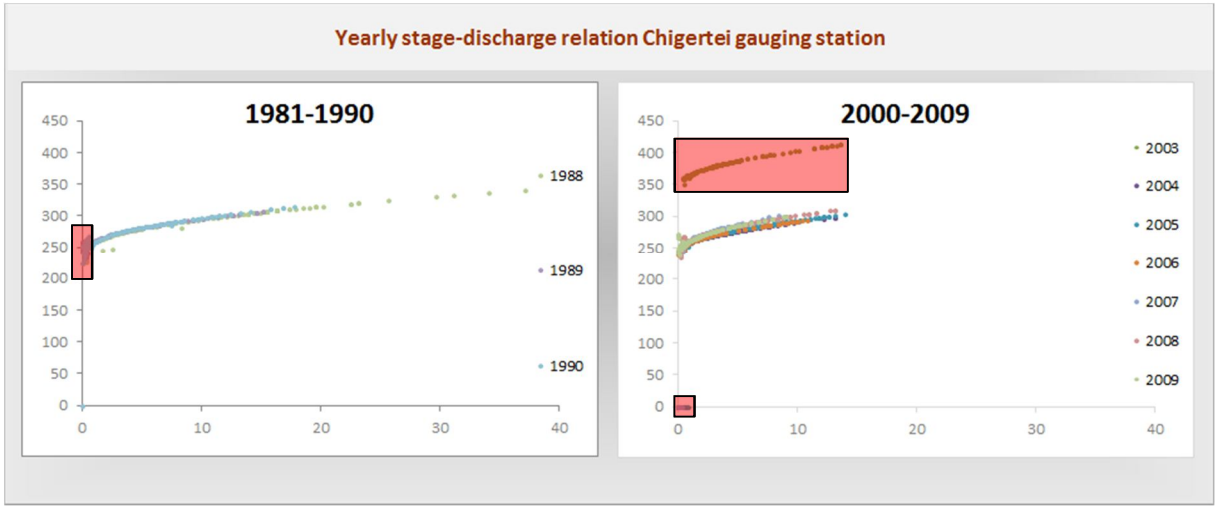

Figure 18 Yearly rating curves which represent the relation between the stage [mm] (vertical axes) and the discharge [m³/s] (horizontal axes) for the river gauging points at Chigertei (IMH Mongolia). Unreliable data has been highlighted by red boxes.

3.3.2.5 Reliability discharge data

By filtering the unreliable data for each individual yearly rating curve the quality of the discharge data can be determined. The discharge graphs for the four river gauging stations are depicted in Figure 19. The green areas represent reliable data and the red areas unreliable data. Unreliable discharge data is mostly observed during winter time, in the months December, January, February and March. This is mainly due to the absence of water level measurements or incorrect relations between water levels and discharge based on the yearly rating curve. Quality of data for the river gauging stations Gantsmod is high compared to the quality at the three other gauging stations. At these stations green areas are more often separated by red areas.

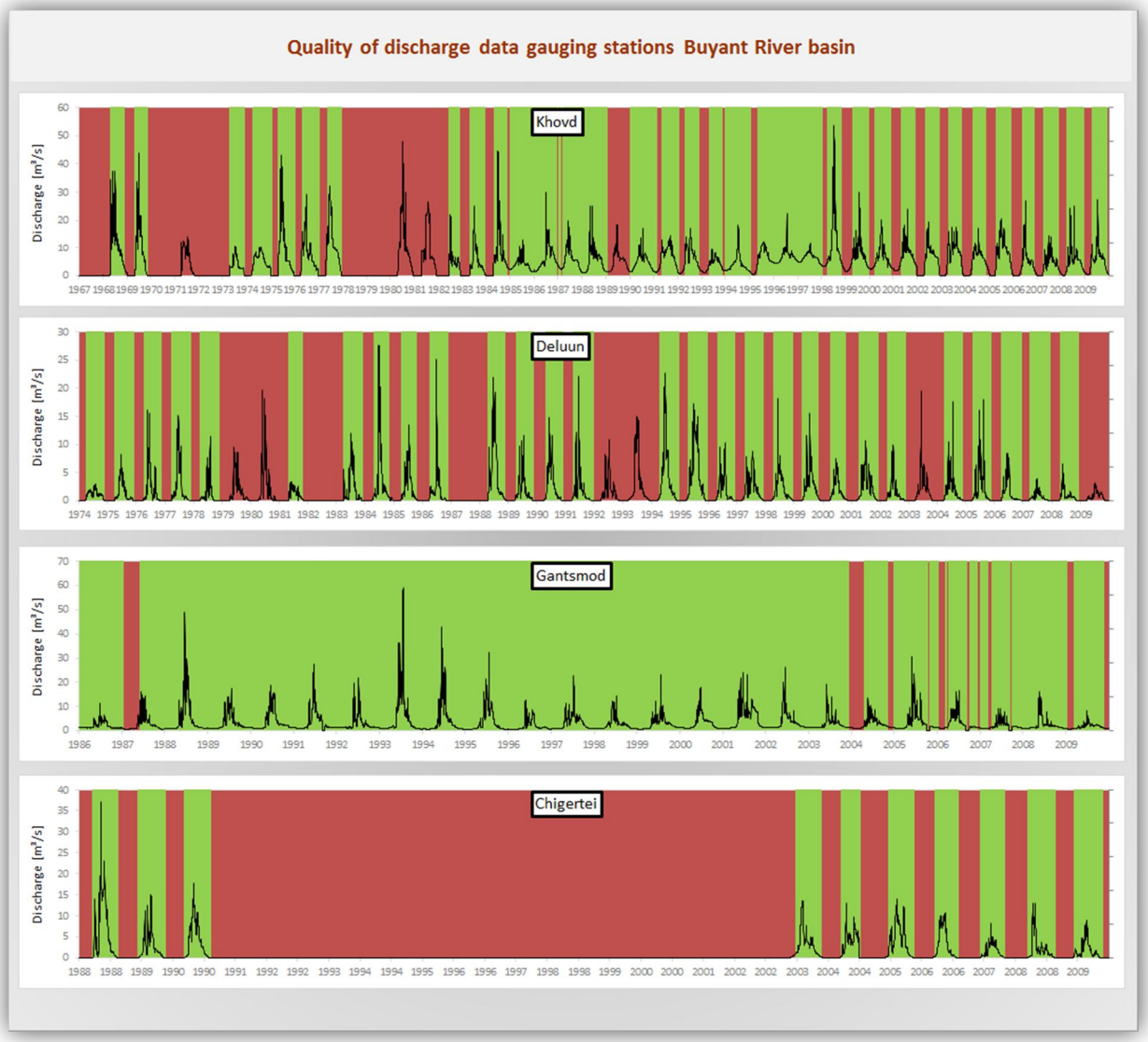

Figure 19 Daily discharge values are plotted against time for all 4 river gauging stations (IMH Mongolia). Green boxes represents reliable data, as the red boxes represents unreliable data.

3.4 Repair

3.4.1 Meteorological data

The obtained precipitation data and temperature data at the meteorological stations rely on point gauge measurements. Within the vicinity of the Buyant River basin there are only 4 metrological stations over an area of 8370 km²; errors can be significant due to this small number of gauges [*Viviroli et al.*, 2009]. Due to the small number of meteorological stations in the Buyant River basin, the simple elevation lapse-rate is considered the best method for calculating the areal precipitation and temperature for ungauged areas [*Shaw et al.*, 2011]. Using this lapse-rate precipitation, temperature and potential evapotranspiration can be calculated for all elevation heights in the Buyant River basin. The lapse-rate calculates the change in precipitation and temperature for a change in elevation height. Determining a weighted station which describes the average of data for each meteorological station is therefore a prerequisite. The area of the Buyant basin which each individual meteorological station covers, determines the weight for the meteorological data at the weighted station. The spatial distribution of the meteorological stations is shown in Figure 20. In this figure the catchment is colored by Thiessen polygons which divide the basin by lines that are equidistant between pairs of adjacent meteorological stations [*Shaw et al.*, 2011].

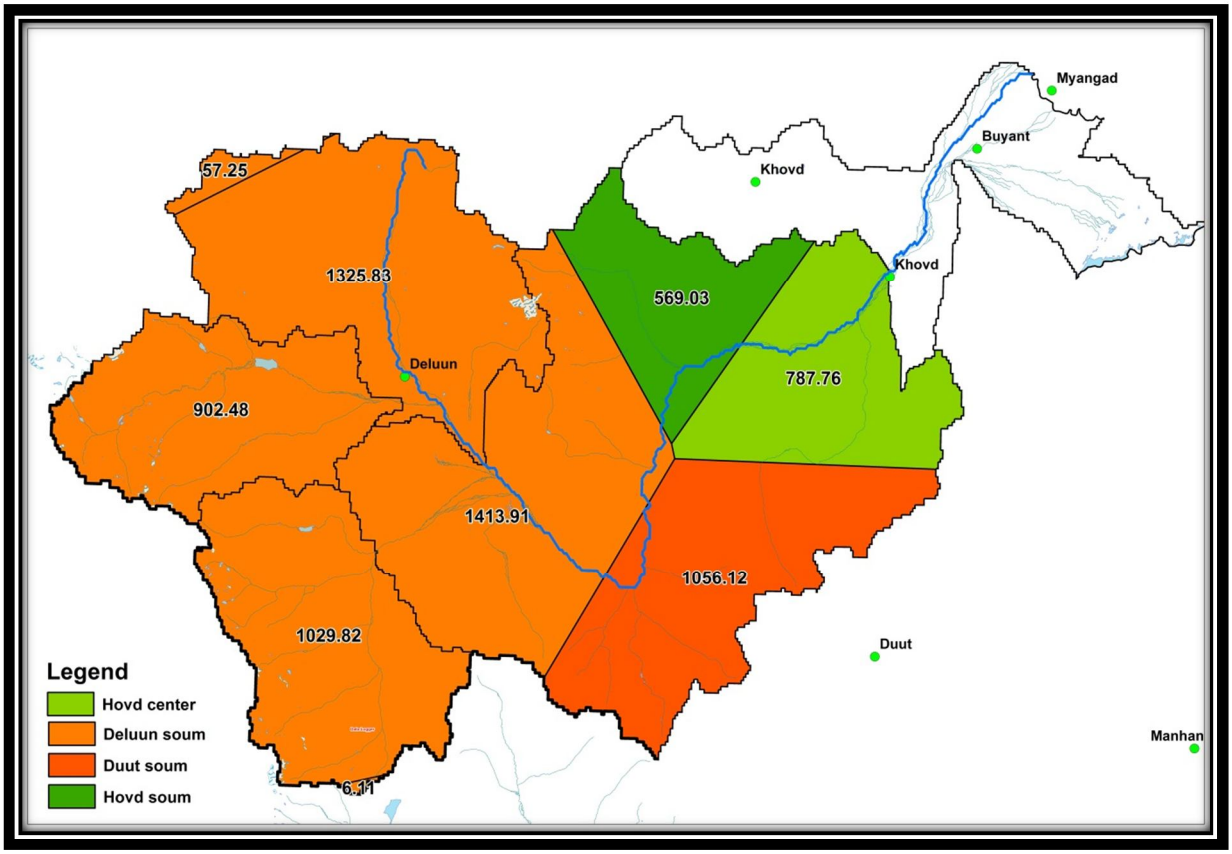

Figure 20 Thiessen polygons, which divide the basin by lines that are equidistant between pairs of adjacent meteorological stations, determine the input of each meteorological stations (IMH Mongolia). This figure is prepared by colleagues of IMH Mongolia

The altitude of the weighted station is determined by the input of the meteorological stations. As can be seen in Figure 20 the area covered by the meteorological station Deluun is highest, which means that the altitude of Deluun counts more heavily than the other stations. Based on the area covered, each station weights a fraction of the total weighted altitude. These fractions are enclosed by brackets in the third column of Table 8. The weighted altitudes for each data period are outlined in the last column.

Table 8 Weighted altitudes for the meteorological data for different data periods

Data period	Input value	Meteorological stations	Weighted altitude [m]
1961-1994	Precipitation	Khovd (1)	1405
1961-1993	Temperature	Khovd (1)	1405
1961-1993	Pot evapotranspiration	Khovd (1)	1405
1994-2005	Precipitation	Khovd(0.26)+Deluun(0.74)	1966
1993-2005	Temperature	Khovd(0.26)+Deluun(0.74)	1966
1993-2005	Pot evapotranspiration	Khovd(0.26)+Deluun(0.74)	1966
2005-2009	Precipitation	Khovd(0.18)+Deluun(0.67)+Duut Soum(0.15)	2040
2005-2007	Temperature	Khovd(0.18)+Deluun(0.67)+Duut Soum(0.15)	2040
2005-2007	Pot evapotranspiration	Khovd(0.18)+Deluun(0.67)+Duut Soum(0.15)	2040
2009-2010	Precipitation	Khovd(0.11)+Deluun(0.66)+Duut Soum(0.15)+Khovd Soum(0.06)	2058
2007-2010	Temperature	Khovd(0.11)+Deluun(0.66)+Duut Soum(0.15)+Khovd Soum(0.06)	2058
2007-2010	Pot evapotranspiration	Khovd(0.11)+Deluun(0.66)+Duut Soum(0.15)+Khovd Soum(0.06)	2058

To determine the weighted precipitation for the Buyant River basin the values for the year 2003 will not be considered due to its poor quality. The graphs presenting the temperature for the four meteorological stations are based on the average daily temperature values obtained by IMH Mongolia. The missing data for the meteorological station Khovd will be replaced by the average of the maximum and minimum data for these missing days. The missing months of temperature data for the meteorological stations Deluun and Duut Soum will be interpolated using the average of the daily temperature values for the two surrounding years, due to missing maxima and minima temperature values. This means that the average temperature at 1-2-1995 at meteorological station Deluun will be calculated by averaging the temperatures of 1-2-1994 and 1-2-1996. The missing data in February 2010 at meteorological station Duut Soum are calculated by averaging the related days of the previous three years. The average temperature at 1-2-2010 at meteorological station Duut Soum is the average of the temperatures of 1-2-2009, 1-2-2008 and 1-2-2007.

The potential evapotranspiration is calculated with the repaired temperature data using the Blaney and Criddle method.

3.4.2 Discharge data

By determining the yearly rating curves of reliable data at the four river gauging stations rating equations for each year can be derived. Using these equations unreliable discharges are repaired with the correlating measured water levels. First the relations between stages and discharges are filtered for each year using the predefined reliability, as described in paragraph 3.3.2. Hereafter the rating curve is determined by an equation of the form,

$$Q = a \cdot h^b$$

The coefficients *a* and *b* vary for each yearly rating curve. Unreliable discharges are then repaired by recalculating the daily discharges with the available measured water levels. This results in reliable discharge data for all days where water levels were measured. Thus using the rating equation daily discharges can be calculated if water levels are available.

4 Results

4.1 Meteorological data

The prepared meteorological data is depicted in Figure 21. All data series are complete for precipitation, temperature and potential evapotranspiration. As described in Table 8, weighted meteorological data is calculated based on the four available data periods obtained by the four meteorological stations. These periods are highlighted with colors in Figure 21, and the correlating altitudes are defined in textboxes.

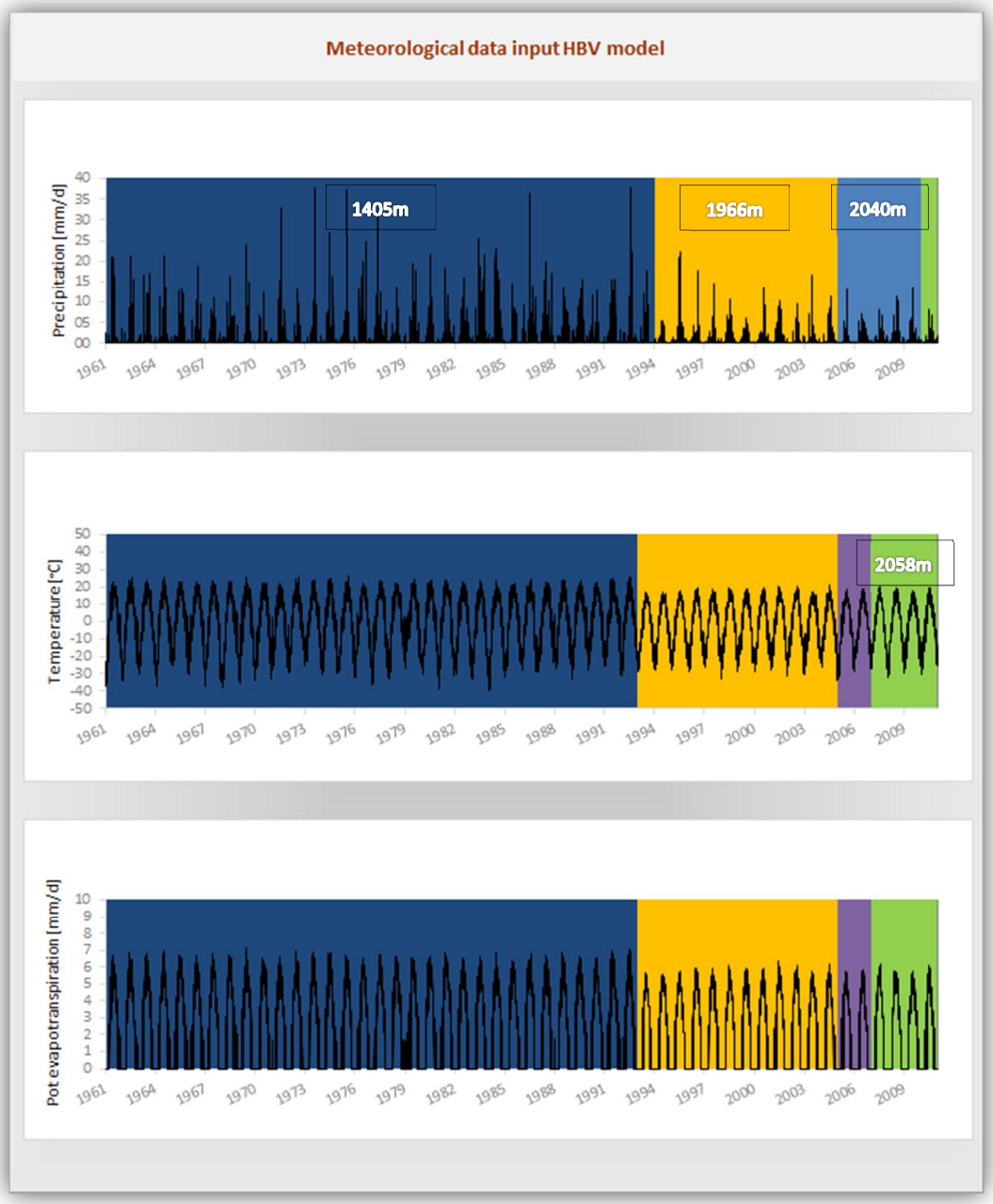

Figure 21 Graphical view of the meteorological data series which are used as input data for the HBV model. The color bars indicating the different data periods with the correlating altitude heights.

4.2 Discharge data

The prepared discharge data is depicted in Figure 22. Using the yearly rating curves of the stage-discharge relationship, quality of data for the gauging points were improved, especially at Khovd and Gantsmod. Discharge data at the gauging stations Khovd, Deluun and Chigertei are only reliable during the months May till October. Due to the missing water level measurement during the winter months at these gauging stations, indicated by red rectangles in Figure 22.

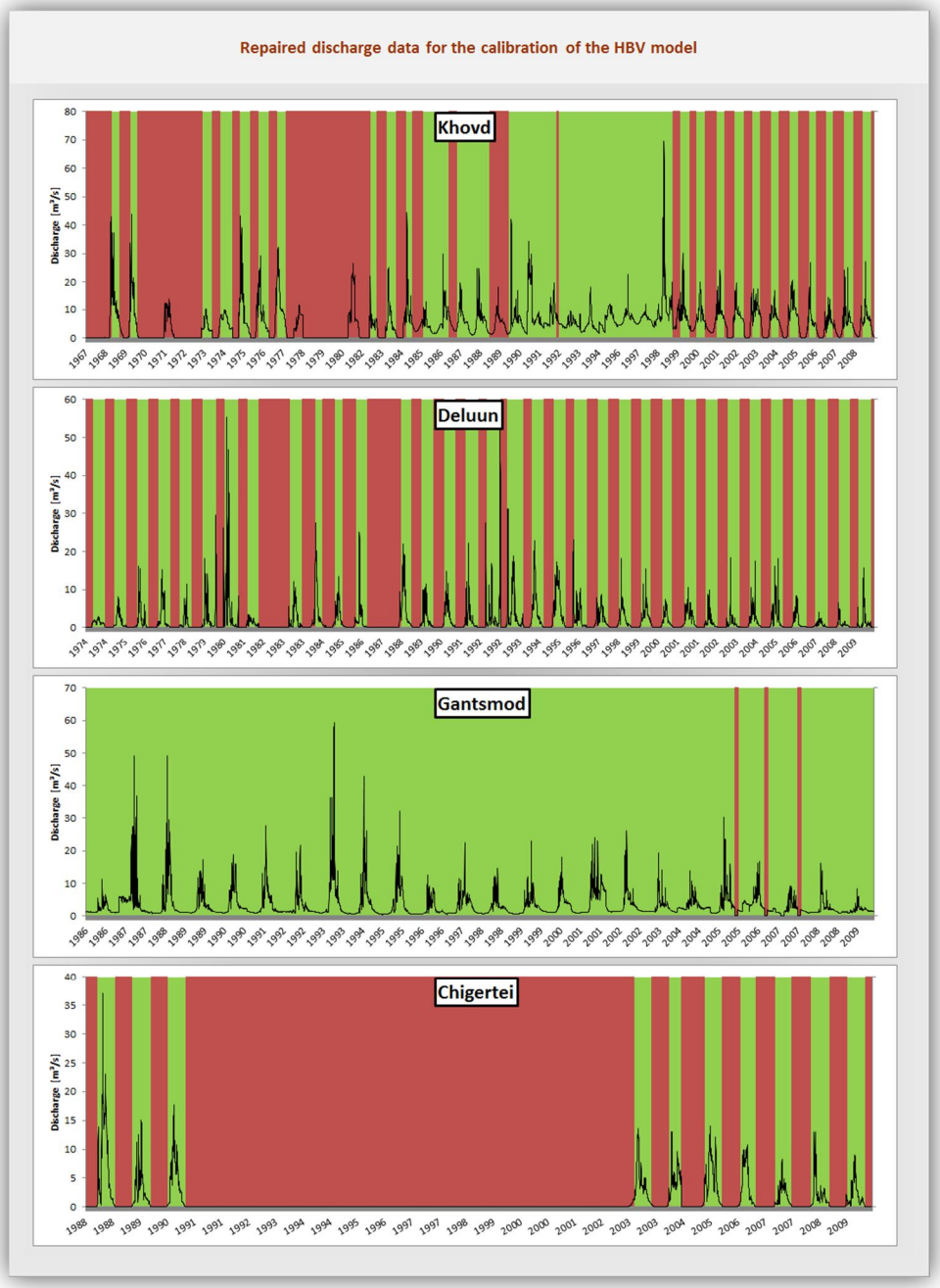

Figure 22 Graphical view of discharge data which should be used during the calibration of the HBV model. Red rectangles represents unreliable data, as the green rectangles represents data which should be used to calibrate the HBV model.

5 Conclusions

The data obtained during the visit to Mongolia has been outlined in this report. Quality of the data has been checked and repaired using interpolation techniques and the stage-discharge relations. Due to the small number of meteorological stations within the relative large Buyant River basin, the elevation lapse rate will be used to determine the areal precipitation, temperature and potential evapotranspiration. With only a small number of meteorological stations errors can be significant for the calculation of areal data. However, the quality of the meteorological data seems reliable and long-term data series are applicable for the Buyant River basin. The error significance will be further more examined during the modeling process of the Buyant River basin.

Next to the small number of meteorological stations, only a few permanent river gauging stations are located in the Buyant River and two of its main tributaries. At first the quality of discharge data was poorly obtained. However by filtering unreliable data better rating curves were determined, making it possible to repair poorly values for more reliable data. During calibration of the HBV model the reliable discharge data should be taken into account. Only these data periods should be compared with the correlating simulated discharges. In general data for the months May till October is considered reliable.

The Buyant River basin is divided into 4 sub-basins and lumped, semi-lumped and semi-distributed strategies are obtained. Working from a lumped model towards a semi-distributed model, parameters can be determined for each sub-basin based on soil characteristics, topography and their contribution to the stream flow at the outlet.

References

Ajami, N. K., H. Gupta, T. Wagener, and S. Sorooshian (2004), Calibration of a semi-distributed hydrologic model for streamflow estimation along a river system, *J Hydrol*, *298*(1-4), 112-135.

Allen, R. G., L. S. Pereira, D. Raes, and M. Smith (1998), Crop evapotranspiration—guidelines for computing crop water requirements.*Rep.*

Blaney, H. F., and W. D. Criddle (1950), Determining water requirements in irrigated areas from climatological irrigation
data*Rep.*, Department of Agriculture, Washington, DC.

Chen, D., G. Gao, C.-Y. Xu, J. Guo, and G. Ren (2005), Comparison of the Thornthwaite method and pan data with the standard Penman-Monteith estimates of reference evapotranspiration in China, *CLIMATE RESEARCH*, *28*, 123-132.

Nandintsetseg, B., and M. Shinoda (2011), Seasonal change of soil moisture in Mongolia: its climatology and modelling, *Int J Climatol*, *31*(8), 1143-1152.

Nandintsetseg, B., M. Shinoda, R. Kimura, and Y. Ibaraki (2010), Relationship between Soil Moisture and Vegetation Activity in the Mongolian Steppe, *Sola*, *6*, 29-32.

Shaw, E. M., K. J. Beven, N. A. Chappel, and R. Lamb (2011), *Hydrology in practice*, Fourth ed., Spon Press, London.

Viviroli, D., M. Zappa, J. Gurtz, and R. Weingartner (2009), An introduction to the hydrological modelling system PREVAH and its pre- and post-processing-tools, *Environmental Modelling & Software*, *24*(10), 1209-1222.

APPENDIX C: PET CALCULATIONS AND PROJECTIONS

Next to the observed precipitation and temperature data, potential evapotranspiration is an important input variable for the HBV model. A large number of empirical methods have been developed over the last 50 years to estimate the evapotranspiration [*Zotarelli et al.*, 2010]. Of these methods the well-known Penman-Monteith equation has been selected because it can estimate the evapotranspiration closely, and the climatic variables are available for the Buyant basin. The Penman-Monteith method combines both energy and mass balances to model the potential evapotranspiration and it is based on fundamental physical principles, which guarantee the universal validity of the method [*Chen et al.*, 2005].

Penman-Monteith equation

The equation uses standard climatological records of solar radiation (sunshine), air temperature, humidity and wind speed:

$$ET_0 = \frac{0.408\Delta(R_n - G) + \gamma \frac{900}{T+273} \cdot u_2 (e_s - e_a)}{\Delta + \gamma(1 + 0.34 u_2)}$$

The FAO [*Zotarelli et al.*, 2010] provided a step-by-step calculation of the reference evapotranspiration for a given location from the available weather data.

To ensure the integrity of computations, the weather measurements are converted to a height of 2m above the surface. The observed measurements were recorded at a height of 10m above the surface (IMHE Mongolia). Table 1 shows a list of parameters required to calculate the potential evapotranspiration:

Table 1 Parameters required to calculate the potential evapotranspiration using the Penman-Monteith equation [Zotarelli et al., 2010]

Symbol	Parameter	Unit
T_{max}	Maximum temperature	°C
T_{min}	Minimum temperature	°C
RH_{max}	Maximum relative humidity	%
RH_{min}	Minimum relative humidity	%
R_s	Average solar radiation	MJ m^{-2} d^{-1}
u_2	Average wind speed	M s^{-1} at 2 m above surface
P	Atmospheric pressure (barometric)	kPa
z	Site elevation above sea level	M
J	Julian day	-
LAT	Latitude	degree

Recorded humidity data ranges from 0 to 10, with no clear distinction between relative or normal humidity. Due to the questionable quality of the humidity data, the actual vapor pressure, e_a, has been obtained by assuming the air temperature is close to T_{min}.

The incoming solar radiations for the two meteorological stations are derived from the NASA website (http://eosweb.larc.nasa.gov/cgi-bin/sse/register.cgi). These data were provided by the Prediction of Worldwide Energy Resource Project and were obtained from the NASA Langley Research Center Atmospheric Sciences Data Center. By filling in the latitude, longitude and altitude of the two meteorological stations, the amount of electromagnetic energy (solar radiation) incident on the surface of the earth was obtained.

Hargreaves equation

To determine the monthly change in potential evapotranspiration the Hargreaves equation is applied [*Hargreaves*, 1984]:

$$EP_{Har} = 0.0022 \cdot R_A \cdot \left[\left(T_{max} + \Delta T_{GCM,SRES}\right) - \left(T_{min} + \Delta T_{GCM,SRES}\right)\right]^{0.5} \cdot \left[\left(T_{mean} + \Delta T_{GCM,SRES}\right) + 17.8\right]$$

Where R_A *[mm/day]* is the mean extra-terrestrial radiation, T_{max} *[°C]* is the maximum observed monthly air temperature, $\Delta T_{GCM,SRES}$ *[°C]* is the monthly temperature change for the each climate change scenario and T_{min} *[°C]* is the minimum observed monthly air temperature.

The monthly mean, maximum and minimum temperature and the radiation for the meteorological station Khovd are obtained from the website http://www.climate-charts.com/Locations/m/MO44218.php. These values, listed in Table 2, are used to calculate the potential evapotranspiration occurring to *Hargreaves* [1984] under the current climate conditions and for the climate change scenarios.

Table 2 Monthly temperature and radiation values for the Buyant River basin.

Month	*Average temperature [°C]*	*Maximum temperature [°C]*	*Minimum temperature [°C]*	*Radiation [mm/day]*
Jan	-24.3	-16.3	-29.9	2.83
Feb	-20.2	-12	-27.1	4.38
Mar	-7.4	0.3	-14.7	6.64
Apr	3.9	11.1	-3.5	9
May	11.9	19.1	4.6	10.79
Jun	17.1	23.8	10.3	11.57
Jul	18.6	24.7	12.3	11.14
Aug	16.7	23.4	10	9.61
Sep	10.6	17.7	3.9	7.43
Oct	1.5	9	-4.7	5.09
Nov	-9.7	-2.3	-15.7	3.22
Dec	-20	-12.9	-25.6	2.39

The projections for the potential evapotranspiration for the period 2080-2100 are shown in Table 3, Table 4 and Table 5. First the monthly potential evapotranspiration is calculated for the current climate with the values from Table 2. Hereafter the mean monthly projections of the temperature for the 4 GCMs are listed. Based on these temperature increase/decrease a new monthly potential evapotranspiration is calculated using the Hargreaves equation. Hereafter the PET projection is determined for the 4 GCMs for the period 2080-2100; dividing the projected monthly potential evapotranspiration by the current climate monthly potential evapotranspiration

Table 3 PET projections for the A2 emission scenario derived from the Hargreaves equation for the period 2080-2100

Current climate		T projection				Hargreaves equation results				PET projection			
Month	**PET by Hargreaves**	**GFDL**	**HadCM3**	**MRICGCM**	**ECHAM5**	**GFDL**	**HadCM3**	**MRICGCM**	**ECHAM5**	**GFDL**	**HadCM3**	**MRICGCM**	**ECHAM5**
1	0.000	5.33	3.51	4.40	5.86	0.000	0.000	0.000	0.000	1.000	1.000	1.000	1.000
2	0.000	4.84	3.86	2.88	6.50	0.091	0.055	0.018	0.154	1.000	1.000	1.000	1.000
3	0.588	7.54	5.78	3.43	8.02	1.015	0.915	0.783	1.042	1.725	1.556	1.330	1.771
4	1.642	4.60	3.91	1.73	4.46	1.989	1.937	1.772	1.979	1.212	1.180	1.079	1.206
5	2.685	5.13	3.09	2.50	4.87	3.148	2.964	2.911	3.125	1.173	1.104	1.084	1.164
6	3.264	4.20	4.52	2.00	5.13	3.657	3.687	3.451	3.743	1.120	1.130	1.057	1.147
7	3.141	4.43	6.13	2.41	5.58	3.524	3.670	3.349	3.623	1.122	1.168	1.066	1.153
8	2.670	5.96	4.75	4.11	6.06	3.131	3.038	2.988	3.139	1.173	1.138	1.119	1.176
9	1.725	5.93	5.27	3.58	5.18	2.084	2.045	1.942	2.039	1.209	1.186	1.126	1.182
10	0.800	4.42	3.72	3.05	4.92	0.983	0.954	0.926	1.004	1.229	1.193	1.158	1.255
11	0.210	4.79	6.26	4.34	5.62	0.334	0.372	0.323	0.356	1.591	1.772	1.536	1.693
12	0.000	4.25	3.81	4.76	5.74	0.038	0.030	0.048	0.066	1.000	1.000	1.000	1.000

Table 4 PET projections for the A1B emission scenario derived from the Hargreaves equation for the period 2080-2100

Current climate		T projection				Hargreaves equation results				PET projection			
Month	**EP by Hargreaves**	**GFDL**	**HadCM3**	**MRICGCM**	**ECHAM5**	**GFDL**	**HadCM3**	**MRICGCM**	**ECHAM5**	**GFDL**	**HadCM3**	**MRICGCM**	**ECHAM5**
1	0.000	2.47	4.64	3.25	6.59		0.000	0.000	0.000	0.002		1.000	1.000
2	0.000	5.85	2.86	3.44	6.41		0.129	0.017	0.039	0.150		1.000	1.000
3	0.588	5.37	6.05	2.50	6.81		0.892	0.931	0.730	0.974		1.517	1.582
4	1.642	6.00	6.32	1.04	2.83		2.096	2.120	1.721	1.856		1.277	1.291
5	2.685	4.44	4.32	1.77	3.95		3.086	3.075	2.845	3.042		1.149	1.146
6	3.264	4.52	4.63	1.90	4.63		3.687	3.697	3.442	3.697		1.130	1.133
7	3.141	5.63	5.72	2.70	5.70		3.627	3.635	3.375	3.633		1.155	1.157
8	2.670	5.71	6.21	3.94	5.24		3.112	3.150	2.975	3.076		1.166	1.180
9	1.725	5.27	3.93	3.60	4.39		2.045	1.963	1.943	1.991		1.186	1.138
10	0.800	4.59	4.62	2.53	5.27		0.990	0.991	0.905	1.018		1.238	1.239
11	0.210	4.90	5.91	4.54	5.14		0.337	0.363	0.328	0.343		1.605	1.729
12	0.000	2.92	3.76	3.90	5.95		0.013	0.029	0.032	0.070		1.000	1.000

Table 5 PET projections for the B1 emission scenario derived from the Hargreaves equation for the period 2080-2100

Current climate		T projection				Hargreaves equation results				PET projection			
Month	**EP by Hargreaves**	**GFDL**	**HadCM3**	**MRICGCM**	**ECHAM5**	**GFDL**	**HadCM3**	**MRICGCM**	**ECHAM5**	**GFDL**	**HadCM3**	**MRICGCM**	**ECHAM5**
1	0.000	5.33	3.51	4.40	5.86		0.000	0.000	0.000	0.000		1.000	NA
2	0.000	4.84	3.86	2.88	6.50		0.091	0.055	0.018	0.154		1.000	NA
3	0.588	7.54	5.78	3.43	8.02		1.015	0.915	0.783	1.042		1.725	NA
4	1.642	4.60	3.91	1.73	4.46		1.989	1.937	1.772	1.979		1.212	NA
5	2.685	5.13	3.09	2.50	4.87		3.148	2.964	2.911	3.125		1.173	NA
6	3.264	4.20	4.52	2.00	5.13		3.657	3.687	3.451	3.743		1.120	NA
7	3.141	4.43	6.13	2.41	5.58		3.524	3.670	3.349	3.623		1.122	NA
8	2.670	5.96	4.75	4.11	6.06		3.131	3.038	2.988	3.139		1.173	NA
9	1.725	5.93	5.27	3.58	5.18		2.084	2.045	1.942	2.039		1.209	NA
10	0.800	4.42	3.72	3.05	4.92		0.983	0.954	0.926	1.004		1.229	NA
11	0.210	4.79	6.26	4.34	5.62		0.334	0.372	0.323	0.356		1.591	NA
12	0.000	4.25	3.81	4.76	5.74		0.038	0.030	0.048	0.066		1.000	NA

APPENDIX D: PARAMETER VALUES HBV MODEL STRUCTURES

Parameter	Description	Ranges		First Calibration		Second Calibration			
		Min.	Max.	SEZ	MEZ	SEZ	MEZ	SEZ-PC	MEZ-PC
ECALT [-]	**Evapotranspiration correction factor for altitude**	**Default**		**0.100**	**0.100**	**0.100**	**0.100**	**0.1000**	**0.1000**
PCALT [-]	**Precipitation correction factor for altitude**	**Default**		**0.100**	**0.100**	**0.100**	**0.100**	**0.1000**	**0.1000**
TCALT [-]	**Temperature correction factor for altitude**	**Default**		**0.600**	**0.600**	**0.600**	**0.600**	**0.6000**	**0.6000**
TT [°C]	**Temperature limit for snow/rain**	**Default**		**0.000**	**0.000**	**0.000**	**0.000**	**0.0000**	**0.0000**
TTI [°C]	**Temperature interval with a mixture of snow and rain**	**Default**		**2.000**	**2.000**	**2.000**	**2.000**	**2.0000**	**2.0000**
WHC [-]	**Water holding capacity**	**Default**		**0.100**	**0.100**	**0.100**	**0.100**	**0.1000**	**0.1000**
CFR [-]	**Refreezing factor**	**Default**		**0.050**	**0.050**	**0.050**	**0.050**	**0.0500**	**0.0500**
TTM [°C]	Temperature limit for melting	*0.1000*	*2.5000*	-0.9066	-0.4175	-0.9066	-0.4175	-0.9066	-0.4175
SFCF [-]	Snowfall correction factor	*0.0000*	*2.0000*	1.4228	1.6972	1.4228	1.6972	1.4228	1.6972
RFCF [-]	Rainfall correction factor	*0.0000*	*2.0000*	1.1475	1.7533	1.1475	1.7533	1.1475	1.7533
ECORR [-]	Evaporation correction factor	*0.0000*	*2.0000*	0.8772	1.9805	0.8772	1.9805	0.8772	1.9805
CFMAX [mm/°C/d]	Degree day factor	*0.1000*	*4.0000*	2.5810	1.6745	2.5810	1.6745	**2.5810**	**1.5976**
FC [mm]	Maximum soil moisture content	*125.0000*	*800.0000*	211.4052	301.7516	211.4052	301.7516	211.4052	301.7516
LP [-]	Limit for potential evapotranspiration	*0.2000*	*1.0000*	0.5306	0.8429	**0.5222**	**0.7560**	**0.3640**	**0.3809**
BETA [-]	Parameter in soil routine	*1.0000*	*4.0000*	1.1846	1.3630	1.1846	**1.8577**	1.1846	**1.0239**
PERC [mm/d]	Percolation rate occurring when water is available	*0.1000*	*2.5000*	2.1516	1.4430	**1.3919**	1.4430	**2.4204**	1.4430
CFLUX [mm/d]	Maximum value of capillary flux	*0.1000*	*2.5000*	0.1137	1.1536	0.1137	1.1536	0.1137	1.1536
ALFA [-]	Measure for non-linearity of flow in upper zone box	*0.1000*	*3.0000*	0.6613	0.2679	**0.1635**	**0.1117**	**0.2862**	**0.1214**
K [d^{-1}]	Recession coefficient for runoff from upper zone box	*0.0005*	*0.1500*	0.0023	0.0025	**0.0064**	**0.0111**	**0.0087**	**0.0124**
K4 [d^{-1}]	Recession coefficient for runoff from lower zone box	*0.0005*	*0.1500*	0.0018	0.0011	0.0018	0.0011	0.0018	0.0011
STCF [-]	Soil temperature correction factor	*0.0000*	*2.0000*	**-**	**-**	-	-	**1.1603**	**1.2820**